Universitat Politècnica de Catalunya

Programa de Doctorado:

Automatización Avanzada y Robótica

Tesis Doctoral

CONTROL AND DESIGN OF PEM FUEL CELL-BASED SYSTEMS

Diego Feroldi

Directores: Dr. Jordi Riera Colomer y Dra. Maria Serra Prat

Institut d'Organització i Control de Sistemes Industrials

Marzo 2009

A mi familia

La utopía está en el horizonte. Me acerco dos pasos, ella se aleja dos pasos. Camino diez pasos y el horizonte se desplaza diez pasos más allá. Por mucho que camine, nunca la alcanzaré. ¿Para qué sirve la utopía? Para eso, sirve para caminar.

Eduardo Galeano

Agradecimientos

En primer lugar quisiera agradecer profundamente a mis directores de tesis Jordi Riera y Maria Serra por su inestimable ayuda y soporte durante toda esta etapa tan importante de mi vida. Sus consejos, guías y su invalorable apoyo en todo momento, tanto a nivel académico como personal, han sido imprescindibles para poder realizar la tesis. Asimismo quisiera agradecer a Marta Basualdo, profesora de la Facultad de Ingeniería Electrónica de la *Universidad Nacional de Rosario*, quien me introdujo en el control automático y quien me alentó y ayudó a comenzar el doctorado. Muchas gracias a los tres por confiar en mí.

Quisiera agradecer igualmente a Joseba Quevedo, Viçenc Puig, Teresa Escobet y Salvador de Lira del grupo *Sistemes Avançats de Control* (*SAC*) por su gran aporte y colaboración. Gracias al trabajo realizado en conjunto ha sido posible el Capítulo 5 de ésta Tesis. Y también a Carlos Ocampo por sus consejos sobre *MPC*.

Al *Institut de Robòtica i Informàtica Industrial* (*IRI*), donde he realizado la tesis doctoral, por el soporte y ayuda que me han brindado tanto a nivel humano como económico y a la *Agència de Gestió d'Ajuts Universitaris i de Recerca* (*AGAUR*) por la beca doctoral que me han concedido y que ha hecho posible llevar a cabo la tesis.

A toda la gente del *IRI* con la que he compartido muy buenos momentos durante estos años y en particular a mis compañeros del grupo de pilas de combustible: Mauricio, Attila, Miguel, Vanesa, Enric y Fran.

Para finalizar, quisiera dar las gracias especialmente a mi familia, que me ha apoyado constantemente a la distancia, y expresar mi agradecimiento y admiración a mis padres Jorge y Stella por su trabajo y sacrificio para que sus hijos pudiesen tener una buena educación y, sobre todo, por su amor.

Abstract

The use of fuel cell systems based on hydrogen is advantageous because of their high efficiency in the energy conversion and null emissions. In this thesis, an extensive study about the control and design of electrical generation systems based on fuel cells is performed. The main focus is in hybrid systems composed of fuel cells and supercapacitors as energy storage elements, oriented to automotive applications. The determination of the hybridization degree (i.e. the determination of the fuel cell size and the number of supercapacitors) is performed through a proposed methodology with the objective to fulfil the conductibility requirements and to consume the lowest amount of hydrogen.

The process of design starts with the determination of the electrical structure and utilizes a detailed model developed using *ADVISOR*, a *MATLAB* toolbox for modelling and studying hybrid vehicles. The energy flow between the vehicle components is analyzed when the vehicle is tested with different *Standard Driving Cycles*, showing how the losses in each component degrade the efficiency of the system and limit the energy recovery from braking. With regard to the energy recovery, a parameter to quantify the amount of energy that is actually reused is defined and analyzed: the *braking/hydrogen* ratio.

To control the energy flow between the fuel cell, the energy storage system, and the electrical load in *Fuel Cell Hybrid Vehicles* (*FCHVs*), three *Energy Management Strategies* (*EMSs*) based on the fuel cell efficiency map are presented and validated through an experimental setup, which is developed to emulate the *FCHV*. The resulting hydrogen consumptions are compared with two references: the consumption of the pure fuel cell case, a vehicle without hybridization, and the optimal case with the minimum consumption. The optimal consumption for a given vehicle is determined through a methodology proposed that, unlike other previous methodologies, avoids the discretization of the state variables.

To operate the fuel cell system efficiently, the system is controlled through a proposed control technique, based on *Dynamic Matrix Control* (*DMC*). This control technique utilizes the compressor voltage as control variable and also a new proposed variable: the opening area of a proportional valve at the cathode outlet. The control objectives are the control of the oxygen

excess ratio at the cathode and the fuel cell voltage. The advantages of this new control variable are analyzed both in steady state and transient state. Simulation results show an adequate performance of the controller when a series of step changes in the load current is applied.

The diagnosis and fault-tolerant control of the fuel cell-based system is also considered. A diagnosis methodology based on the relative fault sensitivity is proposed. The performance of the methodology to detect and isolate a set of proposed failures is analyzed and simulation results in an environment developed to include the set of faults are given. The fault-tolerant control is approached showing that the proposed control structure with two control variables has good capability against faults in the compressor when the oxygen excess ratio in the cathode is controlled.

Resumen

Las pilas de combustible son muy ventajosas debido a su alta eficiencia en la conversión de energía y nula contaminación. En esta tesis se realiza un extenso estudio sobre el control y diseño de sistemas de generación eléctrica basados en pilas de combustible. El núcleo principal de la misma son los sistemas híbridos con pilas de combustible y supercapacitores como elementos almacenadores de energía, orientado a aplicaciones automotrices. La determinación del *Grado de Hibridización* (i.e. la determinación del tamaño de la pila de combustible y del número de supercapacitores) se realiza mediante una metodología propuesta con el objetivo de satisfacer requisitos de conductibilidad y consumiendo la menor cantidad de hidrógeno posible.

El proceso de diseño comienza con la determinación de la estructura eléctrica de generación del vehículo y utiliza un modelo detallado realizado en *ADVISOR*, una herramienta para modelado y estudio de sistemas híbridos. Se analiza el flujo de energía a través de los componentes del vehículo cuando el vehículo sigue diferentes ciclos de conducción estándares, mostrando las pérdidas en cada componente que degradan la eficiencia del sistema y limitan la recuperación de energía de frenado. Con respecto a la recuperación de energía, se ha definido y analizado un parámetro que cuantifica la cantidad de energía que realmente es reaprovechada: el ratio *frenado/hidrógeno*.

Para controlar el flujo de energía entre la pila de combustible, los almacenadores de energía y la carga eléctrica, se proponen tres *Estrategias de Gestión de Energía* (*EMS*) para *Vehículos Híbridos con Pila de Combustible* (*FCHVs*) basadas en el mapa de eficiencia de la pila y se validan mediante un montaje experimental desarrollado para emular el sistema híbrido. Los resultados de consumo de hidrógeno son comparados con dos referencias: el consumo correspondiente al caso del vehículo sin hibridización y el caso óptimo con el menor consumo para el vehículo propuesto. El consumo óptimo se calcula mediante una metodología propuesta que, a diferencia de otras, evita la discretización de las variables de estado.

Para operar el sistema eficientemente, la pila de combustible es controlada mediante una metodología de control, basada en *Control de Matriz Dinámica* (*DMC*). Esta metodología de control utiliza como variables de control el voltaje de compresor y una nueva variable propuesta: la apertura de una válvula proporcional ubicada a la salida del cátodo. Los objetivos de control son controlar el exceso de oxígeno en el cátodo y el voltaje generado

por la pila. Se analiza tanto en régimen estacionario como transitorio las ventajas de emplear esta nueva variable de control y se muestran resultados de funcionamiento por simulación del controlador ante perturbaciones en la corriente de carga.

Por otro lado, se aborda el diagnóstico y el control tolerante a fallos del sistema basado en pila de combustible proponiendo una metodología de diagnóstico basada en las sensibilidades relativas de los fallos y se muestra que la estructura de control con las dos variables propuestas tiene buena capacidad de rechazo a fallos en el compresor cuando se controla el exceso de oxígeno en el cátodo.

Nomenclature

Acronym

$ADVISOR$	ADvanced VehIcle SimulatOR
DC	Direct Current
DMC	Dynamic Matrix Control
$DMFC$	Direct Methanol Fuel Cell
ESS	Energy Storage System
FC	Fuel Cell
FCS	Fuel Cell System
$FCHV$	Fuel Cell Hybrid Vehicle
$FCHS$	Fuel Cell Hybrid System
FTP	Federal Test Procedure
$H_2\text{-}FCV$	Hydrogen Fuel Cell Vehicle
$HWFET$	Highway Fuel Economy Test
ICE	Internal Combustion Engine
MEA	Membrane Electrode Assembly
MFM	Mass Flow Meter
MPC	Model Predictive Control
$NEDC$	New European Driving Cycle
PEM	Proton Exchange Membrane
$PEMFC$	Proton Exchange Membrane Fuel Cell
RGA	Relative Gain Array
SC	SuperCapacitor
$UDDS$	Urban Dynamometer Driving Schedule

Symbol		*Unit*	*Value*
A	Fuel cell active area	cm^2	
A_f	Vehicle frontal area	m^2	
A_t	Cathode output valve area	cm^2	
C_d	Drag Coefficient	-	
C_p	Specific heat capacity of air	$J\,kg^{-1}\,K^{-1}$	1004
C_R	Supercapacitor capacitance	F	

$Cons_{H_2}$	Cumulative consumption of hydrogen	g	
E	Energy	Wh	
E^0	Single cell open circuit voltage	V	
E_{cap}	Maximum storage energy of supercapacitors	Wh	
F	Faraday number	$C\,mol^{-1}$	96485
f	Output free response	-	
f_r	Rolling friction coefficient	-	
G	Dynamic matrix in DMC controller	-	
g	Gravity	$m\,s^{-2}$	9.8
g_i	Dynamic matrix coefficients	-	
h_m	Control horizon	-	
h_p	Prediction horizon	-	
HD	Hybridization degree	$HD = \frac{P_{ess,\,max}}{P_{fcs,\,max}+P_{ess,\,max}}$	
I	Stack current	A	
i	Current density	$A\,cm^{-2}$	
J	Cost function	-	
k_{SC}	Constant depending on the particular SC	-	
m_{veh}	Vehicle mass	kg	
m_T	Vehicle total mass	kg	
M_{H_2}	Hydrogen molar mass	$kg\,mol^{-1}$	2.016×10^{-3}
M_{N_2}	Nitrogen molar mass	$kg\,mol^{-1}$	28×10^{-3}
M_{O_2}	Oxygen molar mass	$kg\,mol^{-1}$	32×10^{-3}
M_v	Water vapor molar mass	$kg\,mol^{-1}$	18.02×10^{-3}
N_c	Number of time steps in a driving cycle	-	
n	Number of cells in a stack	-	
P	Power	W	
p	Pressure	P_a	
p_{H_2}	Hydrogen partial pressure	P_a	
p_{O_2}	Oxygen partial pressure	P_a	
P/E	Storage system $Power/Energy$ ratio	$W\,Wh^{-1}$	
$Q,\ R$	Weight matrices in DMC	-	
$\bar{R}$	Universal gas constant	$J\,mol^{-1}\,K^{-1}$	8.3145
R_d	Internal resistance (DC) of ESS	Ω	
r	Resistance	Ω	
SRa	Air stoichiometry	-	
SoC	State of Charge	$\%$	
SoE	State of Energy	$\%$	
T	Temperature	K	
t	Time	s	
t_c	Duration of the driving cycle	s	
u	Control variable		
V	Voltage	V	
v	Velocity	$m\,s^{-1}$	

w	Disturbance		
W	Mass flow rate	$kg\,s^{-1}$	
y	Output		
$y(k+1|k)$	Prediction of y_i at time $k+1$ done in time k		
y_r	Reference output		

Greek letters		*Unit*	*Value*
α	Road slope	$radians$	
$\Delta(.)$	Variation from the nominal value	-	
ΔH_{LHV}	Lower heating value of hydrogen	$kJ\,g^{-1}$	120
ΔH_{HHV}	Higher heating value of hydrogen	$kJ\,mol^{-1}$	286
Δu	Variation in the control action		
ϕ	Relative humidity	%	
γ	Ratio of the specific heats of air	-	1.4
η	Efficiency	-	
η_{fc}	Efficiency of a single fuel cell	-	
η_{fcs}	Efficiency of the fuel cell system	-	
λ	Coefficient to weight the error in MPC	-	
λ_{O_2}	Oxygen excess ratio	-	
ρ_a	Air density	$kg\,m^{-3}$	1.2
τ	Torque	$N\,m$	

Subscripts and superscripts			
an	Anode		
atm	Atmospheric		
aux	Auxiliary		
ca	Cathode		
cap	Capacity		
cm	Compressor motor		
cp	Compressor		
el	Electrical		
ess	Energy storage system		
fc	Fuel cell		
fcs	Fuel cell system		
gen	Generated		
H_2	Hydrogen		
i	Index		
in	Inlet		
j	Index		
N_2	Nitrogen		
O_2	Oxygen		

out	Outlet
rct	Reacted
rm	Return manifold
sm	Supply manifold
sys	System
T	Transposed
t	Throttle
v	Water vapor
w	Water

Contents

CONTENTS

List of Figures

List of Tables

LIST OF TABLES

Chapter 1

Introduction

1.1 Motivation

Given the serious environmental problems and the anticipated fuel shortage for the next decades it is important to find more efficient forms of using the power resources, affecting minimally the environment. According to different sources, such as [1], global oil reserves are only sufficient for around 40 years with the current level of oil production. However, the global economy is rapidly increasing with a subsequent increase in oil consumption: the total primary energy consumption has grown from $6128\,Mtoe$[1] in 1973 to $11435\,Mtoe$ in 2005 (Fig. 1.1). In the same period, the CO_2 emission has grown from $15661\,Mt$ to $27136\,Mt$ (Fig. 1.2) [2]. Therefore, oil reserves will be probably exhausted in a much shorter time period.

The main fossil alternatives for oil are coal and natural gas. Coal is cheap and global coal reserves are sufficient for 156 years of current coal consumption[2] [1]. However, the CO_2 emissions per MJ are two times higher than for natural gas and pollution abatement is very expensive. Therefore, it is important to promote the development of new energy technologies.

Hydrogen-based fuel cell technology is a promising alternative for electrical energy generation, specially for automotive applications. Hydrogen is a potential energy vector for fuel cell-based vehicles, for reasons of vehicle design, cost and efficiency, as well as

---

[1]The tonne of oil equivalent (*toe*) is the amount of energy released by burning one tonne of crude oil, approximately $42\,GJ$.

[2]Not including sub-bituminous coal and lignite.
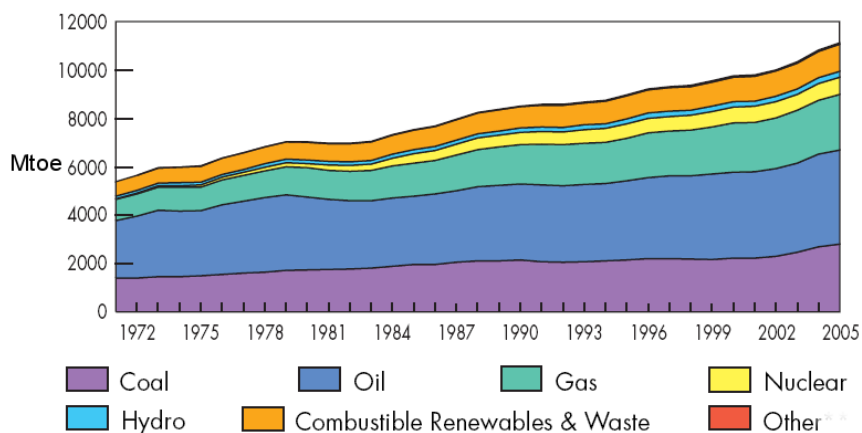
Figure 1.1: Evolution from 1971 to 2005 of World Total Primary Energy Supply by fuel (Other includes geothermal, solar, wind, heat, etc.) [2]

energy supply and environmental benefits (e.g., the possibility for reducing the total fuel cycle greenhouse gas emissions). For the same performance, hydrogen fuel cell vehicles are likely to be simpler in design, lighter, more energy efficient, and less expensive than methanol or gasoline fuel cell vehicles. Moreover, the tailpipe emissions will be strictly zero under all operating conditions [3].

Polymer Electrolyte Membrane Fuel Cells (PEMFCs) are one of the most advanced fuel cell systems together with *Solid Oxide Fuel Cells (SOFCs)*. The *PEMFC* technology is essentially hydrogen-based and is more mature than *SOFCs*. Fundamentally, *PEMFCs* work at temperatures much lower than *SOFCs*, allowing the use of them in multiple applications. However, there are still important areas such as material development (especially relating to electrolyte and catalysts for electrodes) and process control that will further advance the technology [4] permitting lower cost and higher reliability.

The *PEMFCs* are devices that allow transforming directly the chemical energy of an energy vector[1] (hydrogen) into electrical energy. This energy conversion has high efficiency and is clean since the only by-products are water and heat. On account of these reasons, *PEMFC* technology is an interesting alternative of electrical generation

---

[1]Frequently, in the literature it is said that hydrogen is a fuel but this is not completely correct. Hydrogen, in reality, is an energy vector as it is explained in [5, 6], and not an energy source. Hydrogen may be obtained from fossil sources (such as methane) or water electrolysis.
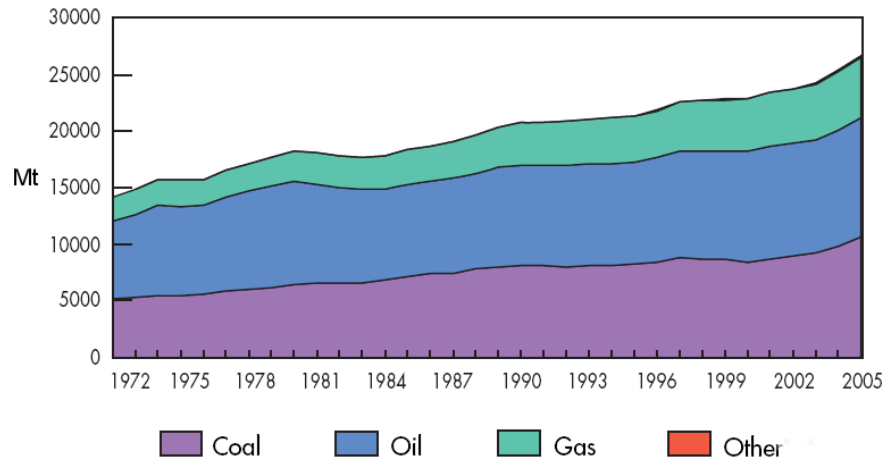
Figure 1.2: Evolution from 1971 to 2005 of World CO_2 Emissions by Fuel [2]

in several applications. These applications can be divided in three great groups [7]:

1. Generation of electricity for stationary applications

2. Automotive applications

3. Portable electronic applications

Particularly, in the last years, the study of fuel cell applications in vehicles has taken more and more importance. The fuel cell running on hydrogen is the most attractive long-term option for passenger cars [8]. The main advantage of the fuel cell vehicles as opposed to those with *Internal Combustion Engine* (*ICE*) is that in the former the energy conversion is direct (without combustion), producing a higher efficiency and practically null emission of polluting agents [9]. Thus, fuel cell vehicles have long term potential to be the mainstream vehicle in the future because the almost zero emission and compatible driving range with *ICE* [10].

However, the *PEM Fuel Cell System* is a complex and interrelated system. With the aim of obtaining an efficient energy conversion and maintaining the durability of the cells, the control of the fuel cell system is crucial. Thus, different control problems must be solved to obtain a correct operation of the system. The main ones are the following:

- Suitable hydrogen and air supply

- Handling of heat and water

- Conditioning of the generated power

- Control of the power flows in the system to fulfill the power load

Solving efficiently these issues allows an energy conversion with high efficiency, diminishing the hydrogen consumption and increasing the fuel cell durability.

Therefore, there is a strong motivation to study the control of *Fuel Cell-based Systems* according to the benefits and challenges enunciated and, in particular, the hybrid systems with fuel cells and energy storage. Moreover, fuel cell systems is a field of study in development and there is great expectancy in the industrial sector and the society in general. During the study of the state of the art of the subject we have found few publications that approach the problem of control these systems as a global system. In fact, a study of the control of the fuel cell hybrid systems is necessary with a global approach, taking account of the complete system and the interaction between the different subsystems.

1.2 Main contributions

This thesis presents an approach to the control and design of *PEM* Fuel Cell-based systems that integrates several subjects: the control of the air supply of the fuel cell system, the diagnosis and fault-tolerant control, the design of fuel cell hybrid systems oriented to automotive applications according to drivability requirements and hydrogen economy, and the development of energy management strategies to control the energy flows in the hybrid system.

The main contributions of this thesis may be summarized as follows:

Fuel cell control

Proposal of a new control structure, which includes an additional manipulated variable, and a new control system for the fuel cell air supply based on dynamic matrix predictive control. Evaluation of the control performance, showing the improvement of the efficiency and transient behavior of the system, and fault-tolerant capabilities of the control structure.

Design of *Fuel Cell Hybrid Systems*

A methodology of design to assess the size of the fuel cell and the energy storage of the *Fuel Cell Hybrid Systems* oriented to automotive applications. This methodology allows to achieve a robust design that fulfils conductibility requirements similar to conventional vehicles, consuming the minimum amount of hydrogen.

Energy management strategy for *Fuel Cell Hybrid Vehicles*

Three *Energy Management Strategies* to determine the fuel cell operation to fulfill the load profiles and minimize the hydrogen consumption, using the fuel cell system efficiency map. The strategies are effective to work in real time and present high performance in the experimental validation.

1.3 Outline of the thesis

This thesis is about the control of power generation systems based on *Polymer Electrolyte Membrane (PEM) Fuel Cells* and, in particular, the *Fuel Cell Hybrid Systems (FCHS)* with an *Energy Storage System (ESS)* acting as a secondary power source. The emphasis is placed on understanding the theoretical advantages and limitations of these systems, and developing methodologies of design and control.

Within the scope of this thesis is the fuel cell control (mainly focused in the air supply control), the analysis of hybrid structures, the study of the convenient hybridization degree[1] and the system modelling. Besides, a study of the design process with particular focus on the interrelation between the hybridization degree and the energy management strategies is done. Special attention is given to the study of *Energy Management Strategies* with the aim of obtaining a more efficient system operation. The *FCHS* are studied with the aim of applying them to electric vehicles.

Fuel cell temperature control, water management, startup and shutdown operation and the control of the power converters are beyond the scope of this thesis.

---

[1]In the context of fuel cell hybrid systems, the hybridization degree (HD) is a parameter that indicates the relation between two installed powers: $HD = \frac{P_{ess,\,max}}{P_{fcs,\,max}+P_{ess,\,max}}$. The formal definition is given in Section 6.3.2.

1. Introduction

In this chapter we presented the motivation and main contributions of this thesis. The rest of the thesis is organized according to the following chapters:

Chapter 2 provides a brief review of *PEM Fuel Cell-based Systems* to introduce the main concepts of this technology.

Chapter 3 presents the state of the art of *Fuel Cell-based Systems*, reviewing previous approaches in the literature to their control, and the design and operation of fuel cell hybrid systems.

Chapter 4 focuses on the control of a power generation system composed of a fuel cell system fed with hydrogen from a pressurized tank and atmospheric air through a compressor. In this chapter, the design of controllers is studied with the control objectives to regulate the oxygen excess ratio in the cathode and the generated voltage in the fuel cell stack. Finally, a controller based on *Dynamic Matrix Control DMC* is proposed and evaluated.

Chapter 5 approaches the *Diagnosis* and *Fault-Tolerant Control* of fuel cell-based systems. In particular, it is shown that using an additional manipulated variable in the air control subsystem permits to introduce a certain degree of fault-tolerance against compressor faults in the critical air feeding control, at the same time that allows to improve the control performance.

Chapter 6 continues the study of *PEMFC* systems, approaching the *Fuel Cell-Hybrid Systems* with an *Energy Storage System* composed of supercapacitors, with the aim of increasing the efficiency and performance of the power generation system through regenerative braking (in automotive applications) and an adequate energy management strategy.

Chapter 7 focuses on the development of *Energy Management Strategies* to determine at each sampling time the power split between the *FCS* and the *ESS* in order to fulfill the power balance and reduce the hydrogen consumption.

Chapter 8 provides the conclusions of this thesis and a proposal of future work to continue the research in the subject.

1.4 Derived publications

The following is a list of the published works derived from this thesis:

1. D. Feroldi, M. Serra, J. Riera. Design and Analysis of Fuel Cell Hybrid Systems Oriented to Automotive Applications, Submitted to *IEEE Transactions on Vehicular Technology*, Nov 25 2008

2. M. Basualdo, D. Zumoffen, L. Nieto Degliuomini, D. Feroldi, J. Riera, Predictive Adaptive Robust Control by Zones for Fuel Cells Hybrid Vehicles, submitted to 10th International Symposium on Process Systems Engineering - PSE2009.

3. D. Feroldi, M. Serra, J. Riera. Energy Management Strategies based on Efficiency Map for Fuel Cell Hybrid Vehicles, *Journal of Power Sources*. In press, accepted manuscript, available online 28 January 2009, DOI: 10.1016/j.powsour.2009.01.040

4. T. Escobet, D. Feroldi, S. de Lira, V. Puig, J. Quevedo, J. Riera and M. Serra. Model based fault diagnosis in PEM fuel cell Systems, *Journal of Power Sources*. In press, corrected proof, available online 9 December 2008, DOI: 10.1016/j.powsour.2008.12.014

5. D. Feroldi, M. Serra, J. Riera. Performance improvement of a PEMFC system controlling the cathode outlet air flow, *Journal of Power Sources*, Vol. 169, pp 205-212, 2007.

6. M. Serra, A. Peter Husar, D. Feroldi, J. Riera. Performance of diagonal control structures at different operating conditions for polymer electrolyte membrane fuel cells, *Journal of Power Sources*, Vol. 127, pp. 1317-1323, 2006.

7. T. Escobet, D. Feroldi, S. de Lira, V. Puig, J. Quevedo, J. Riera, M. Serra, Diagnóstico de Fallos en Sistemas de Generación de Energía basados en Pilas de combustible, *in Proc. III Congreso Nacional de Pilas de Combustible, CONA-PPICE 2008* (Zaragoza, Spain), pp. 223-226.

8. D. Feroldi, E. Roig, M. Serra, J. Riera, Energy Management Strategies for Fuel Cell-Hybrid Vehicles, *in Proc. HYCELTEC 2008* (Bilbao, Spain).

9. V. Puig, D. Feroldi, M. Serra, J. Quevedo, J. Riera, Fault-Tolerant MPC Control of PEM Fuel Cells, *in Proc. 17th IFAC World Congress* (Seoul, Korea) 2008, pp. 11112-11117.

10. D. Feroldi, M. Serra, J. Riera, Control de la respuesta dinámica de la tensión generada y del suministro de aire en sistemas basados en pilas de combustible tipo PEM, *in Proc. II Congreso Nacional de Pilas de Combustible, CONAPPI-CE 2006* (Madrid, Spain), pp. 293-296.

11. D. Feroldi, M. Serra, J. Riera, Control de Sistemas Basados en Pilas de Combustible Tipo PEM, *in Proc. Segones Jornades d'Automàtica, Visión y Robòtica* (Barcelona, España) 2006, pp. 98-105.

12. D. Feroldi, M. Basualdo, M. Serra, J. Riera, Control Multivariable de una Pila de Combustible Tipo Polimérica mediante Control Predictivo de Matriz Dinámica, *in Proc. II Jornadas Iberoamericanas de Pilas de Combustible e Hidrógeno* (Buenos Aires, Argentine) 2006.

Chapter 2

Review of *PEM* Fuel Cell Systems

This chapter provides a review of *PEM Fuel Cell-based Systems* in order to introduce the main concepts and to show the advantages of using these systems in different applications. The chapter is divided in two sections: *Fuel Cell Systems* (Section 2.1) and *Fuel Cell Hybrid Systems* (Section 2.2).

2.1 Fuel Cell Systems

2.1.1 Basic Fuel Cell structure

The *Polymer Electrolyte Membrane Fuel Cell* (*PEMFC*), also known as *Proton Exchange Membrane Fuel Cell*, takes its name from the type of electrolyte: a polymeric membrane with high proton conductivity when the membrane is conveniently hydrated [7]. At the moment, the polymer mostly used in this type of cells is the $Nafion^{\circledR}$ developed by *DuPont* (*USA*), which is fabricated with chemically stabilized perfluorosulfonic acid copolymer [11].

Basically, the physical structure of a *PEMFC* consists of seven components, according to Fig. 2.1 [12]: feeding channels, diffusion layer, and catalytic layer in the anode; membrane; catalytic layer, diffusion layer, and feeding channels in the cathode. The *PEMFC* combines in a very compact unit the electrodes and the electrolyte. This structure, well-known as *Membrane Electrode Assembly* (*MEA*), is not thicker than few

hundreds of microns. It is the heart of the fuel cell, and fed with hydrogen and oxygen[1], generates electrical power with a power density of around $1\,W\,cm^{-2}$ [14].
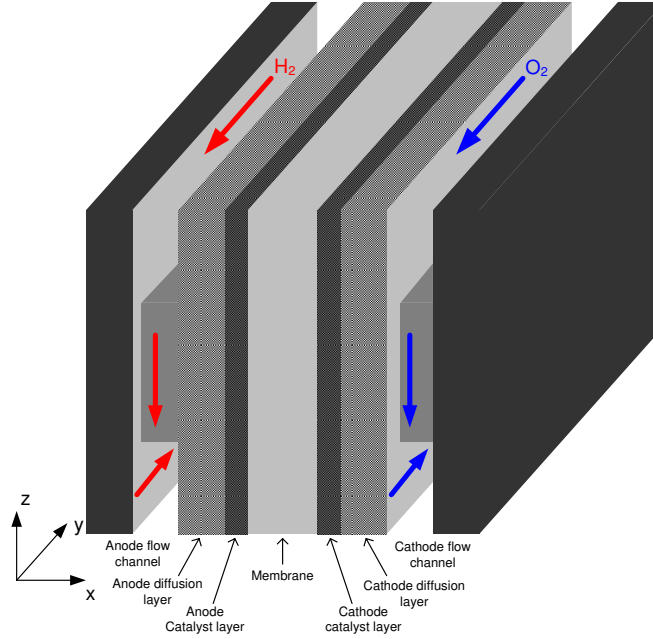
Figure 2.1: 3-dimensional schematic diagram of a fuel cell.

The polymeric solid electrolyte forms a thin electronic insulator and a barrier for gases between both electrodes, allowing a fast proton transport and high current density. The solid electrolyte has the advantage, as opposed to those of liquid type, that allows the *FC* to operate in any spatial position [7].

The electrodes consist of a catalytic layer of great superficial area on a substratum of coal, permeable to gases. Electrocatalyst materials are necessary to obtain a good operation, increasing the speed of the chemical reaction. In this way, the gases can react with a lower energy of activation, allowing that the reaction takes place at a smaller temperature [12]. The electrocatalyst used in *PEMFC* is the platinum, which is one of the major drawback of this technology because of its high cost.

---

[1]Usually, the fuel cell is fed with atmospheric air instead of pure oxygen. The oxygen mole fraction in atmospheric air is 0.21 [13].

2.1.2   Basic principle of operation

The principle of operation of the fuel cell is quite simple and the first development was made by the scientist William Grove in 1839 [5]. The *PEMFC* is an electrochemical device that transforms directly chemical energy into electrical energy [15].

The hydrogen flows through the feeding channels of the anode, spreads through the diffusion layer and reaches the catalytic layer where it is oxidized releasing electrons and protons, according to

$$2\,H_2 \rightarrow 4\,H^+ + 4\,e^-. \tag{2.1}$$

The released electrons are lead through the catalytic metal and the granulated coal of the catalytic layer of the anode, arriving at the cathode via the external circuit, whereas the protons are transported through the membrane to the catalytic layer of the cathode. At the same time, oxygen is injected in the feeding channels of the cathode and spreads through the diffusion layer toward the catalytic layer, where it reacts with protons and electrons, generating water, according to

$$O_2 + 4\,H^+ + 4\,e^- \rightarrow 2\,H_2\,O. \tag{2.2}$$

Therefore, the global reaction in the fuel cell is

$$2\,H_2 + O_2 \rightarrow 2\,H_2\,O. \tag{2.3}$$

The reaction on the cathode is exothermic: the heat release is dependent upon the voltage, which is directly related to its efficiency. The previous explanation is schematically shown in Fig. 2.2.

The water management in the cell is critical for an efficient operation. As mentioned previously, a requirement for this type of cells is to maintain a high water content in the electrolyte to assure high protonic conductivity [15]. The protonic conductivity of the electrolyte is high when the membrane is completely saturated of water, and thus offers minimum resistance to the ion passage, increasing the efficiency of the cell specially at high current densities [16]. The water content in the cathode and the anode is determined by the water balance in the respective volume, being the water balance the result of the inputs and outputs of water: there is normally an input of water in the incoming gas and there is water transport trough the membrane. The water transport
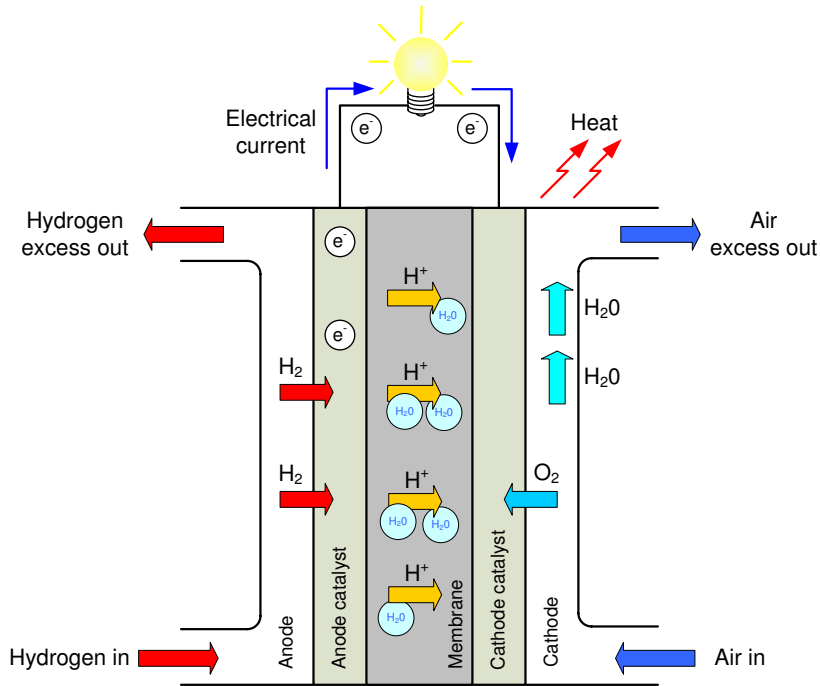
Figure 2.2: Schematic diagram showing the *PEM Fuel Cell* principle of working.

during the operation is a function of the cell current and the characteristics of the membrane and the electrodes. The main mechanism of water transport through the membrane is the drag of water molecules by the protons: each proton drags between 1 and 2,5 water molecules [7]. If more water leaves the cell than it is produced, it is important to humidify the incoming gas in the anode and/or in the cathode. Nevertheless, if there is too much humidification, the diffusion layers are flooded, which cause problems in the gases diffusion.

2.1.3   Advantages and disadvantages of *PEM Fuel Cells*

The main advantage of *PEM Fuel Cells* is their high efficiency compared with other energy conversion devices [17]. This allows that the efficiency of a fuel cell vehicle using direct-hydrogen FC[1] is twice than in a gasoline vehicle [9, 18]. Moreover, unlike the internal combustion engines, the *FC* efficiency is also high with partial loads: in the standard driving cycles, urban and suburban, most of the time the vehicle is demanding

---

[1]Direct-hydrogen *FC* refers to a *FCS* that is directly fed with hydrogen from a pressurized tank opposite to the case where the hydrogen is produced with an on-site reformer.

a small fraction of the nominal *FC* power [19]. Thus, a *FC* vehicle will be working most of the time at high efficiencies. At the same time, using direct-hydrogen *FC*, the local emissions problem in densely urban areas can be eliminated.

Another important advantage of *PEMFC*, in contrast to other types of fuel cells, is the low operation temperature (below 80ºC) [15], allowing to reach the operation point quickly. In addition, the cost of the materials is smaller than for the high temperature fuel cells (except the catalyst, which is based on platinum) and their operation is safer. All these characteristics turn *PEMFC* particularly appropriate for applications in vehicles. Nevertheless, it is necessary to use better, and more economic, catalyst so that the reaction occurs at lower temperatures.

The main disadvantage of fuel cells is their high cost and the high production cost of hydrogen. Hydrogen is preferred because of the fast electrochemical reaction, and its high specific energy[1]. Nevertheless, as it was mentioned, hydrogen is not a primary fuel. Usually, it is produced from hydrocarbon reforming or water electrolysis [5, 7]. The use of electrolysis is advisable specially when some type of renewable energy is used, avoiding fossil fuel use. It is expected that the cost of fuel cells and hydrogen will diminish with the technology progress. Thus, hydrogen has possibilities of becoming an alternative to fossil fuels with the joint use of renewable energies.

2.1.4 Fuel Cell voltage

The standard potential E^0 is a quantitative measurement of the maximum cell potential, i.e., the open circuit voltage. For a hydrogen-oxygen cell, in which there is a transfer of two electrons by each water molecule, $E^0 = 1.229\ V$ if the produced water is in liquid state and $E^0 = 1.18\ V$ if the produced water is in gaseous state [5]. These values correspond to normalized conditions: cell temperature T_{fc} equal to 298.5 K and the partial pressures of oxygen p_{O_2} and hydrogen p_{H_2} equal to 1 atm. In the work of Amphlett *et al.* [21], the following expression of E^0 is given, depending on the temperature and the reactant partial pressures, which is used in several models of fuel cell

---

[1]The Specific Energy of hydrogen at ambient pressure is 8890 $Wh\,kg^{-1}$, meanwhile the corresponding one of petrol is 694 $Wh\,kg^{-1}$. However, the necessary volume for its storage is greater. The energy density of petrol is 500 $Wh\,dm^{-3}$, meanwhile for hydrogen(300 bar) is 55 $Wh\,dm^{-3}$ [20].

e.g., [13, 22]:

$$E^0 = 1.229 - 8.5 \times 10^{-4} \left(T_{fc} - 298.5\right) +$$
$$+ 4.3085 \times 10^{-5} T_{fc} \left[\ln\left(p_{H_2}\right) + \frac{1}{2} \ln\left(p_{O_2}\right)\right]. \tag{2.4}$$

However, in the practice the cell potential is significantly lower than the theoretical potential because there are some losses even when no external load is connected.

Moreover, when a load is connected to the fuel cell, the voltage in the terminals decreases still more due to a number of factors, including polarization losses and interconnection losses between cells. The main voltage losses in a fuel cell are the following [5, 7, 23]:

Activation loss The *activation losses* v_{act} are caused by the slowness of the reaction that takes place in the surface of the electrodes. A proportion of the generated voltage is lost in maintaining the chemical reaction that transfers electrons from the negative electrode toward the positive electrode. This phenomenon is strongly nonlinear and more important at low current densities.

Fuel crossover and internal currents These energy losses results from the waste of fuel passing through the electrolyte and from electron conduction through the electrolyte. In *PEMFC*, the fuel losses and internal current are small and their effects are usually negligible.

Ohmic loss The *ohmic losses* v_{ohm} are caused by the resistance to the transport of electrons through the electrodes and the different interconnections, and also to the passage of ions through the electrolyte. The behavior of v_{ohm} is approximately linear with the current density.

Concentration loss The *concentration losses* v_{conc} are caused by the diffusion of ions through the electrolyte which produces an increase of the concentration gradient, diminishing the speed of transport. The relation between the voltage of the cell and the current density is approximately linear until a limit value, above of which the losses grow quickly.

Therefore, the fuel cell voltage of a simple cell can be expressed as

$$v_{fc} = E^0 - v_{ohm} - v_{act} - v_{conc}. \tag{2.5}$$

A typical polarization curve showing the potential and power density as a function of the current density is shown in Fig. 2.3. This curve is obtained using the fuel cell model developed in [13]. In practice, a succession of cells are connected in series in order to provide the necessary voltage and power output, constituting a *Fuel Cell Stack System.*
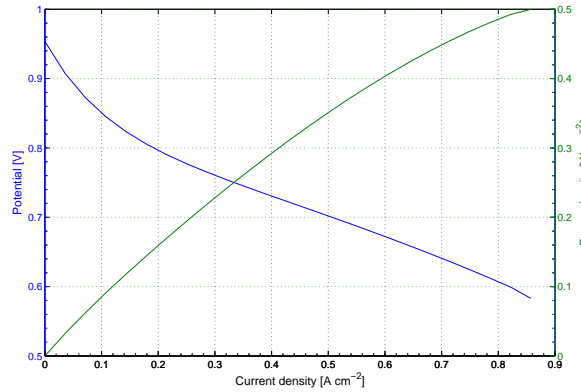
Figure 2.3: Polarization curve showing the cell potential and the power density vs. the cell current density at $p_{H_2} = p_{O_2} = 2.28 \ atm$ and $T_{fc} = 353 \ K$.

2.1.5 Theoretical and real fuel cell efficiency

The efficiency of any energy conversion device is defined as the ratio between the useful energy output and the energy input. In a fuel cell, the useful energy output is the generated electrical energy and the energy input is the energy content in the mass of hydrogen that is supplied. The energy content of an energy carrier is called the *Higher Heating Value* (ΔH_{HHV}). The ΔH_{HHV} of hydrogen is 286.02 $kJ \, mol^{-1}$ or 141.9 $MJ \, kg^{-1}$. This is the amount of heat that may be generated by a complete combustion of 1 mol or 1 kg of hydrogen, respectively. The ΔH_{HHV} of hydrogen is experimentally determined by reacting a stoichiometric mixture of hydrogen and oxygen in a steel container at 25 ^oC. If hydrogen and oxygen are combined, water vapor emerges at high temperatures. Then, the container and its content are cooled down

to the original 25 ^oC and the ΔH_{HHV} is determined by measuring the heat released between identical initial and final temperatures. On the contrary, if the cooling is stopped at 150 ^oC, the reaction heat is only partially recovered (241.98 $kJ\,mol^{-1}$ or 120.1 $MJ\,kg^{-1}$). This is known as the *Lower Heating Value* (ΔH_{LHV}) of hydrogen [24].

Assuming that all the Gibbs free energy of hydrogen[1], ΔG, can be converted into electrical energy, the maximum possible (theoretical) efficiency of a fuel cell is [23]

$$\eta_{HHV} = -\Delta G/-\Delta H_{HHV} = 237.34/286.02 = 83\%. \tag{2.6}$$

However, the ΔH_{LHV} is used very often to express the fuel cell efficiency to compare it with the internal combustion engine, whose efficiency has traditionally been expressed using the fuel lower heating value. In this case, the maximum theoretical fuel cell efficiency results in a higher number:

$$\eta_{LHV} = -\Delta G/-\Delta H_{LHV} = 228.74/241.98 = 94.5\%. \tag{2.7}$$

If both ΔG and HHV in (2.6) are divided by $2\,F$, where 2 is the number of electrons per molecule of H_2 and F is the Faraday number, the fuel cell efficiency may be expressed as a ratio of two potentials:

$$\eta_{HHV} = \frac{-\Delta G}{-\Delta H_{HHV}} = \frac{\frac{-\Delta G}{2\,F}}{\frac{-\Delta H_{HHV}}{2\,F}} = \frac{1.23}{1.482} = 83\%, \tag{2.8}$$

where

$\frac{-\Delta G}{2\,F} = 1.23\,V$ is the theoretical cell potential, and

$\frac{-\Delta H_{HHV}}{2\,F} = 1.482\,V$ is the potential corresponding to the HHV, or thermoneutral potential.

In this section, we analyzed the theoretical fuel cell efficiency. However, as explained in previous sections, in a real fuel cell the efficiency is quite lower and also depends on the fuel cell current. The fuel cell efficiency η_{FC} can also be defined as the ratio between the power produced and the power of hydrogen consumed [23]:

$$\eta_{HHV} = \frac{P_{FC}}{P_{H_2}} = \frac{V_{fc}\,I_{fc}}{\frac{-\Delta H_{HHV}\,I_{fc}}{2\,F}} = \frac{V_{fc}}{1.482}, \tag{2.9}$$

$$\eta_{LHV} = \frac{P_{FC}}{P_{H_2}} = \frac{V_{fc}\,I_{fc}}{\frac{-\Delta H_{LHV}\,I_{fc}}{2\,F}} = \frac{V_{fc}}{1.254}, \tag{2.10}$$

---

[1]The Gibbs free energy is used to represent the available energy to do external work. The changes in Gibbs free energy $\Delta\,G$ are negative, which means that the energy is released from the reaction, and varies with both temperature and pressure [25].

where V_{fc} is the generated voltage and I_{fc} is the fuel cell current. Thus, the FC efficiency is related to the actual voltage, which is related to the fuel cell current through the polarization curve.

Moreover, in a real system it is necessary to incorporate some auxiliary systems which consume a fraction of the generated power. As a result, the efficiency of the fuel cell system, η_{fcs}, is even lower than the expressed in (2.9):

$$\eta_{fcs} = \eta_{HHV} \frac{P_{net}}{P_{fc}} = \eta_{HHV} \frac{P_{fc} - P_{aux}}{P_{fc}} = \eta_{HHV} \left(1 - \frac{P_{aux}}{P_{fc}}\right), \qquad (2.11)$$

where P_{net} is the net power output, P_{fc} is the fuel cell power, and P_{aux} is the power consumed by the auxiliary components, which include, in particular, the air compressor. The efficiency curve of a fuel cell system of 50 kW modelled in $ADVISOR$[1] is shown in Fig. 2.4.
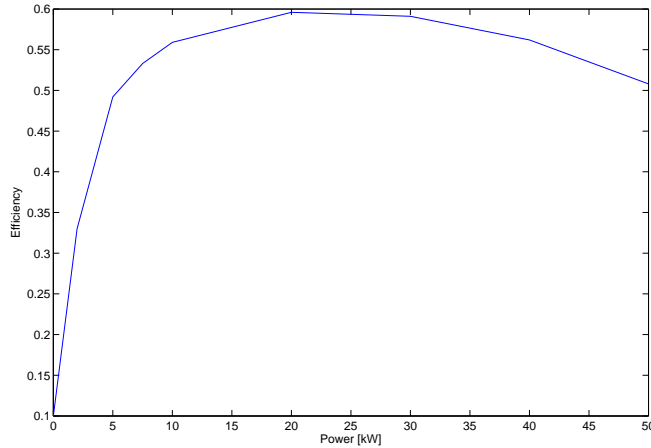
Figure 2.4: Fuel cell efficiency curve from ADVISOR data.

2.1.6 Generic structure of a fuel cell-based power generation system

In order to be able to produce energy, it is necessary to integrate the fuel cell stack with other components to form a fuel cell-based power generation system. A generic

---

[1] *ADVISOR, ADvanced VehIcle SimulatOR*, is a toolbox developed by the National Renewable Energy Laboratory with the aim of analyzing the performance and fuel economy of conventional, electric, and hybrid vehicles [26, 27].

scheme showing the interrelation between the main components of the power generation system is presented in Fig. 2.5. These components can be divided into the following subsystems [25]:

Reactant Flow Subsystem The reactant flow subsystem consists of the hydrogen and the air supply circuits. The objective is to supply the adequate reactant flow to ensure fast transient response and minimal auxiliary power consumption. The hydrogen supply circuit is generally composed of a pressurized tank with pure H_2 connected to the anode through a pressure-reduction valve and a pressure-controlled valve, meanwhile, the air supply circuit is generally composed of an air compressor which feeds the cathode with pressurized air from the atmosphere. The anode output is generally operated in *dead-ended* mode and a purge valve in the anode output is periodically opened to remove the water and accumulated nitrogen gas. In the case the anode output is not closed it is possible to reinject the out-flowing hydrogen into the anode input. On the other hand, the cathode output is normally open through a fixed restriction. The cathode air supply will be studied in Chapter 4 where we propose to close the cathode output with a controlled valve.

Heat and Temperature Subsystem The heat and temperature subsystem includes the fuel cell stack cooling system and the reactant heating system. The thermal management of the fuel cell is critical since the performance depends strongly on the temperature. The stack temperature control can be done using a fan or a water refrigeration subsystem.

Water Management Subsystem The objective of the water management subsystem is to maintain an effective hydration of the polymer membrane and an adequate water balance, because the fuel cell performance is also strongly dependent on membrane hydration. Both, the air and the hydrogen, are usually humidified before entering the fuel cell with humidifiers in both circuits. The water that leaves the cathode can be recovered in a water separator and reinjected in the humidifiers through a pump.

Power Conditioning Subsystem The fuel cell generates an unregulated DC voltage which drops off when the current increases according to the polarization curve.
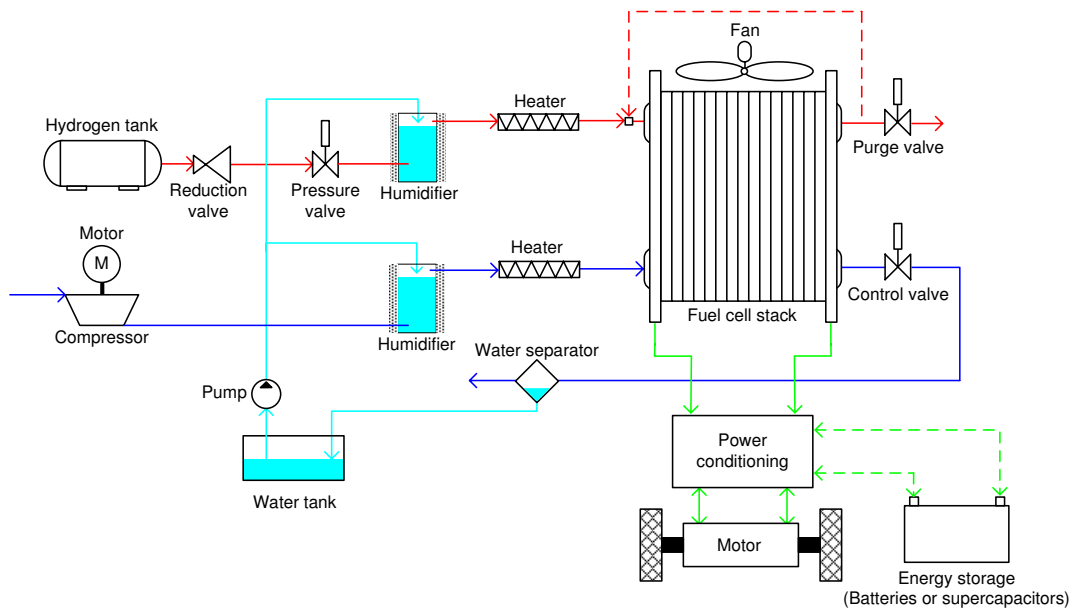
Figure 2.5: General scheme of a *FCS* oriented to automotive applications.

Excluding some applications where this is not a trouble, some power conditioning actions are necessary. Such actions make necessary the use of *DC/DC* regulators and/or inverter regulators.

Power Management Subsystem The power management subsystem controls the power drawn from the fuel cell stack. If no energy storage devices is used, the full load must be supplied by the fuel cell and no power management is necessary. However, if an energy storage system is included, such as batteries or supercapacitors, it is necessary to implement a power management between this two power sources. A review of *Fuel Cell Hybrid Systems* is described in next section and a detailed study is done in Chapter 6.

2.2 Fuel Cell Hybrid Systems

The *Fuel Cell Hybrid Systems* (*FCHS*) are composed of a *Fuel Cell System* (*FCS*), which is the primary power source and an *Energy Storage System* (*ESS*), e.g., a battery or supercapacitor bank that contributes to supply the load power demand.

2.2.1 How hybridization works

Given a load power $P_{load}(t)$, this can be supplied with a fraction of the power from the *FCS*, $P_{fcs}(t)$, being the rest of power supplied by the *ESS*, $P_{ess}(t)$:

$$P_{load}(t) = P_{fcs}(t) + P_{ess}(t) \qquad \forall t. \tag{2.12}$$

A diagram with the energy and power flows between the elements in the hybrid system is shown in Fig. 2.6. The $P_{fcs}(t)$ is produced by the fuel cell stack, which is fed with
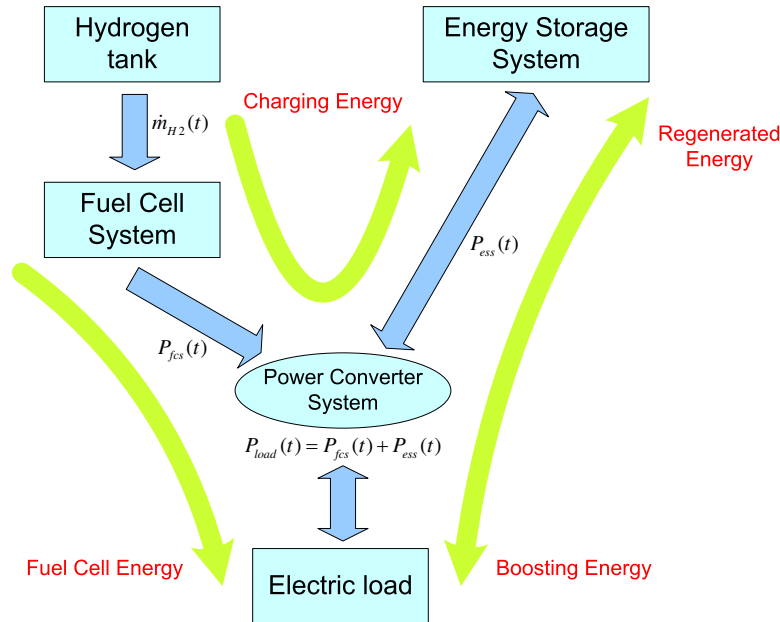
Figure 2.6: Diagram showing the energy and power flows in a Fuel Cell Hybrid System.

a hydrogen flow $\dot{m}_{H_2}(t)$ from a H_2-pressurized tank, whereas, the bidirectional power flow $P_{ess}(t)$ can come from two different sources: the *FCS* or the load, through a regenerative process in automotive applications. The regenerative braking is covered in Chapter 6. In the *FCHS* of Fig. 2.6, four energy flows can be distinguished:

Fuel cell energy flow The *FCS*, which is the primary power source, supplies energy directly to the load.

Charging energy flow It is possibly to charge the *ESS* with energy from the *FCS* to subsequently supply the load.

Regenerated energy flow When the load power is negative, e.g., during regenerative braking in automotive applications, it is possible to regenerate energy and charge the *ESS* with energy from the load.

Boosting energy flow It is possibly to boost the *FCS* supplying energy to the load from the *ESS* with energy previously charged from the *FCS* or regenerated from the load.

How to manage efficiently this energy flows is the function of the *Energy Management Strategies (EMS)*, which are covered in Chapter 7.

2.2.2 Advantages and disadvantages of fuel cell hybrid systems

The potential advantages of fuel cell hybrid systems are the following [18, 28]:

- Improve the hydrogen economy

- Overcome the relatively slow fuel cell system transient response

- Reduce the cost and weight of the global system[1]

- Reduce the warm-up time of the fuel cell system to reach full power

The disadvantages of the hybridization are the following:

- Greater complexity of the vehicle system

- Greater complexity of the control system

The advantages and disadvantages of fuel cell hybrid systems can be better understood analyzing the roles of the *Energy Storage System* in a fuel cell hybrid vehicle, which is the most promising application of hybrid systems. These roles are the following [29]:

---

[1]This is true if the cost per unit power of the storage elements is lower than the corresponding to the fuel cells. Otherwise, it can become a disadvantage. In the same way, the weight per unit power of the storage elements must be lower than the corresponding to the fuel cell.

Supply traction power during fuel cell start-up. Under ambient and cold-start conditions the *FCS* output power is lower than its rated power. Thus, the energy storage system is expected to compensate this drawback until the fuel cell reaches its rate power.

Supply power assistance during drive cycles. The stored energy in the *ESS* can supply the transitory demands of energy, allowing to assist the fuel cell operation in two ways. First, it is possible to reduce the fuel cell power, supplying only a fraction of the full load. Secondly, the energy storage can be used to improve the transient response in a system in which the fuel cell alone is not capable of responding quickly enough to an increase in power. The maximum *power* demands from a vehicle typically take place during maximum accelerations, while the highest *energy* demands take place when driving with slope. The energy storage system can improve significantly the acceleration performance supplying instantaneous power to compensate the relatively slow fuel cell dynamic. However, the contribution to the performance of driving with slope is expected to be minimal since the capability of energy storage is limited.

Recapture regenerative braking energy. The possibility of recovering energy from regenerative braking in automotive applications allows to improve the hydrogen economy recuperating energy that, otherwise, is dissipated at the friction brakes. This amount of energy depends on the driving cycle considered and goes from 5% in a highway cycle to almost 18% in a city cycle.

Supply electrical accessory loads. A fuel cell hybrid vehicle may include several electric loads such as radiator fans, power-assisted steering, electric brake, air conditioning system, etc. These loads vary during the driving cycle but the total net load could be considered as a constant value. It is potentially be expected that the energy storage system could maintain these electrical loads for certain periods during the cycle (e.g., if the fuel cell is shutdown).

Fuel cell startup and shutdown. In fuel cell hybrid vehicles it would be desirable to have start/stop capability. This means that while the vehicle is running, the primary power plant (i.e., the fuel cell) can be shut down and restarted according

to an energy management strategy. This type of operation is beyond the scope of this thesis.

2.2.3 Applications of fuel cell hybrid systems

Stand-Alone Residential application

Fuel cell-based systems are very attractive for stationary energy generation, since they allow the production of electricity and heat in a decentralized, quiet, efficient and environmentally friendly way [30]. However, for stationary applications, a *FC* stack may not be sufficient to satisfy the load demands, especially during peak demand periods or transient events.

The problem of the slow dynamic response is more pronounced when the *FC* stack is fed with hydrogen coming from a reformer instead of a H_2-pressurized tank because of the dynamic response of the reactor. Moreover, in stationary applications the prospective arrangement is composed of a reformer. In addition, it is expected that the load has an aggressive behavior: sudden load switching and load conditions such as active-reactive power and loads with high harmonic distortion [31]. As a result, it may be necessary an auxiliary energy storage system such as a battery or supercapacitor bank to meet all load demands.

A dynamic electrochemical simulation model of a grid independent *PEMFC* power plant is presented in [32]. The model includes the methanol reformer, the *PEM* stack, and the power conditioning unit. In addition to these components, the system is equipped with storage batteries connected in parallel with the DC bus. The model is used to study the transient response of the *PEMFC* power plant when subjected to rapid changes in a residential load connected to it. The results show the fast response capabilities of the *PEMFC* following the changes of the load.

In the same way, in [33] and [31], it is concluded based on experimental results that the parallel combination of a *FCS* and a *SC* bank exhibits good performance for stand-alone residential applications during the steady-state, load-switching, and peak power demand. On the contrary, without the *SC* bank, the *FCS* must supply an extra power, thereby increasing the size and cost of the *FCS*.

2. Review of *PEM* Fuel Cell Systems

In addition, a residential *CHP*[1] system based on *PEMFC* is studied in [30]. The system is a co-generative unit, converting natural gas into electricity and heat, that can works both under grid-connected and stand alone configurations. The system considered in this work is also equipped with a set of batteries enabling load tracking and peak loads. Results show that the prototype can satisfy the energy needs of small residential applications.

Fuel Cell Hybrid Vehicles application

Most of the major automobile manufacturers are developing prototypes of fuel cell vehicles. During the 1990s, several car companies began to work on developing the *PEMFC* for passenger car propulsion motivated by the increasing environmental issue. Hydrogen fuel cell vehicles ($H_2 - FCVs$) are a good alternative to conventional internal combustion engine (ICE) vehicles. Actually, fuel cells and hydrogen are considered as the best overall solution in the long run, although significant technical improvements are necessary [8].

The advantages of $H_2 - FCVs$ are

- The $H_2 - FCVs$ have no local contaminant emissions allowing to reduce the urban pollution: the only emissions created during vehicle operation is water vapor. In addition to this advantage, the use of hydrogen for transportation makes possible to introduce alternative energy sources (e.g., biomass, biofuels, solar power, wind power, wave power, etc.), in order to reduce the dependence on petroleum.

- *FCS*, in contrast to *ICE*, have the characteristic that the efficiency does not degrade at part load and, in fact, can be higher. A typical urban vehicle operates mostly at part load conditions. In [34], it is concluded that the hydrogen economy of $H_2 - FCVs$ can be $2.5 - 3$ times the fuel economy of conventional *ICE* vehicles.

- It is possibly to improve the hydrogen economy by recovering energy through regenerative braking adding an energy storage system: the *fuel cell hybrid vehicles* (*FCHVs*).

---

[1]Combined Heat and Power.

- The specific energy of hydrogen is much larger than batteries, which converts $H_2 - FCVs$ into a more competitive solution than pure battery electric vehicles: 1600 $Wh\,kg^{-1}$ for hydrogen at 70 MPa contrary to 35 $Wh\,kg^{-1}$ for lead-acid batteries, 70 $Wh\,kg^{-1}$ for nickel-metal-hydride batteries, and 120 $Wh\,kg^{-1}$ for Lithium-ion batteries [8].

Therefore, in this thesis we concentrate our attention on the *Fuel Cell Hybrid Vehicles* (*FCHVs*) with some kind of *Energy Storage System*.

Chapter 3

State of the Art in control aspects of PEM Fuel Cell-Based Systems

In this chapter, a state-of-the-art review of fuel cell-based systems is done. The first part of this study is focused on the literature works dealing with the control of fuel cell systems with the anode fed from a high-pressure hydrogen tank and the cathode fed with air from a compressor. The major control problem covered in this review is the air supply control loop. In the second part of the state-of-the-art study, a review of the control problem of *Fuel Cell Hybrid Systems* (*FCHS*) with *Energy Storage System (ESS)* is done, focusing on the literature works dealing with the energy management strategies to perform the determination of the fuel cell operation.

3.1 State of the Art in control and design of Fuel Cell-based Systems

The transient behavior of the electrochemical reaction that takes place in the fuel cell is very fast. Nevertheless, the transient behavior of the stack power is limited by the dynamics of the hydrogen and air flow, the pressure regulation and the water and heat management [16]. When a load is connected to the FC, the control system must maintain the temperature, the membrane hydration and the partial pressure of gases at both sides of the membrane to avoid voltage degradation and, consequently, a reduction in the efficiency. Besides, it is important to control the mentioned variables to assure

the *FC* durability. These critical variables must be controlled for a wide range of power, with a series of actuators such as valves, pumps, compressors, expansors, ventilators, humidifiers and condensers [35].

The control issues covered in this section of the state-of-the-art study are

1. Regulation of the stack power

2. Control of the *oxygen excess ratio*

3. Control of the hydrogen supply

4. Controllability of the system

5. Improvement of the system efficiency

3.1.1 Regulation of the stack power

One of the main control objectives is to control the *FCS* so that the power output meets the power load. Among possible applications of *PEMFC* are electrical vehicles propulsion where the load fluctuates strongly. Indeed, the power required by a car depends heavily on the driving profile. There are different standard driving cycles, representing urban and suburban driving situations, which are widely used in the automotive literature to compare the performance and emissions in different vehicles. One of these cycles is the *New European Driving Cycle (NEDC)*. The standard driving cycles will be seen in detail in Section 6.4.3.

The control system must match the power demand, manipulating appropriately the control variables. Theses variables include: the hydrogen and air inlet flow, the hydrogen and air inlet pressure, the stack temperature, the membrane humidification, the coolant temperature and the coolant flow. There is a degree of uncertainty in the behavior of the *FCS* components due to material degradation and the external temperature and pressure [36]. Thus, the control system must be sufficiently robust.

In the work of Golbert and Lewin [36], *Model-based Predictive Control (MPC)* is used with the objective to demonstrate that the *MPC* can be used to obtain a robust control and to improve the system efficiency reducing the hydrogen consumption. Since that work is focused on applications with vehicles, the objective is to meet a certain

speed more than an output power. In practice, the car driver manipulates the accelerator and brake pedals according to the desired speed. This behavior can be simulated using a *PID* controller together with a simple vehicle model. This model calculates the required power to meet the required speed according to the vehicle characteristics. In the simulations, the *FCS* controller based on *MPC* is implemented as a slave of a master controller based on *PID* control, which provides the power set-point to the *MPC* controller. Then, this controller manipulates the control variables of the *FCS* to achieve the required *FCS* power. The *MPC*-based controller uses a nonlinear reduced order model of the *FCS* model developed in [37]. In this work is concluded that it is possible to satisfy the fluctuating power demands and to optimize the system efficiency, with a significant hydrogen consumption reduction.

3.1.2 Control of oxygen excess ratio

One of the most important problems in *FCS* control is to guarantee the sufficient oxygen supply during abruptly changes in the load demand. This objective is difficult to obtain since oxygen reacts instantaneously to load demands whereas, as was mentioned, the air supply is limited by the gas feeding dynamics and the air compressor dynamics. Several publications approach this problem [35, 38, 39, 40]. When the current demanded increases quickly, the present oxygen level in the cathode diminishes drastically as a result of the electrochemical reaction. The abrupt oxygen diminution can cause damages to the membrane and degradation of the *FCS* efficiency. This phenomenon is known in the literature *PEMFC* as *"Oxygen Starvation"*. This term describes the operation condition of a fuel cell in sub-stoichiometric reactants feedings and is one of the potential causes of fuel cell failure [41]. A parameter that indicates the excess of oxygen in the cathode, namely *Oxygen Excess Ratio (λ_{O2})*, is defined [25, 38, 40]:

$$\lambda_{O2} = \frac{W_{O2,in}}{W_{O2,rct}}, \tag{3.1}$$

where $W_{O2,in}$ is the cathode inlet oxygen mass flow and $W_{O2,rct}$ is the reacting oxygen mass flow in the cathode electrochemical reaction. This flow depends on *FCS* current I_{fcs}:

$$W_{O2,rct} = M_{O2} \frac{n\, I_{fcs}}{4\, F}, \tag{3.2}$$

3. State of the Art in control aspects of PEM Fuel Cell-Based Systems

where M_{O2} is the molar mass of oxygen, n is the stack cell number, and F is the Faraday number ($F = 96485\,C\,mol^{-1}$). Therefore, when the FCS current increases, the value of λ_{O2} diminishes instantaneously. It is necessary to implement a control strategy that allows a fast recovery of the oxygen level. In order to do that the controller must provide more air to the FCS increasing the air compressor voltage.

In the work of Pukrushpan *et al.* [35], the oxygen level regulation is obtained by means of a *PI* controller in the compressor. The oxygen transitory response is improved using linear observability techniques. The observability improves when the FCS voltage is included as a measured variable in the feedback controller. It is demonstrated that there is a severe conflict between the oxygen excess control and the net power temporary response. The limitation in the temporal response comes from the fact that all the auxiliary equipment is power supplied directly by the FCS without any secondary power source. In this publication is mentioned that with the use of an energy storage system (e.g., batteries or supercapacitors) it is possible to overcome this conflict, although this configuration is not developed.

In the work of Grujicic *et al.* [38], the optimization of the transitory behavior in a *PEMFC* is analyzed with strategies of model based control. The controller in this work has the objective to maintain a necessary level of oxygen partial pressure in the cathode during steep changes in the demanded current. The results obtained indicate that the oxygen level in the cathode can satisfactorily be maintained by means of feedforward control, manipulating the air compressor motor voltage. Nevertheless, the FCS power does not respond adequately during the transitory, which also suggests the necessity of a power management by means of a secondary power source (battery or another storage energy system). In [39], a feedback controller is added to the feedforward controller to reduce the stationary state error. Again is concluded that it is necessary to implement a hybrid configuration with storage of energy in order to improve the transitory response.

In the work of Vahidi *et al.* [40], a *Model based Predictive Control (MPC)* is proposed to solve the oxygen supply problem during steep changes in the current. In this article a hybrid system composed of FC and supercapacitors is analyzed. *MPC* is based on minimization of a cost function of the predicted response of a system over a future horizon. Excellent results in the oxygen level control are obtained, although the transitory behavior of the FCS power is not analyzed.

3.1.3   Hydrogen supply control

The hydrogen supply control objective is to feed the *FCS* with hydrogen at the same pressure than air independently of the hydrogen consumed, which is proportional to the current load [16]. It is very important to reduce the differential pressure through the membrane to avoid damaging it. When pressurized hydrogen is used, the hydrogen flow can be regulated by a servo valve. Since the valve is fast, it is assumed that the flow can be controlled with a proportional controller based on the feedback of the differential pressure [42]. Commonly, a purge valve is installed at the anode output to remove the water in excess. The purge valve can also be used to reduce the anode pressure quickly in case of necessity.

It is generally accepted that the hydrogen supply control is not critical when the system is fed with pressurized hydrogen. However, the hydrogen supply control problem is critical when the hydrogen production is made with an on-board fuel processor with a relatively slow transitory response [25]. This is the case when reforming a hydrocarbon fuel, for example natural gas, in a rich hydrogen gas [43]. This drawback can originate a phenomenon known as *"Hydrogen Starvation"* [25, 43].

3.1.4   System controllability

The efficiency improvement in a fuel cell system is very important, but also it is important to maintain the system controllability. The efficiency and the controllability of the system in two operating points for a determined net power is studied in the work of Serra *et al.* [44]: one point corresponding to the minimum current necessary to obtain the required power and the other one with a greater current. A conflict between controllability and efficiency was found. The operating point corresponding to minimum current has greater efficiency whereas the point with higher current has better controllability. Therefore, it is necessary to obtain a convenient balance between efficiency and controllability.

3.1.5   Improvement of the system efficiency

It is meaningful to study the manner of operating a *FCS*, specially at low loads. An adequate operation produces important benefits, increasing the system efficiency in

3. State of the Art in control aspects of PEM Fuel Cell-Based Systems

terms of hydrogen reduction and allowing a greater peak power. In a direct-hydrogen *FCS*, the air supply subsystem has a crucial role in the improvement of the performance of the system [19]. In fact, there are two external variables that have greater impact in the polarization curve: the air pressure and the air stoichiometry (*SRa*).

The air pressure and the air stoichiometry control the oxygen partial pressure in the catalytic layer of the cathode, which determines the cathode polarization and, therefore, the efficiency. In [16], it is also stated the importance of the air pressure control to improve the *FCS* efficiency. The efficiency improvement for a given load is based on a trade-off between the increase of the air pressure and the *SRa*, and the increase of the parasitic compressor power.

In the work of Friedman and Moore [19], it is shown that a *FCS* can be optimized to obtain high peak power and high efficiency over a broad range of output powers. The key to obtain this objective is to vary the pressure and the air flow. Based on this result, it could be concluded that a *FCS* must be operated to the greater possible pressure and *SRa*. Nevertheless, if the energy necessary to compress the air is considered, the result is different: for a fixed air flow, the compressor power consumption increases significantly when the pressure is increased. This means that it is possible to find an optimal combination of pressure and air flow.

A similar conclusion is stated in [38]. In this work, it is assumed that the *FCS* net power P_{net} can be approximately defined as the difference between the power produced by the *FCS*, P_{fcs}, and the consumed compressor power P_{cm}. For each load current, an air flow increment increases the cathode pressure and, therefore, increases the oxygen partial pressure, increasing the *FCS* voltage. This also leads to an increment in the oxygen excess ratio in the cathode, λ_{O2}. The initial increase in the oxygen excess is translated in a *FCS* power increase and a net *FCS* power. Nevertheless, if a limit λ_{O2} is exceeded, an excessive compressor power produces that the net power falls. Thus, for each current there is an optimal value of λ_{O2}, for which the net power has its maximum.

A plot of net power as a function of the oxygen excess ratio at different currents for a 40-*kW FCS* is shown in Fig. 3.1 [38]. The *FCS* is operated in standard conditions: temperature $T_{fcs} = 353K$ and relative humidity in the cathode $\phi_{ca} = 100\%$.
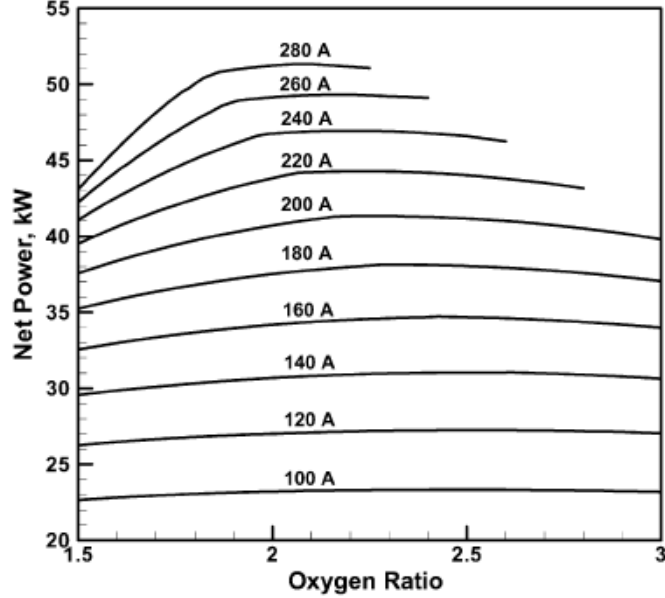
Figure 3.1: Net *FCS* power at different currents and Oxygen Excess Ratio [38].

3.2 State of the Art in Control of Fuel Cell Hybrid Systems

In this section, we present the state of the art of the control of *Fuel Cell Hybrid Systems*, which is separated in three subsections for clarity:

1. Electrical topology

2. Hybridization degree

3. Energy management strategies

3.2.1 Electrical topology

One important issue in *Fuel Cell Hybrid Systems* is to determinate the proper electric topology. Some configurations for fuel cell vehicles and their control strategies are studied in [9, 45]. Some of these configurations include the use of a propulsion battery. On the other hand, in the work of Santi *et al.* [46], a case study of a domestic fuel cell-based uninterruptedly power supply is presented. In that work, different configurations

are also analyzed. Because of the slow dynamics of the fuel cell compared to the electrical system requirement, it is concluded that the use of energy storage elements is necessary. The rate at which the energy from the storage system is required is a significant parameter to choose the correct technology for storage and the use of batteries is decided after an analysis of different options.

An approach for the design of a *Power Conditioning System* (*PCS*) for fuel cell generation systems is studied in [47] with the help of several *PCS* examples. From this study, it is noted that full-bridge, half-bridge and push-pull converters are fundamentally used and various different topologies. Also, the comparison of the voltage source and current source topologies has been done, so that a system designer can select the proper topology according to the applications. From this comparison, it is concluded that it is better to connect the energy storage unit to the *DC*-link in parallel through a bidirectional converter. A similar conclusion is found in [48].

3.2.2 Hybridization degree

In the work of Atwood *et al.* [49], the influence of the hybridization degree on the system efficiency is analyzed, looking for an optimal value. Results for a wide range of combinations between batteries and *FC* sizes are presented, from a purely electrical vehicle to a pure fuel cell vehicle (without storage batteries). The results of hydrogen economy that are shown demonstrate that hybridization can improve the power efficiency. As it is expected, the presence of batteries allows the capture of regenerated energy from braking. The main conclusion of this work is that the optimal degree is not independent of the driving cycle considered. The results also show that the control strategy, the power spectrum of the considered cycle, and the *FCS* and battery efficiency interact in a complex form. It is also concluded that the efficiency at low powers depends on the air compressor power and its minimum speed, combined with the hybridization degree.

In the same way, in the work of Friedman [50], it is also investigated the convenience of using a hybrid configuration of *FCS* and batteries. In this work, comparisons between two hybrid systems are made (which differ in the size of the battery bank). A pure *FCS* system is also considered. Different driving cycles are used to compare the performance. The results are not conclusive about the convenience of the hybrid systems, although

the work clarifies that they depend on the technology used. In fact, with the new technologies in batteries and supercapacitors it is possible to achieve better results.

An economic comparison between vehicles with different hybridization degrees is done in [18], considering the initial cost of the vehicle, the fuel cell, the batteries and the hydrogen. The initial cost of a fuel cell vehicle is reduced by means of hybridization when the price of the fuel cell is high. In addition, the operation cost is affected mainly by the hydrogen cost. Since one of the advantages of hybridization is the hydrogen reduction, it is possible to reduced the operative cost of the vehicle. In this work, a hybrid vehicle model was simulated using the *Federal Urban Driving Schedule* (*FUDS*) for different *HD*, including the case of null hybridization (no batteries). The results show that the best hydrogen economy was obtained for a *HD* of 33%, meanwhile for a *HD* of 73% the economy is worse than in the case of pure *FC* vehicle. Concerning to the initial vehicle cost, the results also show that if the fuel cell price is less than $400\,US\$/kW$ the hybridization has no benefits.

It is also concluded in [51] that an auxiliary power source can be used in *FCV* to alleviate the performance limitation, specially when the *FC* is fed with an on-board fuel reformer. It is shown that for a given vehicle, motor and *FCS* configuration, there is an optimal choice for the energy capacity for different battery technology. However, in this work the effect of different driving cycles is not taken into account.

The results of an energy analysis for a load-following fuel cell vehicle (without any energy storage device) versus a battery-hybrid fuel cell vehicle are presented in [52]. The major conclusion from this study is that only for cycles with a large amount of regenerative braking at low to mid power levels (e.g., the *FUDS* cycle) there are significant advantages in terms of overall hydrogen economy. The fact that the hydrogen economy occurs only in certain driving cycles can be attributed to the hybrid configuration and, fundamentally, the energy recovery from regenerative braking. However, the energy management strategy employed to perform the power split between the energy storage system and the fuel cell is quite elementary. As a result, it is expected to achieve better results implementing a more elaborated strategy exploiting the capabilities of the recovered energy from regenerative braking and operating the *FCS* in a more advantageous way. Besides, and probably more important, as this study was

done with batteries in the energy storage system the use of supercapacitors increase the benefits of the hybrid system as it will be shown.

3.2.3 Energy management strategies

The coordination between several power sources in a *Fuel Cell Hybrid System* requires a high level control: the *Energy Management Strategy*. Different approaches are found in literature. In the work of Thounthong *et al.* [53], the strategy implemented is based on *DC* link voltage regulation by controlling the power converters. The *FCS* is operated in almost steady state conditions in order to minimize the mechanical stresses of the *FCS* and to ensure a good synchronization between hydrogen flow and *FCS* load current. Supercapacitors are only functioning during transient energy delivery or transient energy recovery. This strategy addresses the link voltage regulation but not the system efficiency.

In the work of Paganelli *et al.* [54], a general formulation about the instantaneous power split between the fuel cell and the *Energy Storage System (ESS)* in a *FCHV* is presented. The proposed method is based on a control strategy called *Equivalent Consumption Minimization Strategy (ECMS)*. This formulation is based on fitting the instantaneous distribution of power between the *FC* and the *ESS* to diminish the global hydrogen consumption using an appropriate analytical formulation suited for real time control. For that, a first step consists in converting the electrical powers that take part in the system in equivalent hydrogen consumptions. Unlike the previous works, the *ECMS* strategy demonstrates to be robust under a wide range of operating conditions. Nevertheless, the efficiency is sensible to several crucial parameters: average consumption, the function penalty employed and the limit values of the load range. They conclude that greater investigation is necessary to surpass these problems.

In the same line, in the work of Rodatz *et al.* [28, 55], it is implemented a real time control to distribute the power between the *FC* and the *ESS*, with the objective of diminishing the hydrogen consumption maintaining, at the same time, the controllability of the system, using the same concept of equivalent hydrogen consumption. Experimental results are shown in [55] with a *FC-supercapacitors* hybrid vehicle (experimental Volkswagen HyPower vehicle).

An algorithm is implemented in [28], which resolves an optimization problem at each sampling time and the cost function is constructed from variables considered at the present time. This cost function takes into account the use of the hydrogen energy, since the major objective is to reduce the hydrogen consumption, but also considers the amount of recovered energy. The conclusion of the work is that the efficiency is not significantly improved with the use of this control strategy. This might be due to the small margin for optimization with respect to the case study of the work of Rodatz *et al.* [55], which is utilized to make the comparisons. Nevertheless, this technique has the advantage that it does not need more adjustment than the horizon time. In addition, *ECMS* control involves a hydrogen consumption model as a function of the net output power. This feature makes *ECMS* inherently self-adaptive to achieve full efficiency with any system configuration and operating condition such as temperature.

In the work of Kotz *et al.* [56], a pilot system on small scale that represents a hybrid vehicle with *FC* and supercapacitors is analyzed. The *FC-SC* hybrid system is tested with the *New European Driving Cycle, (NEDC)*[1], demonstrating that supercapacitors are excellent energy storage devices that can be used efficiently in vehicle applications for energy recovering from braking and peak power reinforcing. The recovered energy in different driving cycles for two different car sizes are presented: in an urban driving cycle it is possible to recover until a 25% of the traction energy and the general efficiency of the recovering process is near 70%. The main conclusion of this work is that supercapacitors have a great potential for applications with short duration peak powers, such as in hybrid electrical vehicles. In addition, it is concluded that an elaborated energy management strategy is necessary as is presented in [28].

In the work of Caux *et al.* [57, 58], the energy management between a *FCS* and supercapacitors is studied in a tramway application. An algorithm that determines two power references (one for the *FCS* and another one for the supercapacitors) is presented with the main objective to fulfill the power demand. Other objectives are the following: *1)* recover the maximum of braking energy, *2)* supply the power consumed by the auxiliary systems with the *FCS*, *3)* the *FCS* must operate preferably at rated power $(400\,kW)$, *4)* employ the storage elements as little as possible, *5)* restrict the *FCS* power variation, and *6)* perform the starting and stoping with the storage elements

---

[1]The characteristic load profiles are covered in Section 6.4.3.

totally charged. The algorithm computes all possible references and, with the losses and the efficiency estimation of all components, an effective solution is found for a given profile. The conclusion is that a different number of supercapacitors is required depending on the profile in study.

For the development of a correct energy management strategy, it is necessary both a good *FCS* model and an estimation of the energy losses produced in the storage elements and the converters. The losses in the supercapacitors by Joule effect ($P_{loss} = r_{sc} \cdot I_{sc}^2$) and the losses produced by conduction and commutation in each converter are calculated in [58]. These losses are function of the commutation frequency (f_c), and the current and voltage on the converter ($P_{loss} = f(f_c, I_{DC}, V_{DC})$).

In the work of Jung *et al.* [59], a control strategy with two objectives is proposed: one objective is to obtain high efficiency in the hybrid system and the other is to maintain a minimum state of charge in the batteries. If both objectives cannot be fulfilled simultaneously, the priority is given to the battery state of charge. The system efficiency can be improved controlling the power split between the fuel cell and the battery. The value of reference for the battery state of charge can be determined considering the optimal efficiency of charge and discharge. The operation is divided into five different modes of operation: *1) charge* mode, *2) discharge* mode, *3) fuel cell* mode, *4) regenerative* mode and *5) electrical vehicle* mode (only batteries). The operation mode is determined according to the battery state of charge and the power required. The effectiveness of the control strategy proposed was evaluated by experimental results, although the obtained effectiveness is not quantified.

In the work of Kim *et al.* [60], a combined *power management/design optimization problem* approach for the performance optimization of *FCHVs* is formulated. Their results indicates that optimality consists in downsizing the fuel cell compressor, decreasing the hybridization degree without compromising regenerative braking and employing adequate control strategies.

Schiffer *et al.* [61] also shows the benefits of using a *fuel cell-supercapacitor* system for *FCHVs*. Their results show that it is a good strategy to use the supercapacitors with their maximum power during acceleration and deceleration phases and to control the voltage of the supercapacitors during standstill and constant speed phases to reach an optimum voltage that depends on the vehicle speed. The fuel cell is used as

little as possible during acceleration and deceleration phases while used to charge the supercapacitors during standstill and constant speed phases if necessary.

3. State of the Art in control aspects of PEM Fuel Cell-Based Systems

Chapter 4

The control of *PEM* Fuel Cell Systems

The behavior of the generated power in a fuel cell system depends on the hydrogen and air flows, the regulation of the pressure, and the management of water and heat [16]. When a load is connected to the fuel cell, the control system must control the temperature, the membrane hydration and the partial pressure of gases at both sides of the membrane to avoid voltage degradation and, therefore, a reduction in the efficiency [42]. Besides, it is important to control efficiently the mentioned variables to assure the durability of the cells. These critical variables must be controlled for a wide range of power, with a series of actuators such as valves, pumps, compressors, expanders, fans, humidifiers and condensers [35]. Figure 4.1 shows a scheme of a generic fuel cell system.

The control of the fuel cell system without any energy storage is approached in this chapter with the following structure. Firstly, the model that is employed to simulate the fuel cell system response is presented. Secondly, the control objectives are stated. Thirdly, a controller is designed.

4.1 Overview of the model employed for control purposes

Validated mathematical models provide a powerful tool for the development and improvement of fuel cell-based systems. Mathematical models can be used to describe the fundamental phenomena that take place in the system to predict the behavior under

4. The control of *PEM* Fuel Cell Systems
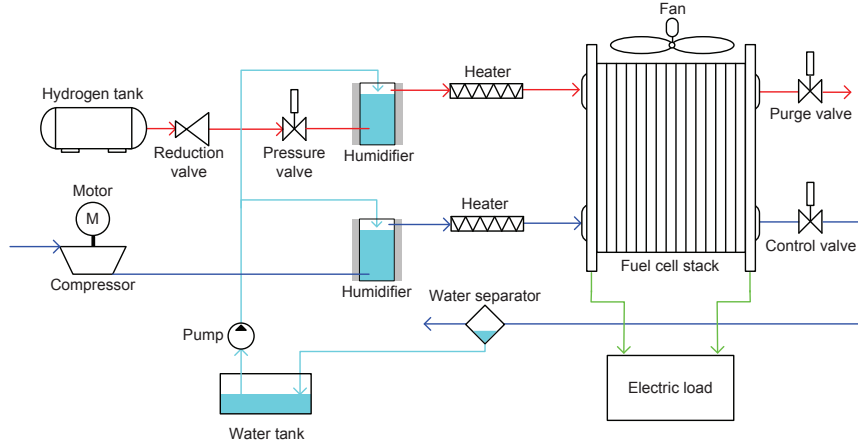
Figure 4.1: Scheme of a generic fuel cell system

different operating conditions and to design and optimize the control of the system.

The models of fuel cell systems describe quantitatively the physical and electrochemical phenomena that take place into the cells. They can be divided in two groups: empirical models and mechanistic models. Most of the empirical models are focused in the prediction of the polarization curve, which is used to characterize the electrical operation of the *FC*, by means of empirical equations. One example is the model developed by Amphlett *et al.* [62], which incorporates as much empirical properties as mechanistic to obtain the *FC* voltage as a function of the current, the *FC* temperature and the hydrogen and oxygen partial pressures for a 35-cell 5 *kW PEM* fuel cell. On the other hand, the mechanistic model considers the fundamental phenomena in detail such as, heat and mass transport, forces, and electrochemical processes. In the work of Yao *et al.* [12], an extensive review of models for hydrogen polymeric fuel cells and direct methanol polymeric fuel cells is made. The first *FC* mechanistic models were one-dimensional models, e.g., [63]. Only variation of magnitudes in the direction across the *FC* are considered. More recently, several models of two and three dimensions have been developed, e.g., the model developed by Nguyen *et al.* [64], which is a three-dimensional model of a *PEM* fuel cell with serpentine gas channels.

Nevertheless, in spite of having many models that study the cells in stationary state there are few dynamic models. In the work of Pukrushpan *et al.* [13] a dynamic model for *PEMFCS* that is suitable for the control study has been developed. The model

captures the transitory behavior of the air compressor, the gasses filling dynamics (in the cathode and in the anode), and the effect of the membrane humidity. These variables affect the cell voltage and, therefore, the efficiency and the output power. The polarization curve in this model is a function of the hydrogen and oxygen partial pressures, the stack temperature and the membrane water content. This allows to evaluate the effect of variations of oxygen concentration and membrane humidity in the output voltage, which are necessary to make the control during transitory operation.

The model developed by Pukrushpan *et al.* [13], which has been employed in [38, 40, 43] for control purposes, is utilized in this work as a base to represent the behavior of a generic fuel cell system. The principal equations of this model are described in Appendix A. In our work, this base model has been modified to adapt it to the proposed control structure described in Section 4.2. In the original model there is only one control variable: the compressor motor voltage. In this thesis it is proposed to add an extra variable, the throttle opening area in the cathode output, A_t, adding a control valve in the cathode output. The advantages of this new configuration are covered in detailed in Section 4.2.3.

The model in [13] contains four main subsystems that interact with each other: *i)* the FC voltage subsystem, *ii)* the membrane hydration subsystem, *iii)* the cathode flow subsystem, and *iv)* the anode flow subsystem. The spatial variation of parameters is not considered and, thus, they are treated as lumped parameters. On the other hand, the time constants of the electrochemical reactions are in the order of magnitude of 10^{-19} s despite another work [65] argues that this constants are significatively lower (10^{-9} s). In any case, all the literature agrees in the fastness of the electrochemical reactions, what is remarked in [66] and [67]. Thus, for control purpose, these time constants can be assumed negligible compared to other constants much slower: temperature (10^2 s) and dynamics of volume filling (10^{-1} s).

Usually, in model-based control, it is necessary to find simplified models, derived from the complete ones or from experimental data, to be used as inner models into the controller. In this work the step response is utilized to obtain a simplified model that is used as internal model to predict the future process response in the control strategy implemented in Section 4.2.5. The main advantage of this simplified model is that is

easily obtainable through experimental data with good agreement with respect to the original nonlinear system in the considered operating point.

4.2 Design of controllers for Fuel Cell Systems

PEMFC systems are efficient devices which allow the transformation of the chemical energy stored in hydrogen into electric energy. In order to obtain this transformation efficiently, all the subsystems must work properly. The air supply is one of these subsystems, which has a great influence in the system efficiency. In fact, one of the most important challenges in fuel cell control is to assure sufficient amount of oxygen in the cathode when current is abruptly drawn from the fuel cell stack. In this study, the air supply subsystem is composed by an air compressor, which supplies air to the cathode. On the other hand, the hydrogen supply subsystem relies on a hydrogen-pressurized tank and the hydrogen inlet flow rate is regulated by an independent control loop to maintain the working pressure in the anode close to the pressure in the cathode.

4.2.1 Control objectives

The main objectives of fuel cell systems control found in literature were exposed in Section 3.1 and, as mentioned, the control of the air supply is the more critical with regard to the efficiency improvement since the compressor consumption is the major parasitic power. The efficiency of the *FCS* was defined in (2.11).

At a given fuel cell current I_{fcs}, if the compressor motor voltage is increased, the compressor flow rate augments the cathode pressure and, in turn, this also leads to a higher level the oxygen excess ratio λ_{O_2} in the cathode. However, an increment of λ_{O2} above a certain limit generally requires an excessive increase in the compressor motor power consumption which causes a reduction in the net power since $P_{net} = P_{fcs} - P_{cp}$. Thus, it is concluded that at each level of the fuel cell current there is an optimal value of λ_{O2} at which the net power is maximum [38]. This result is reproduced in Fig. 3.1. Thus, the control of λ_{O2} is an indirect way to improve the system efficiency.

On the other hand, since the efficiency is a function of the fuel cell voltage V_{fc}, any voltage reduction is translated in an efficiency degradation. Thus, it is necessary to regulate the fuel cell voltage. Therefore, the control objectives proposed are:

1. to regulate the oxygen excess ratio in the cathode, λ_{O2}

2. to regulate the generated voltage in the fuel cell system, V_{fcs}

4.2.2 Control variables

The only variable used to control the air supply in the cathode, from the literature review, is the compressor motor voltage [13, 37, 38, 40]. The cathode outlet flow $W_{rm,out}$ is a function of the upstream pressure and the downstream pressure at the cathode nozzle. The downstream pressure is assumed to be fixed at p_{atm}. If the pressure difference is small, the flow rate can be approximated by the linearized expression

$$W_{rm,out} = k\left(p_{rm} - p_{atm}\right). \tag{4.1}$$

On the contrary, a more complex expression is necessary to calculate the outlet mass flow as a function of the return manifold pressure p_{rm} as it is shown in (4.2) and (4.3) [13]:

$$W_{rm,out} = \frac{C_{D,rm}\,A_t\,p_{rm}}{\sqrt{\bar{R}\,T_{rm}}}\left(\frac{p_{atm}}{p_{rm}}\right)^{\frac{1}{\gamma}}\left\{\frac{2\gamma}{\gamma-1}\left[1-\left(\frac{p_{atm}}{p_{rm}}\right)^{\frac{\gamma-1}{\gamma}}\right]\right\}^{\frac{1}{2}}$$
$$\text{for}\quad \frac{p_{atm}}{p_{rm}} > \left(\frac{2}{\gamma+1}\right)^{\frac{\gamma}{\gamma-1}} \tag{4.2}$$

and

$$W_{rm,out} = \frac{C_{D,rm}\,A_t\,p_{rm}}{\sqrt{\bar{R}\,T_{rm}}}\,\gamma^{\frac{1}{2}}\left(\frac{2}{\gamma+1}\right)^{\frac{\gamma+1}{2(\gamma-1)}} \qquad \text{for}\quad \frac{p_{atm}}{p_{rm}} \le \left(\frac{2}{\gamma+1}\right)^{\frac{\gamma}{\gamma-1}}, \tag{4.3}$$

where $C_{D,rm}$ is the return manifold throttle discharge coefficient ($C_{D,rm} = 0.0124$ in the used model), $\bar{R} = 8.3145\ J\ mol^{-1}\ K^{-1}$ is the universal gas constant, and $\gamma = 1.4$ is is the ratio of the specific heat of air.

As mentioned, the compressor power consumption is the greater parasitic power and has a major effect in the system efficiency. Therefore, it is important to find efficient procedures to control the cathode air flow. We propose in this thesis work to consider the throttle opening area A_t as a variable area. This is achieved adding a proportional valve at the cathode output. Thus, this new variable is a new control variable that regulates the outlet air flow in conjunction with the compressor motor voltage. Note that this control variable by itself is not capable to regulate the air
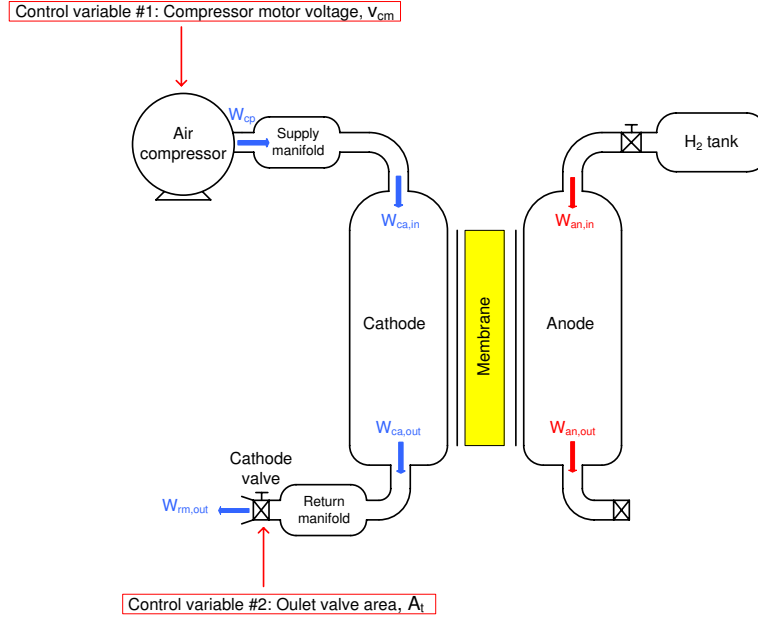
Figure 4.2: *PEMFC* reactant flow scheme with the variables proposed for control purposes.

flow since the compressor is always necessary to get pressure in the supply manifold and the cathode. The advantages of this configuration are analyzed in Section 4.2.3. Therefore, the manipulated variables are $u_1 = V_{cm}$ (compressor motor voltage) and $u_2 = A_t$ (outlet valve area). A schematic diagram of the system is shown in Fig. 4.2.

4.2.3 Performance analysis using an extra control variable

In this section, the performance improvement achieved through the use of the extra control variable described before is analyzed. The analysis is done in two parts. Firstly, a stationary analysis is done with the aim of showing the advantages in steady state using this new control variable. Secondly, a transient analysis is done in order to show the dynamic improvement.

Stationary analysis

As mentioned before, the air supply subsystem has a strong influence in the fuel cell performance. On the one hand, an insufficient air supply may cause oxygen starvation in the cathode, which causes voltage reduction and membrane life shortening. On the

other hand, the compressor operation implies a power consumption that diminishes the system efficiency (see (2.11)).

The operation of the fuel cell system at high pressures increases the generated voltage as a result of the increase in the cathode oxygen partial pressure and anode hydrogen partial pressure (see (2.4)). Especially, an increase in the cathode pressure produces an increase in the supply manifold pressure and thus, an increase in the pressure ratio across the compressor and in the compressor power consumption contributing to a reduction in the system efficiency. The power consumed by the air compressor is

$$ P_{cp} = \frac{C_p \, T_{atm}}{\eta_{cp}} \left[\left(\frac{p_{sm}}{p_{atm}} ^{\frac{\gamma - 1}{\gamma}} \right) - 1 \right] W_{cp}, \tag{4.4} $$

where W_{cp} is the compressor air flow rate, P_{cp} is the compressor power, T_{atm} is the inlet air temperature in the compressor, η_{cp} is the compressor efficiency, p_{sm} is the supply manifold pressure, $C_p = 1004 \, J \, kg^{-1} \, K^{-1}$ is the specific heat capacity of air, and $\gamma = 1.4$ is the ratio of the specific heat of air. The compressor motor voltage as a control input allows to regulate the oxygen partial pressure in the cathode. Augmenting the compressor voltage, the oxygen partial pressure increases. However, the compressor power consumption also increases.

A diminution of the area of the valve that closes the cathode air flow with a fixed V_{cm} contributes to increase the cathode pressure and, at the same time, contributes to modify the input air flow, the stoichiometry, and the oxygen concentration. The power consumption of the compressor has two opposite trends when the valve is partially closed: the trend to increase due to the pressure rise and the trend to decrease due to the flow reduction. When all these effects are taken into account, there is a positive balance in the total efficiency diminishing the valve area as we can observe analyzing the curves of polarization (see Fig. 4.3), efficiency (see Fig. 4.4), power compressor consumption (see Fig. 4.5) and oxygen partial pressure (see Fig. 4.6) plotted for two different valve areas and a certain compressor voltage ($V_{cm} = 140V$).

It is important to note that the increase in the efficiency is not for all current densities. When the current density is high, the flow and concentration reduction have a greater influence than the pressure increase and the result is a decrease in the oxygen partial pressure. In effect, the oxygen consumption is higher at higher current densities:

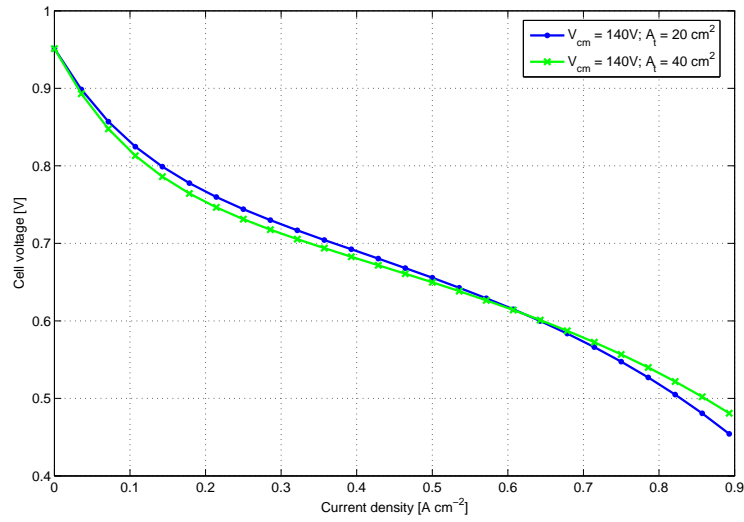$$ W_{O2, \, rct} = \frac{M_{O2} \, n \, A}{4 \, F} \, i, \tag{4.5} $$

Figure 4.3: Polarization curves for $V_{cm} = 140\,V$ and different valve areas.
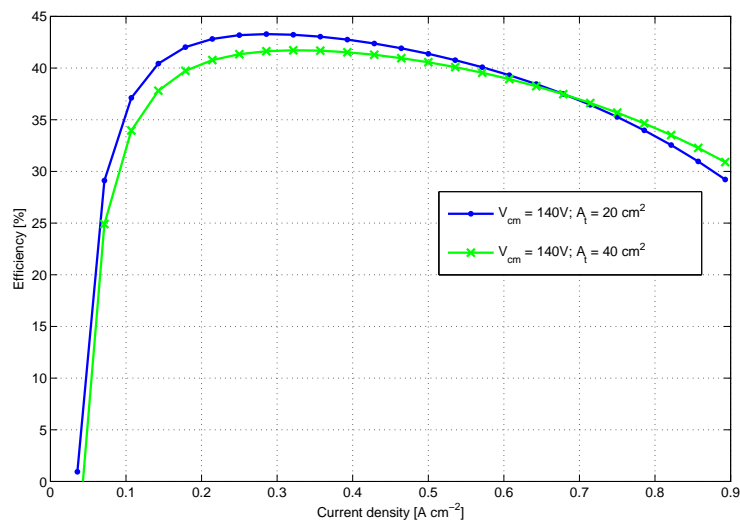
Figure 4.4: Efficiency curves for $V_{cm} = 140\,V$ and different valve areas.
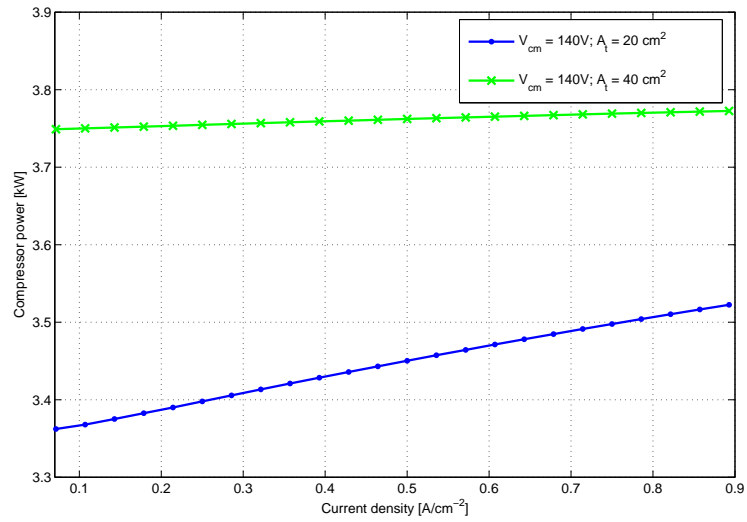
Figure 4.5: Compressor power consumption curves for $V_{cm} = 140\,V$ and different valve areas.
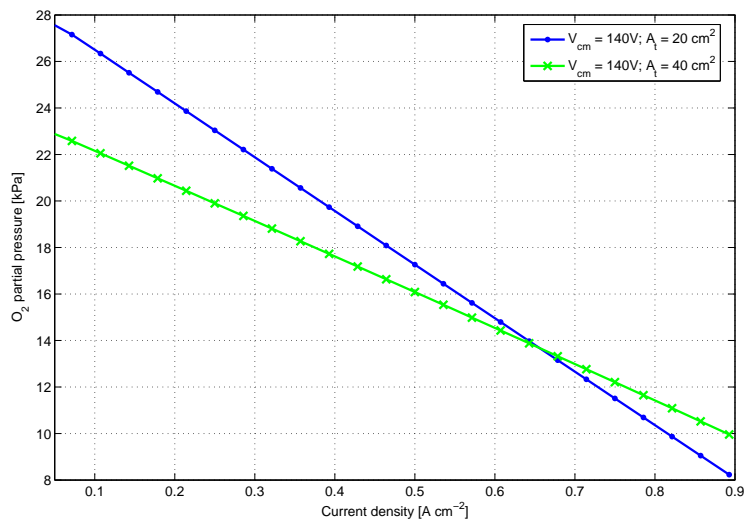
Figure 4.6: Oxygen partial pressure curves for $V_{cm} = 140\,V$ and different valve areas.
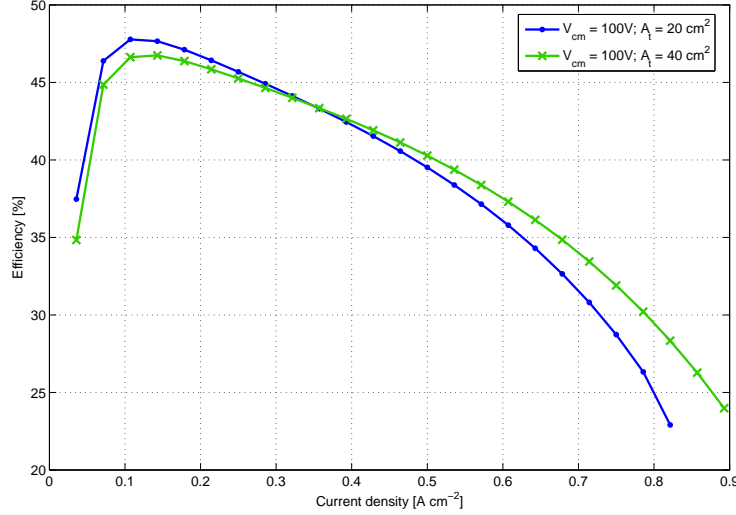
Figure 4.7: Efficiency curves for $V_{cm} = 100\,V$ and different valve areas.

where $W_{O2,rct}$ is the rate of oxygen reacted, $M_{O2} = 32 \times 10^{-3} kg\,mol^{-1}$ is the molar mass of oxygen, n is the number of cells, A is the active cell area equal to $381\,cm^2$, $F = 96485\,C\,mol^{-1}$ is Faraday number, and i is the current density. Depending on the operating pressure, the increment in efficiency happens along different current density ranges. With low operating pressures (lower compressor voltage V_{cm}) the system efficiency increment due to the valve closure occurs only at low current densities, whereas with higher operating pressures (higher compressor voltage) the increment in system efficiency occurs along greater current densities ranges. This can be seen in Fig. 4.7 to Fig. 4.9. For $V_{cm} = 100\,V$ the efficiency increment occurs only for current densities below $0.34\,A\,cm^{-2}$ (see Fig. 4.7), for $V_{cm} = 140\,V$ the increment occurs for current densities below $0.67\,A\,cm^{-2}$ (see Fig. 4.4), while for $V_{cm} = 180\,V$ the increment occurs for all the current densities analyzed (see Fig. 4.8).

As can be seen in Fig. 4.9 for $V_{cm} = 180\,V$, the oxygen partial pressure rise, as a result of diminishing the valve area, occurs at all current densities.

In Fig. 4.10, it can be seen how the efficiency changes with A_t for values between 20 to $40\,cm^2$. As a conclusion of this stationary analysis, it can be stated that the cathode output valve area as well as the compressor motor voltage have to be adjusted in order to have high efficiency.
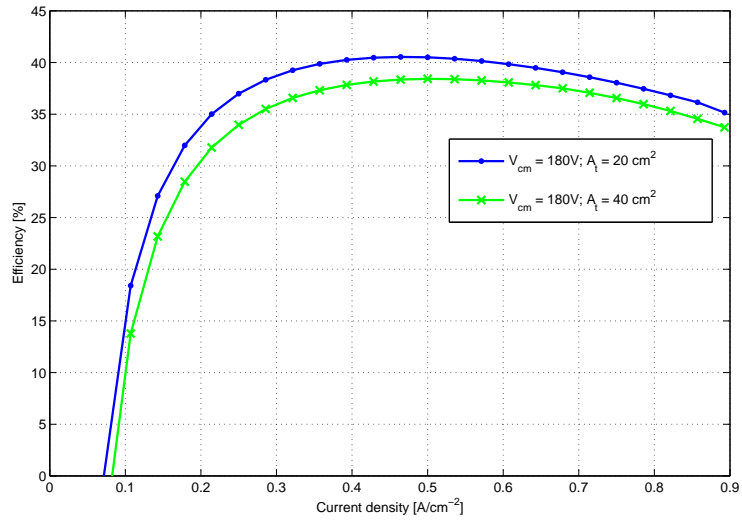
Figure 4.8: Efficiency curves for $V_{cm} = 180\,V$ and different valve areas.
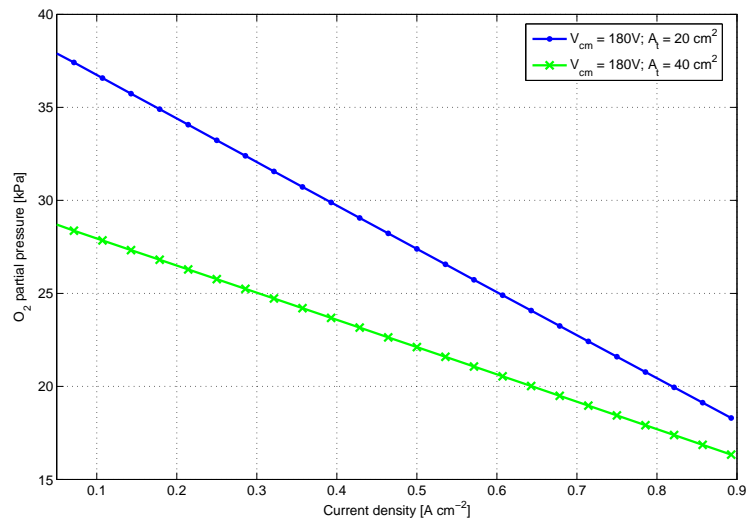
Figure 4.9: Oxygen partial curves for $V_{cm} = 180\,V$ and different valve areas.
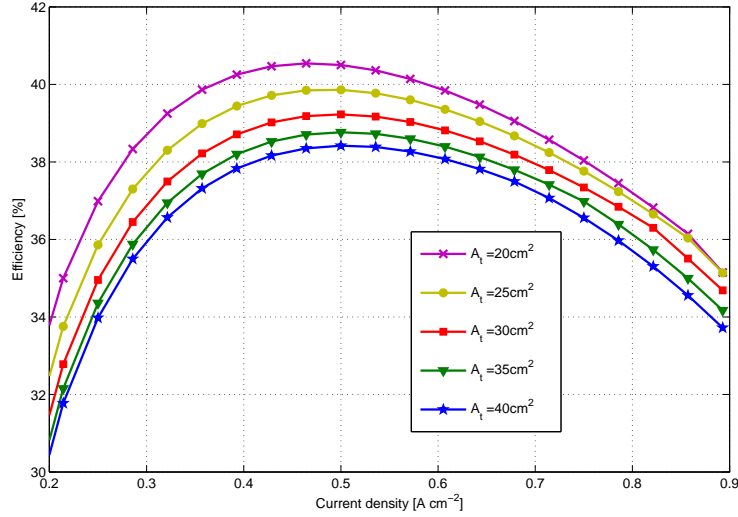
Figure 4.10: Efficiency curves for $V_{cm} = 180\,V$ and different valve areas.

Transient analysis

Besides the possible performance improvement observed in the stationary analysis, there is also an improvement in the transient behavior using the cathode air flow valve as a manipulated variable. A preliminary transient analysis is made employing a *DMC strategy* (the details of this control strategy are explained in Section 4.2.5). The controlled variable in this analysis is the stack voltage. A stack current disturbance from $200\,A$ to $210\,A$ is applied to the fuel cell system in order to compare the disturbance rejection capability of the system. A comparison between the transient responses obtained using only the compressor voltage as a control variable and the one obtained by using the opening valve area in combination with the compressor voltage is showed in Fig. 4.11. The later shows a better behavior with a reduction in the stack voltage time response from $0.6\,s$ to $0.4\,s$.

4.2.4 Control strategy

The advantages of using the outlet valve area together with the compressor voltage are exploited implementing a control strategy. However, there is an interaction between the manipulated variables and the controlled variables, which makes difficult the realization
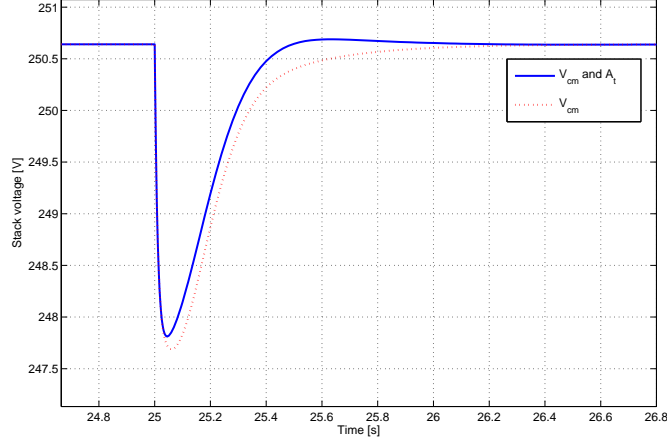
Figure 4.11: Comparative between stack voltage responses.

of a decentralized control of the system [44]. An analysis of interaction and sensitivity is done using the *Relative Gain Array* (*RGA*). The *RGA* is the ratio of the *open loop* and *closed loop* gains, and can be computed as

$$RGA = G \times (G^{-1})^T, \tag{4.6}$$

where $\times$ denotes element-by-element multiplication and G is the gain matrix of the system. Each element of the gain matrix, g_{ij}, is the response for steady-state in output y_i when input u_j is altered but with input u_i kept constant:

$$G = \begin{bmatrix} \left. \frac{\Delta V_{fcs}}{\Delta V_{cm}} \right|_{A_t^0} & \left. \frac{\Delta \lambda_{O_2}}{\Delta V_{cm}} \right|_{A_t^0} \\ \left. \frac{\Delta V_{fcs}}{\Delta A_t} \right|_{V_{cm}^0} & \left. \frac{\Delta \lambda_{O_2}}{\Delta A_t} \right|_{V_{cm}^0} \end{bmatrix}. \tag{4.7}$$

In this analysis, the nominal values are: $I_{fcs}^0 = 190\,A$, $V_{cm}^0 = 187.5\,V$, and $A_t^0 = 20\,cm^2$. The step in the inputs are: $\Delta A_t/A_t^0 = 0.1$ and $\Delta V_{cm}/V_{cm}^0 = 0.1$. The step response is shown in Fig 4.12. Thus, the *RGA* is

$$RGA = \begin{bmatrix} 0.94 & 0.06 \\ 0.06 & 0.94 \end{bmatrix}. \tag{4.8}$$

Analizing the resulting *RGA* matrix, seems convinient to pair V_{cm} with V_{fcs} and A_t with λ_{O_2}. However, we propose the use of a centralized multivariable controller based on *Dynamic Matrix Predictive Control* (*DMC*), which avoids pairing variables,
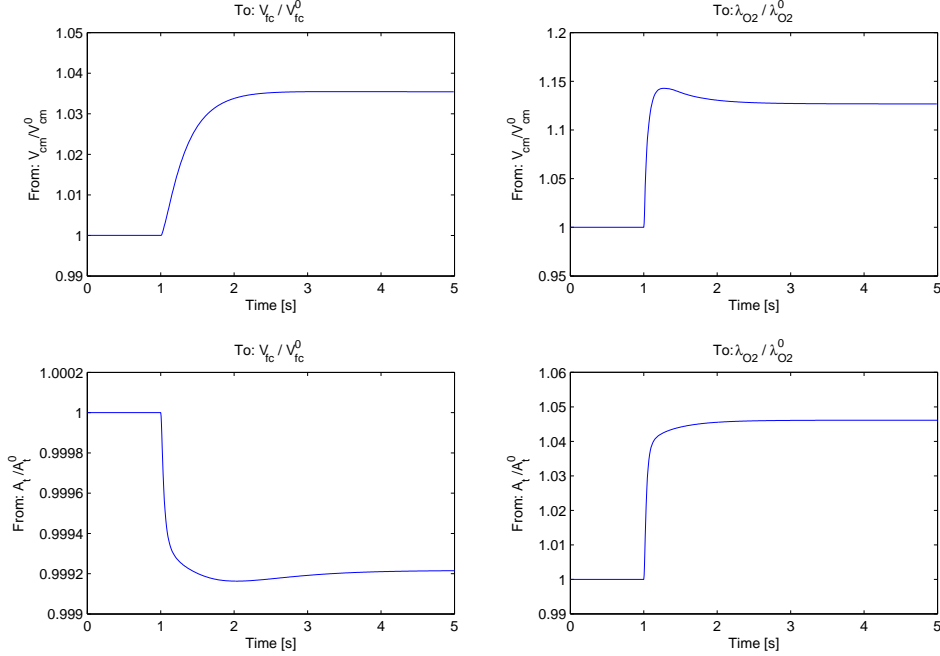
Figure 4.12: Step response.

to resolve efficiently the interaction and sensitivity problem between the manipulated variables and the controlled variables.

The two control objectives and the two control variables are explained in Section 4.2.1 and Section 4.2.2, respectively. The control scheme is shown in Fig. 4.13 where the load current I_{fcs} is considered as a disturbance to the fuel cell system.

4.2.5 Dynamic Matrix Control strategy

The *Dynamic Matrix Control* (*DMC*) [68] is a particular type of predictive control strategy that uses the step response to determine the so-called *Dynamic Matrix G*. This matrix is interpreted as a model of the process that takes into account only the h_p first samples until the response tends to a constant value, assuming therefore that the process is asymptotically stable. Thus, the predicted output can be expressed as

$$y = G\,u + f, \tag{4.9}$$
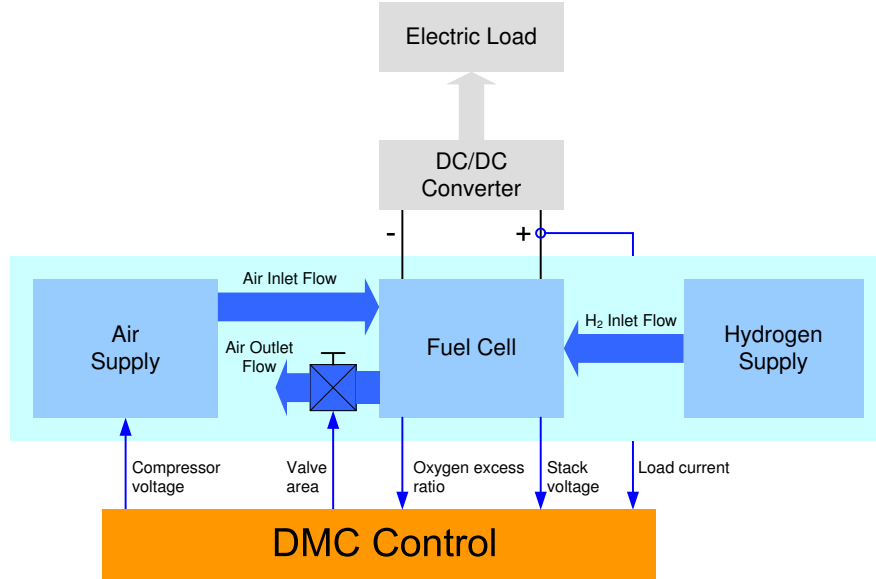
Figure 4.13: *PEM* fuel cell system control scheme.

where y is the time-vector of predicted outputs, $y = \begin{bmatrix} y_1 & \vdots & y_2 \end{bmatrix}^T$, with y_i representing the time-vector of the *i-th* output

$$y_i = [y_i(k+1|k), \cdots, y_i(k+h_p|k)]^T, \tag{4.10}$$

where $y_i(k+1|k)$ denotes the prediction of y_i at time $k+1$ done in time k. The control vector $u = \begin{bmatrix} u_1 & \vdots & u_2 \end{bmatrix}^T$ is the sequence of future control actions where each vector u_j represents the h_m-dimensional vector of control corresponding to the *j-th* control variable

$$u_j = [u_j(k), u_j(k+1), \cdots, u_j(k+h_m-1)]^T, \tag{4.11}$$

and $f = \begin{bmatrix} f_1 & f_2 \end{bmatrix}^T$ is the free response vector, that means, the response that does not depend on future control movements, where

$$f_i = [f_i(k+1|k), \cdots, f_i(k+h_p|k)]^T. \tag{4.12}$$

A graphical description of a general *predictive control strategy* can be seen in Fig. 4.14.

The dynamic matrix G is constructed from the coefficients obtained from the step response with prediction horizon h_p and control horizon h_m:

$$G = \begin{bmatrix} G_{11} & \vdots & G_{12} \\ \hline G_{21} & \vdots & G_{22} \end{bmatrix}, \tag{4.13}$$
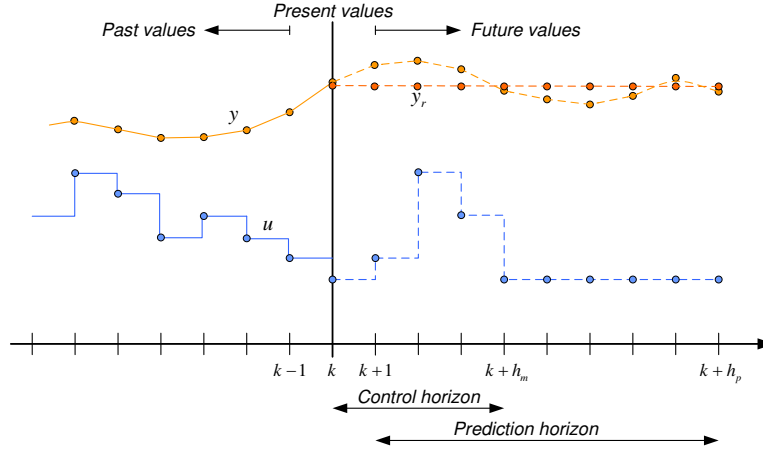
Figure 4.14: Predictive control strategy

and each matrix G_{ij} of dimension $h_p \times h_m$ contains the coefficients of the step response of the *i-th* output corresponding to the *j-th* input:

$$
G_{ij} = \begin{bmatrix}
g_1 & 0 & \cdots & 0 \\
g_2 & g_1 & \cdots & 0 \\
\vdots & \vdots & \ddots & \vdots \\
g_{h_m} & g_{h_m-1} & \cdots & g_1 \\
\vdots & \vdots & \ddots & \vdots \\
g_{h_p} & g_{h_p-1} & \cdots & g_{h_p-h_m+1}
\end{bmatrix}.
\tag{4.14}
$$

The objective of the *DMC* controller is to minimize the difference between the references y_{r_1} and y_{r_2}, and the predictions of the process outputs y_1 and y_2 over a horizon h_p in a least square sense with the possibility of including a penalty term on the control signal large movements:

$$
\min_u J(k).
\tag{4.15}
$$

The cost function $J(k)$ is defined as

$$
J(k) = \sum_{j=1}^{h_p} \left[y\left(k+j|k\right) - y_r \right]^T R \left[y\left(k+j|k\right) - y_r \right] +
$$

$$
+ \sum_{j=0}^{h_m} \left[\Delta u\left(k+j|k\right) \right]^T Q \left[\Delta u\left(k+j|k\right) \right],
\tag{4.16}
$$

where $\Delta u(k+j|k) \triangleq u(k+j|k) - u(k-1+j|k)$, $R = \text{diag}[r_1, r_2]$ is a matrix to compensate the different ranges of values of the process outputs, and $Q = \text{diag}[q_1, q_2]$ is a

matrix that allows to penalize the control effort. If there are no restrictions in the manipulated variables, the minimization of the cost function $J(k)$ can be realized making its derivative equal to zero, resulting

$$\Delta u = \left(G^T R_{2h_p \times 2h_p} G + Q_{2h_m \times 2h_m} \right)^{-1} G^T R_{2h_p \times 2h_p} \mathbf{e}, \qquad (4.17)$$

where $R_{2h_p \times 2h_p}$ and $Q_{2h_m \times 2h_m}$ are expanded matrices from R and Q, respectively:

$$R_{2h_p \times 2h_p} = \mathrm{diag}[\underbrace{r_1, \cdots, r_1}_{h_p}, \underbrace{r_2, \cdots, r_2}_{h_p}], \qquad (4.18)$$

$$Q_{2h_m \times 2h_m} = \mathrm{diag}[\underbrace{q_1, \cdots, q_1}_{h_m}, \underbrace{q_2, \cdots, q_2}_{h_m}], \qquad (4.19)$$

and $\mathbf{e}$ is the vector of future errors along the prediction horizon:

$$\mathbf{e} = [y_{r_1} - y_{p_1}(k), \ y_{r_1} - y_1(k+1|k), \cdots, \ y_{r_1} - y_1(k+h_p-1|k),$$
$$y_{r_2} - y_{p_2}(k), \ y_{r_2} - y_2(k+1|k), \cdots, \ y_{r_2} - y_2(k+h_p-1|k)]^T, \quad (4.20)$$

where y_{p_i} is the *i-th* plant output measured at present instant k. The measurement of the plant outputs provides a compensation mechanism to rectify the inevitable model errors and deal with non-measured disturbances, and thus, assures zero error at steady-state.

In all the predictive control strategies, only the first element of each calculated control sequence u_j is applied to the plant and, in the next iteration, the sequence of control is calculated again using actualized information from the plant. The theoretical bases of the method are given in [68].

4.2.6   Simulation results

The internal model utilized by the *DMC* controller has been obtained through the linearization of the nonlinear model described in Section 4.1 around the operating point corresponding to $u_1 = V_{cm} = 187.5\,V$, $u_2 = A_t = 20\,cm^2$, $w = I_{st} = 190\,A$, which gives a net power of $40\,kW$. The reference values for the outputs are $y_{r_1} = \lambda_{O_2} = 2.36$ and $y_{r_2} = V_{fc} = 250.6\ V$

The control horizon h_m, the prediction control h_p, and the matrices R and Q were adjusted to achieve an adequate dynamic behavior of the fuel cell system. The values of

R and Q have a strong influence on the transient response obtained. This is especially true for the weight matrix Q, which reduces the control effort. The higher are the values in Q, the lower is the control effort, but the response time is greater. Thus, the values chosen for the elements of the weight matrices are: $q_1 = 1$, $q_2 = 0.5$, $r_1 = 5$, $r_2 = 1$. The values of h_p and h_m are 100 and 15, respectively.

The simulation results of the controlled system with variations in the load current (Fig. 4.15(a)) are presented in Fig. 4.15(b) to Fig. 4.15(e). Figure 4.15(b) and Fig. 4.15(c) show the controlled variables (λ_{O2} and V_{fc}), while Fig. 4.15(d) and Fig. 4.15(e) show the manipulated variables (V_{cm} and A_t).

As can be observed in the figures, the implemented controller has a good disturbance rejection: a 17.5% of variation in the stack current at $t = 20\,s$ is demanded, $I_{fc} + \Delta I_{fc} = 170A + 30\,A$, the stack voltage response has a peak $\Delta V_{fc}/V_{fc} = -3.5\%$, which disappears in less than $0.5\,s$. At the same time, the oxygen excess ratio response presents a peak $\Delta\lambda_{O2}/\lambda_{O2} = -27.9\%$ that vanishes in $0.62\,s$. On the contrary, if only V_{cm} is controlled, λ_{O2} has error in steady-state and the transitory response is inadequate, especially when the step in the stack current is negative (e.g., in $t = 10\,s$), as can be seen in Fig. 4.16.

4.2.7 Addition of a disturbance model

The controller performance can be improved if the stack current is measured and a step disturbance model, which reflects the response of the plant output to a disturbance in the stack current ($w = I_{fc}$), is included in the control model used to predict the plant behavior. Thus, the expression of the predicted output in (4.9) becomes

$$y = Gu + Dw + f, \tag{4.21}$$

where the matrix D is

$$D = \left[\frac{D_1}{D_2} \right] \tag{4.22}$$

and each matrix D_i of dimension $h_p \times h_m$ contains the coefficients of the step response of the *i-th* output corresponding to the disturbance w with the same structure than G_{ij} in (4.14).
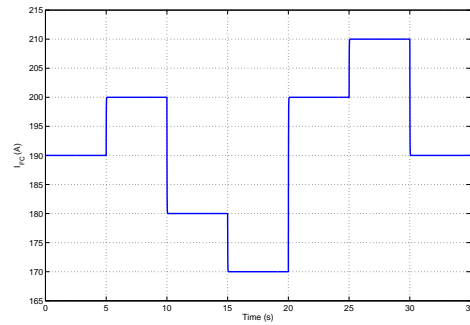
(a) Fuel cell stack current
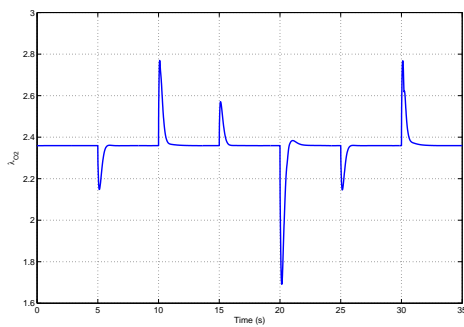
(b) Oxygen excess ratio
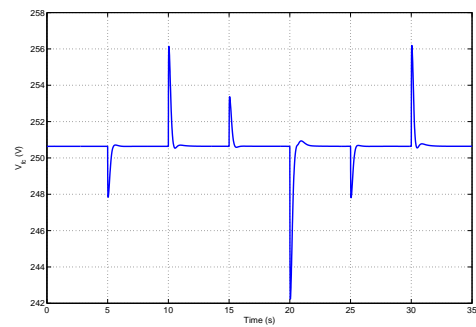
(c) Fuel cell stack voltage
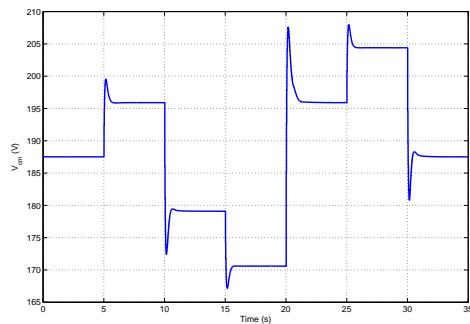
(d) Compressor motor voltage
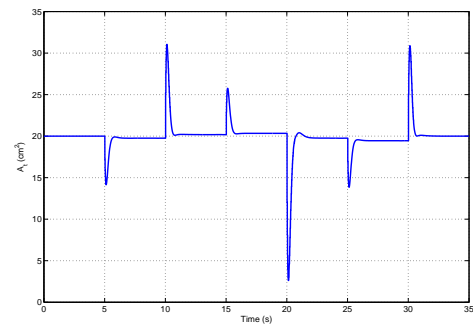
(e) Cathode output valve area

Figure 4.15: Simulation results with *DMC*: disturbance profile (fuel cell stack current), controlled variables (oxygen excess ratio and fuel cell stack voltage), and manipulated variables (compressor motor voltage and cathode output valve area).
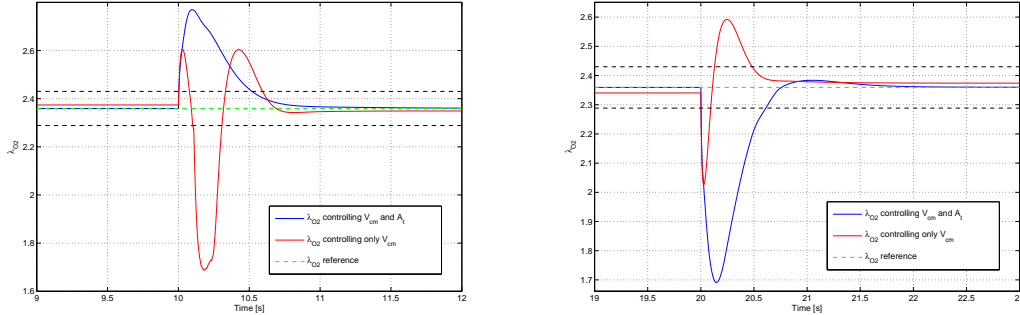
(a) λ_{O_2} response when the step current is negative (b) λ_{O_2} response when the step current is positive

Figure 4.16: Comparative between the λ_{O_2} response controlling V_{cm} and A_t respect to the case where only V_{cm} is controlled.

Comparisons between measured and non-measured disturbance approaches have been made. Details of the voltage stack and the oxygen excess ratio responses are shown in Fig. 4.17(a) and Fig. 4.17(b), respectively. The results obtained show a slight improvement in the generated voltage response. The oxygen excess ratio response can be changed by adjusting the values of the weight matrices. The simulation analysis shows a good performance in a wide operating range around the linearization point despite the internal controller model is linear.

4.3 Conclusions

High efficiency level, long durability, and good transient behavior are fundamental issues for the success of fuel cell systems in energy and automotive market. Through a steady-state analysis it is showed that the system efficiency, in most of the current density range, can be improved by manipulating the cathode outlet air flow valve. The dynamic analysis performed also shows a transient response improvement with this additional manipulated variable.

Taking advantage of the results of the two previously mentioned analysis, a control strategy based on predictive control (*Dynamic Matrix Control*) is proposed, using the compressor motor voltage together and the cathode air flow valve area as manipulated variables. The controlled variables are the stack voltage and the oxygen excess ratio.
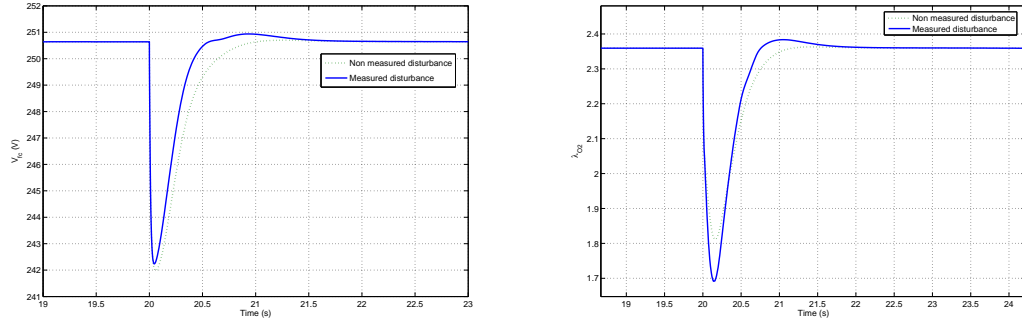
(a) Comparative between stack voltage response

(b) Comparative between oxygen excess ratio response

Figure 4.17: Comparative of the output response with measured and non-measured disturbance

To predict the future process response, the control strategy makes use of a process model that is easily obtainable through step response.

The simulation results show an appropriate dynamic response, which can still be improved with the inclusion of the disturbance model. Moreover, the control objectives have been accomplished with reduced control effort. This effort can be further reduced modifying the values of the matrix Q. This is particularly important because of practical limitations in the manipulated variables.

Chapter 5

Diagnosis and Fault-Tolerant Control of *PEM* Fuel Cells Systems

The energy generation systems based on fuel cells are complex since they involve thermal, fluidic and electrochemical phenomena. Moreover, they need a set of auxiliary elements such as valves, compressor, sensors, regulators, etc. to make the fuel cell work at the pre-established optimal operating point. For these reasons, they are vulnerable to faults that can cause the stop or the permanent damage of the fuel cell. Therefore, it is useful to use systematic techniques, like the recent methods of *Fault-Tolerant Control* (*FTC*), to guarantee the safe operation of the fuel cell systems [69, 70].

The results of this chapter are the product of the collaboration with the Sistemes Avançats de Control (SAC) group of the Universitat Politècnica de Catalunya in Diagnosis and Fault-Tolerant Control of *PEM* Fuel Cell Systems. This results are basically collected in [71] and [72]. The Fault Diagnosis of *PEM* Fuel Cell Systems using a model-based methodology is addressed in Section 5.1, whereas the Fault-Tolerant control based on Model Predictive Control is addressed in Section 5.2. This chapter is complementary to Chapter 4, showing that the proposed control architecture with two actuators adds fault-tolerant control capabilities to the fuel cell systems.

5.1 Model-based Fault Diagnosis in *PEM* Fuel Cell Systems

The first task to achieve active tolerant control consists of the inclusion of a fault diagnosis system operating in real-time. The diagnosis system should not only allow the fault detection and isolation but also the fault magnitude estimation. In this section, a model based fault diagnosis is proposed as a way to diagnose faults in fuel cell systems. The model-based fault diagnosis is based on the on-line comparison between the real behavior of the monitored system by means of sensors and a dynamic model of the system. In case that a significant discrepancy (residual) is detected between the model and the measurements obtained by the sensors, the existence of a fault is assumed.

If a set of measurements is available, it is possible to generate a set of residuals (indicators) that present a different sensitivity to the set of possible faults. Then, analyzing in real-time the evolution of the residuals, it is possible, in some cases, to isolate the fault, and even in some cases, it is also possible to determine its magnitude. The innovation of the fault diagnosis methodology proposed is based on the use of a residual fault sensitivity analysis that allows to isolate faults that otherwise would not be separable.

5.1.1 Foundations of the proposed Fault Diagnosis Methodology

The methodology of fault diagnosis that is proposed and applied to a fuel cell system is mainly based on the classic theory of model-based diagnosis described for example in [73, 74, 75, 76]. Model based diagnosis can be divided in two subtasks: fault detection and fault isolation. The principle of model-based fault detection is to check the consistency of the observed behavior while fault isolation tries to isolate the component that is in fault.

The consistency check is based on computing residuals $r(k)$. The residuals are obtained from measured input signals $u(k)$ and outputs $y(k)$ and the analytical relationships obtained by system modelling:

$$r(k) = \Psi(y(k), u(k)), \tag{5.1}$$

where Ψ is the residuals generator function that depends on the type of detection strategy used (parity equation [73] or observer [77]). At each time step, k, the residual is compared with a threshold value, which is zero in ideal case or almost zero in real case. The threshold value is typically determined using statistical methods that take into account the effect of noise and model uncertainty [69]. When a residual is bigger than the threshold, it is determined that there is a fault in the system; otherwise, it is considered that the system is working properly. In practice, because of input and output noise, and modelling errors, robust residuals generators must be used. The robustness of a fault detection system means that it is only sensitive to faults, even in the presence of model-reality differences and noise [77].

Robustness can be achieved at residual generation phase (active) or at evaluation phase (passive). Most of the passive robust residual evaluation methods are based on an adaptive threshold changing in time according to the plant input signal and taking into account model uncertainty even in the time domain [78]. In this work, a passive method in time domain has been proposed for robust fault detection, where the detection threshold has been obtained using statistical techniques. Robust residual evaluation allows obtaining a set of *fault signatures* $\Phi(k) = [\phi_1(k),\ \phi_2(k), \ldots,\ \phi_{n_\Phi}(k)]$, where each indicator of fault is obtained as follows:

$$\phi_i(k) = \left\{ \begin{array}{ll} 0 & \text{if } |r_i(k)| \leq \tau_i \\ 1 & \text{if } |r_i(k)| > \tau_i \end{array} \right. , \tag{5.2}$$

and τ_i is the threshold associated to the residual $r_i(k)$.

Fault isolation consists in identifying the faults affecting the system and it is carried out on the basis of fault signatures Φ that is generated by the detection module and their relation with all the considered faults $f(k) = \{f_1(k),\ f_2(k), \ldots, f_{n_f}(k)\}$. The method most often applied is a relation defined on the Cartesian product of the sets of faults $FSM \subset \phi \times f$, where FSM is the *theoretical signatures matrix* [73]. One element of that matrix FSM_{ij} will be equal to one if the residual $r_i(k)$ is affected by the fault $f_j(k)$ and in this case the value of the fault indicator $\phi_i(k)$ must be equal to one when the fault appears in the monitored system. Otherwise, the element FSM_{ij} will be zero.

The isolation approach previously presented use a set of binary detection tests to compose the observed fault signature. When applying this methodology to dynamic

systems, the use of binary codification of the residual produces a loss of information, since they may exhibit symptoms with different dynamics [79]. This can be the origin of false isolation decisions, especially because some detection tests have a transient behavior in response to the faults, for example in dynamic slow/delayed systems. Also, in complex systems, some faults could present the same theoretical binary fault signature not allowing fault isolation. In both cases, it is possible to use other additional information associated with the relationship between the residuals and faults, as the sign, sensitivity, order or time activation, to improve the isolation results [79].

What is proposed in our case is the use of information provided by the fault residual sensitivity in the design of the diagnosis system in order to increase fault isolability. According to [73], the sensitivity of the residual to a fault is given by

$$S_f = \frac{\partial r}{\partial f},\tag{5.3}$$

which is a transfer function that describes the effect on the residual r of a given fault f. Sensitivity provides a quantitative information of the effect of the fault on the residual and a qualitative information in their sense of variation (sign). The use of this information at the stage of diagnosis will allow to separate faults that even presenting the same theoretical binary fault signature, present, qualitatively or quantitatively, different sensitivities.

In order to perform diagnosis, the algorithm uses the theoretical signatures matrix *FSMsensit* with the residual sensitivity in the rows, the faults in columns, and each value of this matrix is noticed as $S_{r_i f_j}$. Although sensitivity depends on time in case of a dynamic system, here the steady-state value after a fault occurrence is considered as it is also suggested in [73]. The theoretical value of $S_{r_i f_j}$ describes how easily a fault will cause a violation of the threshold of the *i-th* residual and can be computed analytically using (5.1) and (5.3) or by simulation.

In order to perform real time diagnosis, the observed sensitivity $S_{r_i f_j}^{obs}$ should be computed using the value of the residuals at instant k, $r_i(k)$, and the magnitude of the fault at the same instant, $f(k)$:

$$S_{r_i f_j}^{obs} = r_i(k)/f(k).\tag{5.4}$$

Table 5.1: Observed fault signature matrix using relative sensitivity with respect to r_1.

	f_1	f_2	$\cdots$	f_n
r_2/r_1	$S^{rel,obs}_{r_2r_1f_1}$	$S^{rel,obs}_{r_2r_1f_2}$	$\cdots$	$S^{rel,obs}_{r_2r_1f_n}$
r_3/r_1	$S^{rel,obs}_{r_3r_1f_1}$	$S^{rel,obs}_{r_3r_1f_2}$	$\cdots$	$S^{rel,obs}_{r_3r_1f_n}$
$\vdots$	$\vdots$	$\vdots$	$\ddots$	$\vdots$
r_m/r_1	$S^{rel,obs}_{r_mr_1f_1}$	$S^{rel,obs}_{r_mr_1f_2}$	$\cdots$	$S^{rel,obs}_{r_mr_1f_n}$

5.1.2 The proposed Fault Diagnosis Methodology

From (5.4), it can be seen that using *FSMsensit* in real time requires the knowledge of the fault magnitude or making an estimation of it. In order to overcome this drawback, the diagnosis is designed using the new concept of relative sensitivity rather than the absolute sensitivity given in (5.3). The observed *relative fault sensitivity* is defined as

$$S^{rel,\,obs}_{r_ir_1f_j} = \frac{S_{r_if_j}}{S_{r_1f_j}} = \frac{r_i(k)/f_j(k)}{r_1(k)/f_j(k)} = \frac{r_i(k)}{r_1(k)}, \tag{5.5}$$

which corresponds to the ratio of the *ith* residue at instant k, $r_i(k)$, with another one, for example $r_1(k)$. Then, the relative sensitivity will be non dependent on to the magnitude of that unknown fault. In the case of a set of n fault, a relative fault sensitivity matrix *FSMsensit-rel* as the one shown in Table 5.1 should be used.

The diagnostic algorithm is used to obtain real-time observed relative sensitivities using (5.5), as a ratio of residuals, which provides a vector of relative sensitivities. The generated vector is compared with the vectors of theoretical faults stored into the relative sensitivity matrix *FSMsensit-rel*. The theoretical fault signature vector with a minimum distance with respect to the fault observed vector is postulated as the possible fault:

$$min\left\{d_{f_1}(k), \ldots, d_{f_n}(k)\right\}, \tag{5.6}$$

where the distance is calculated using the Euclidean distance between vectors

$$d_{f_i}(k) = \sqrt{\left(S^{rel,\,obs}_{r_2r_1f_i} - S^{rel,\,teo}_{r_2r_1f_i}\right)^2 + \ldots + \left(S^{rel,\,obs}_{r_mr_1f_i} - S^{rel,\,teo}_{r_mr_1f_i}\right)^2}. \tag{5.7}$$

5.1.3 Application to a *PEM* Fuel Cell System

To show the validity of the proposed model based fault diagnosis approach when applied to a *PEM* fuel cell system (*PEMFC*), the model developed by Pukrushpan *et al.* [42]
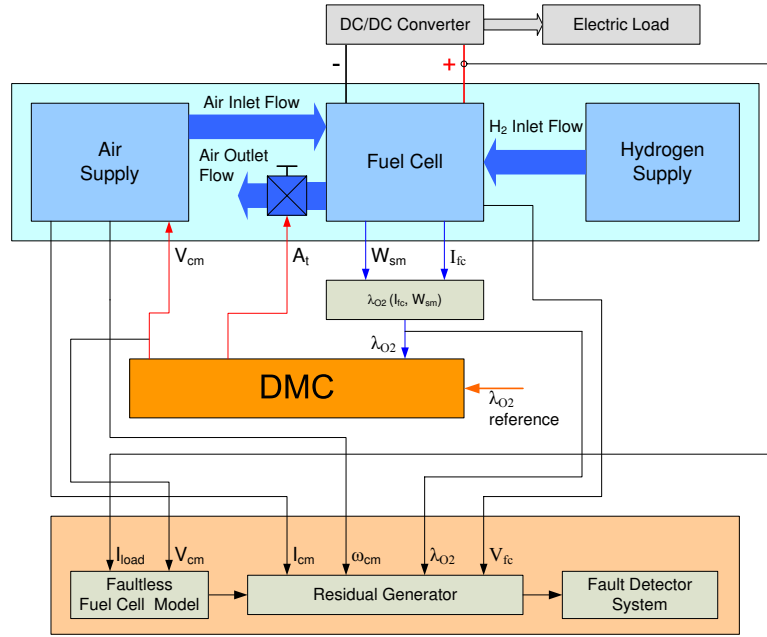
Figure 5.1: Implementation of the fault diagnosis system

(described in Section 4.1 and Appendix A) has been modified in order to include a set of typical faults. With this modified simulator, it is possible to reproduce any of the faults presented in Table 5.2. The implementation of the fault diagnosis system is shown in Fig. 5.1 and, in the simulation set-up, the fuel cell is the modified fuel cell model.

The set of available measurements is compared with its predicted value using a non-faulty fuel cell model. The differences between the predicted and measured values generate a set of residuals that are sent to the fault diagnosis system. When a fault appears, the residuals that are sensitive to this fault take a value different from zero. When some of the residual values cross the detection threshold, the fault diagnosis starts reasoning with all the violated residuals. The reasoning (described in Section 5.1.2) is based on computing the minimum distance between the observed fault signature and a theoretical one. The fault that approaches the most to one of the fault signatures is the one indicated as a possible fault.

The fault f_1 is simulated with an increment Δk_v in the compressor constant k_v and, similarly, the fault f_2 is simulated with an increment ΔR_{cm} in the compressor motor

Table 5.2: Description of the fault scenarios.

Fault	Description
f_1	Increase of the compressor motor friction.
f_2	Overheating of the compressor motor.
f_3	The fluid resistance increases due to water blocking the channels or flooding in the diffusion layer.
f_4	Air leak in the air supply manifold.
f_5	Increase of the voltage value below which the compressor motor does not turn.
f_6	Increase of the stack temperature due to a failure in the temperature controller.

resistance R_{cm}. Both faults result in a change in the compressor torque τ_{cm}:

$$\tau_{cm} = \frac{\eta_{cm}\, k_t}{(R_{cm} + \Delta R_{cm})}\left(v_{cm} - (k_v + \Delta k_v)\omega_{cm}\right), \tag{5.8}$$

where η_{cm} is the motor mechanical efficiency, k_t is a motor constant, and ω_{cm} is the compressor speed.

The fault f_3 is simulated with an increment $\Delta k_{ca,out}$ in the orifice constant of the cathode output, $k_{ca,out}$, which produces a change in the outlet air flow in the cathode, $W_{ca,out}$:

$$W_{ca,out} = (k_{ca,out} + \Delta k_{ca,out})\left(p_{ca} - p_{rm}\right), \tag{5.9}$$

where p_{ca} is the cathode pressure and p_{rm} is the return manifold pressure.

The fault f_4 is simulated with a diminution in the supply manifold outlet flow constant , which is translated into a change in the supply manifold outlet air flow $W_{sm,out}$:

$$W_{sm,out} = (k_{sm,out} + \Delta k_{sm,out})\,,(p_{sm} - p_{ca}) \tag{5.10}$$

where p_{sm} is the supply manifold pressure.

The fault f_5 is simulated with an increment in the voltage value below which the compressor motor does not turn, $V_{cm,low}$, that the controller supplies to the compressor motor, a boundary that also influences the compressor torque in (5.8). The fault f_6 is simulated with an increment ΔT_{fc} in the stack temperature T_{fc}, which has an impact on the open circuit voltage of the stack, the partial pressure of gases, the relative

humidity, and the water diffusion coefficient in the membrane. Therefore, the open circuit voltage E defined in (2.4) becomes

$$
\begin{aligned}
E = {} & 1.229 - 0.85 \times 10^{-3} \left(T_{fc} + \Delta T_{fc} - 298.15\right) + \\
& + 4.3085 \times 10^{-5} \left(T_{fc} + \Delta T_{fc}\right) \left[\ln(p_{H2}) + 0.5 \ln(p_{O2})\right],
\end{aligned}
\tag{5.11}
$$

where p_{H2} and p_{O2} are the partial pressure of hydrogen and oxygen, respectively.

The partial pressure of gases p_i in the anode is

$$
p_{i,an} = \frac{M_{i,an} \, R_i (T_{fc} + \Delta T_{fc})}{V_{an}},
\tag{5.12}
$$

where the subscript i is either H_2-hydrogen or v-vapor, M is the molar mass, R is the gas constant, and V_{an} is the anode volume. The partial pressure of gases in the cathode is

$$
p_{i,ca} = \frac{M_{i,ca} \, R_i (T_{fc} + \Delta T_{fc})}{V_{ca}},
\tag{5.13}
$$

where the subscript i is O_2-oxygen, N_2-nitrogen or v-vapor and V_{ca} is cathode volume. The relative humidity ϕ_j is

$$
\phi_j = \frac{p_{vj}}{p_{sat}(T_{fc} + \Delta T_{fc})},
\tag{5.14}
$$

where the subscript j is either an-anode or ca-cathode and the saturation pressure of vapor is calculated using the following expression:

$$
\begin{aligned}
\log_{10}(p_{sat}) = {} & \\
& -1.69 \times 10^{-10} \, T_{fc}^4 + 3.85 \times 10^{-7} \, T_{fc}^3 - 3.39 \times 10^{-4} \, T_{fc}^2 + 0.14 \, T_{fc} - \\
& -20.92,
\end{aligned}
\tag{5.15}
$$

where the pressure is in kPa and the temperature is in Kelvin. The stack temperature also affects the water diffusion coefficient in the membrane:

$$
D_w = D_\lambda \, exp \left(2416 \left(\frac{1}{303} - \frac{1}{T_{fc} + \Delta T_{fc}} \right) \right),
\tag{5.16}
$$

where D_λ is a constant which depends on the water content in the membrane.

Table 5.3: Theoretical fault signature matrix *FSM* using binary and sign information.

	f_1	f_2	f_3	f_4	f_5	f_6
r_1	(-)1	(-)1	(-)1	(-)1	1	(-)1
r_2	(-)1	(-)1	(-)1	(-)1	1	1
r_3	(-)1	(-)1	(-)1	(-)1	1	(-)1
r_4	(-)1	(-)1	1	1	1	1

Residual generation and fault sensitivity analysis

The variables that are considered as measured and consequently can be used for residual generation are the oxygen excess ratio λ_{O2}, the compressor motor rotational speed ω_{cm}, the compressor motor current I_{cm}, and the fuel cell system voltage V_{fc}. Using these variables and the non linear model presented in [42], four residuals can be derived:

$$
\begin{aligned}
r_1 &= \lambda_{O_2} - \hat{\lambda}_{O_2}, \\
r_2 &= V_{fc} - \hat{V}_{fc}, \\
r_3 &= I_{cm} - \hat{I}_{cm}, \text{ and} \\
r_4 &= \omega_{cm} - \hat{\omega}_{cm}.
\end{aligned}
\tag{5.17}
$$

Using the *PEMFC* fault simulator previously described, it has been determined if the faults defined in Table 5.2 affect or not each of the previous residuals. From these results, the theoretical binary fault signature matrix presented in Table 5.3 can be derived. It can be noticed that all the considered faults affect all the residuals. Thus, the faults are not diagnosable. Even taking into account the sense (sign) in which the fault affect the residual not all the faults are diagnosable: f_1 can not be distinguished from f_2 and, similarly, f_3 from f_4.

Alternatively, using the relative fault sensitivity (5.5), the fault signature table *FSMsensit-rel* can be calculated. The values of this matrix are shown in Table 5.4[1]. It can be noticed that in this case all the considered faults can be isolated since the following condition is satisfied:

$$
S^{rel,teo}_{r_i r_1 f_j} \neq S^{rel,teo}_{r_i r_1 f_k} \text{ for all } j \neq k.
\tag{5.18}
$$

This can be seen by representing the values of the theoretical fault signatures (see Fig. 5.3(a)) in the three-dimensional space r_2/r_1, r_3/r_1, and r_4/r_1. Since there is no overlapping, the six faults can be detected and isolated and thus, can be diagnosed.

---

[1]This table has been derived from the *PEMFC* model in the operating point described in Section 4.2.6.

Table 5.4: Theoretical fault signature matrix *FSMsensit-rel*.

|	f_1	f_2	f_3	f_4	f_5	f_6
r_2/r_1	1	0.824	0.118	0.643	0.036	-0.221
r_3/r_1	0.854	1	0.197	0.206	0.039	0.151
r_4/r_1	1	0.937	-0.128	-0.134	0.168	-0.098

5.1.4 Results

In order to evaluate the model-based fault diagnosis methodology proposed, the fault scenarios and fault simulator presented in Section 5.1.3 are used. As discussed in previous sections, the fault detection is based on checking at every time the difference (residual) between the signal monitored by a sensor and its estimation using the detection model (5.17).

The simulation results for the fault scenario f_1 are shown to illustrate how the methodology works: Fig. 5.2(a) shows the temporal evolution of the residuals and the detection threshold for each of them and Fig. 5.2(b) illustrates the time that the diagnosis system takes for detecting and isolating the fault. The fault is introduced into the system at time $50\,s$ and some time after, all the fault signals cross their detection threshold (dash line) activating the four indicators of fault (5.2). The detection subsystem stores the fault at the time that one of the thresholds is violated by any of the residuals and, as soon as it is detected that a fault is present, the isolation process begins. The isolation process is based on evaluating the distance of the observed relative fault sensitivity vector to the theoretical fault sensitivity vector.

Figure 5.3(a) shows the location of the faults in the space of ratios using the relative fault sensitivities matrix, described in Section 5.1.2, and the time evolution of the minimum distance between the observed and theoretical relative fault sensitivity (5.6) (drawn in continuous line).

Figure 5.3(b) presents the Euclidean distance between the observer and the theoretical sensitivity fault signatures for each fault (5.7). It can be noticed that since fault f_1 has a similar fault signature than f_2 (see also Table 5.4) at the beginning of the fault isolation process f_2 is the fault proposed as the possible fault, since presents a smaller distance than f_1. However, from time instant $82\,s$, f_1 can be isolated. It is seen that the proposed methodology, after some isolation time delay, allows isolate the true fault.
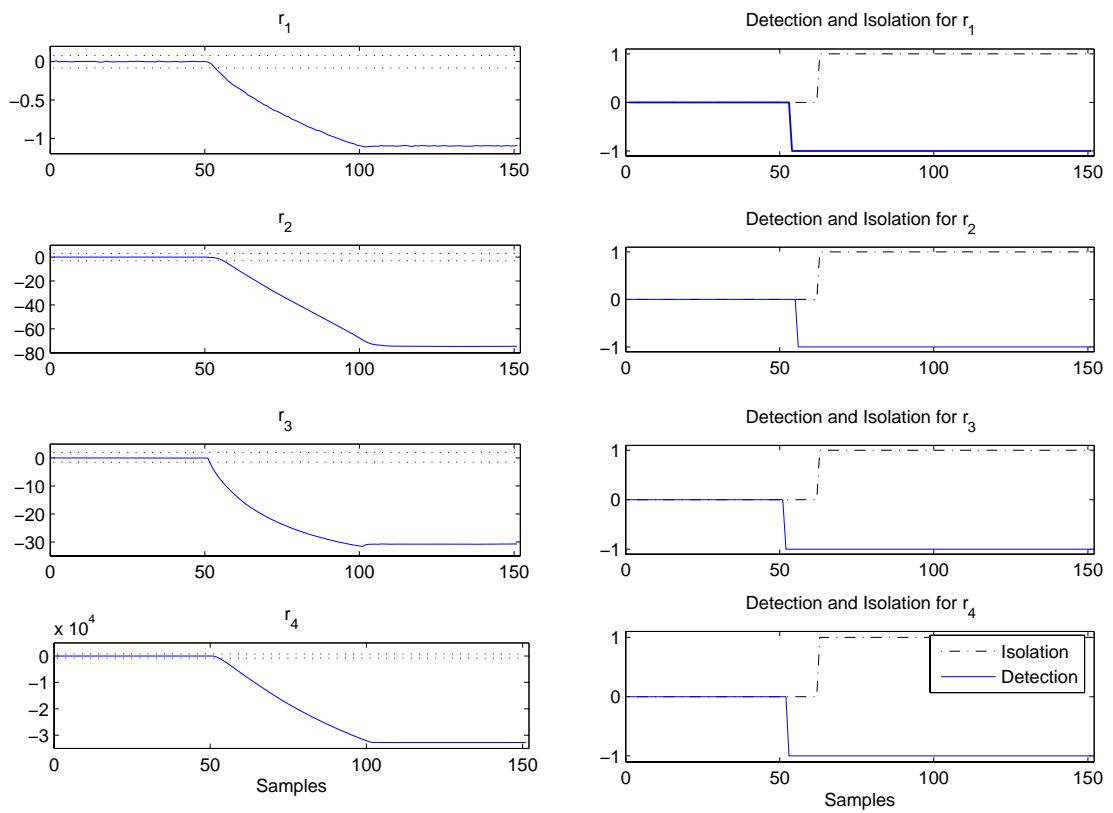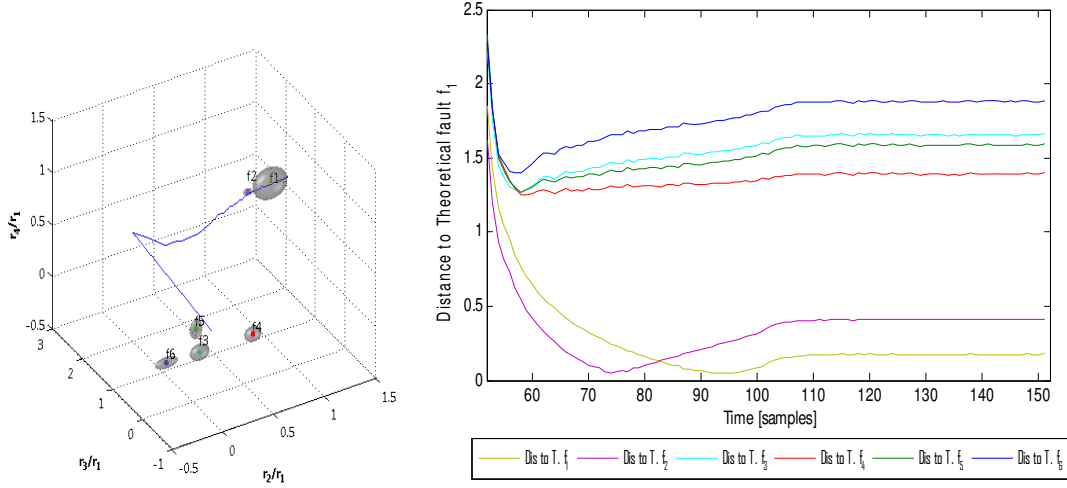
(a) Time evolution of the residuals.

(b) Time evolution of fault detection and isolation indicators.

Figure 5.2: Simulation results corresponding to fault scenario f_1.

(a) Time evolution of the minimum distance according to (5.6).

(b) Time evolution of the distance between observed and theoretical relative fault sensitivity for each fault.

Figure 5.3: Results of the fault diagnosis methodology proposed for fault scenario f_1.

Similarly, it is possible to detect and isolate the other five fault scenarios using the proposed methodology. However, the time that the methodology takes to isolate is different for each fault scenario. It is remarkable that the process of isolation needs considerably more processing time with the fault scenarios f_1 and f_2 because of the similarity between their fault signatures.

5.2 Fault-Tolerant Model Predictive Control of *PEM* Fuel Cells

As it was mentioned in Chapter 4, a main control objective is to avoid a lack of oxygen in the cathode ("oxygen starvation") by maintaining the oxygen excess ratio close to a pre-established set-point, in spite of the disturbance introduced by the current load. However, because of the complexity of the fuel cell system, it is prone to suffer faults during the operation [80]. Therefore, some fault-tolerant capabilities should be added to the control system in order to maintain the fuel cell system under control even in the presence of faults.

This section explores the possibility of making use of the known inherent fault-tolerant capabilities of *Model Predictive Control* (*MPC*) when applied to *PEMFC*.
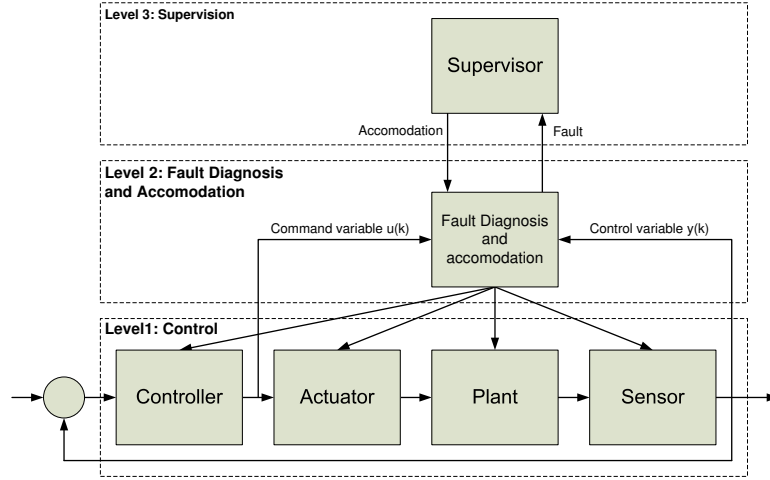
Figure 5.4: Fault-tolerant architecture

In particular, it is shown that the controller architecture based on manipulating two actuators (the compressor and the outlet air valve) that was proposed in Section 4.2.2 offers better fault-tolerant capabilities and improves the system performance.

5.2.1   Fault-Tolerant Model Predictive Control

Fault-tolerant Model Predictive Control is an incipient research area in the automatic control field [69]. One way of achieving fault-tolerance is to employ a fault detection and isolation (*FDI*) scheme on-line. This system will generate a discrete event signal to a supervisor system when a fault is detected and isolated. The supervisor, in turn, will activate some accommodation action in response, which can be predetermined for each fault or obtained from real-time analysis and optimization. Because of the discrete-event nature of fault occurrence and the reconfiguration/accommodation, a *FTC* system is a hybrid system by nature. For design purposes of these systems, the hybrid nature has been traditionally neglected in order to facilitate a simple design, reliable implementation, and systematic testing. The whole *FTC* scheme can be expressed using the three-level architecture for *FTC* systems proposed by Blanke [69] (see Fig. 5.4):

- Level 1: **Control Loop**. This level comprises a traditional control loop with sensors and actuator interfaces, signal conditioning and filtering, and the controller.

- Level 2: **Fault Diagnosis and Accommodation**. The second level comprises a given amount of detectors, usually one per each fault effect to be detected, and actuators that implement the desired reconfiguration or other corrective actions given by the autonomous supervisor.

- Level 3: **Supervision**. The supervisor is a discrete-event dynamical system which comprises state-event logic to describe the logical state of the controlled object. The supervisor functionality includes an interface with *FDI* detectors and generates remedial actions to accommodate a fault.

5.2.2 Inclusion of fault tolerance in *MPC*

Fault tolerance can be embedded in *MPC* relatively easily [81]. This can be done in several ways:

1. Changing the constraints of the *MPC* in order to represent certain kinds of faults, being especially easy to adapt the algorithms for faults in actuators, assuming that the fault has been located and their effects have been estimated using a *FDI* module.

2. Modifying the internal plant model used by the *MPC* in order to reflect the fault influence over the plant using the information provided by the *FDI* module.

3. Relaxing the initial control objectives in order to reflect the system limitations under fault conditions.

5.2.3 One actuator vs. two actuator *MPC* control architecture for Fuel Cell control

In Chapter 4, it was explained that a common practice in the *PEM* fuel cell control is to control the hydrogen supply using the anode inlet valve in such a way that the anode pressure tracks the cathode pressure whereas the control of the air supply is achieved controlling the oxygen excess ratio.

In this section, two architectures to control the oxygen excess ratio are compared: the common architecture in the literature with one actuator (the compressor motor voltage) and a proposed architecture with two actuators: the compressor voltage and the

(a) One actuator control architecture   (b) Two actuator control architecture
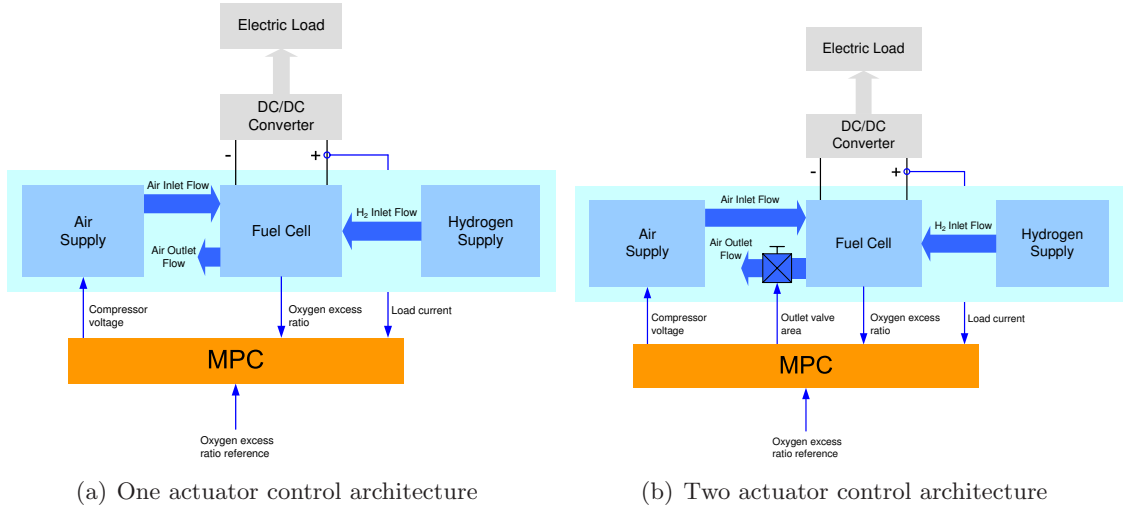
Figure 5.5: One actuator vs. two actuator *MPC* architecture for fuel cell control.

opening area in the cathode outlet valve. The two architectures are shown in Fig. 5.5. In Chapter 4, it was shown that the use of these two actuators offers better control performance and efficiency improvement in the case of regulation of the stack voltage and the oxygen excess ratio at the same time. Here, the two control structures are compared in terms of fault-tolerant capability. The objective is to regulate the oxygen excess ratio around the reference value $\lambda_{O_2,\ ref} = 2.3$, i.e., $\lim_{k \to \infty} |\lambda_{O_2}(k) - \lambda_{O_2,\ ref}| = 0$.

The control architectures are implemented using *MATLAB MPC* Toolbox and the fuel cell system linear model used to implement the *MPC* is derived through a linearization of the nonlinear model proposed in [42] at the selected operating point: $P_{net} = 40\,kW$, $\lambda_{O_2} = 2.3$, $V_{fc} = 235\,V$, $I_{fc} = 191\,A$, $V_{cm} = 164\,V$, and $A_t = 20\,cm^2$.

An open-loop optimal control problem is solved at each sampling time where the future control action is calculated over a finite horizon h_m, i.e.,

$$u = \left[\begin{array}{l} u_1(k),\, u_1(k+1), \cdots,\, u_1(k+h_m) \\ u_2(k),\, u_2(k+1), \cdots,\, u_2(k+h_m) \end{array} \right], \tag{5.19}$$

minimizing a cost function $J(k)$ over a finite prediction horizon h_p:

$$\min_{\Delta u} J(k), \tag{5.20}$$

subject to

$$\begin{aligned}
x(k+1) &= A\,x(k) + B\,u(k),\\
y(k) &= C\,x(k),\\
u(k) &\in [\underline{u},\,\overline{u}]\,,\text{ and}\\
y(k) &\in [\underline{y},\,\overline{y}]
\end{aligned} \qquad (5.21)$$

for $k = 0,\,1,\,2,\cdots$. The cost function is defined as follows:

$$J(k) = \sum_{j=1}^{h_p} \lambda\,[y(k+j|k) - y_r)]^2 + \sum_{j=0}^{h_m} \Delta u(k+j|k)^T Q \Delta u(k+j|k), \qquad (5.22)$$

where $\Delta u(k+j|k) \stackrel{\triangle}{=} u(k+j|k) - u(k-1+j|k)$, λ is a coefficient to weight the error, and Q is a diagonal matrix of dimension 2×2 to weight the control increments.

Only the first value of the calculated control sequence $u(k)$ is applied and the computation is repeated at the next sampling time starting from the new state and over a shifted horizon, leading to a moving horizon policy. The solution relies on a linear dynamic model, respecting all input and output constraints and optimizing a quadratic performance index. The *MPC* weights λ and Q are tuned to achieve the desired control goal, that is to maintain the oxygen excess ratio, penalizing the control effort: λ has been selected to have a value of 5 while the diagonal elements of Q have been selected to have a value of 0.1 for a good performance control, after some trial and error experimentation.

The air compressor voltage is considered as a constrained input due to physical limits: the maximum compressor voltage cannot exceed $230\,V$ and the voltage value is never negative. The oxygen excess ratio is represented as a constrained output: the operating range is between 1.5 and 3 in order to avoid starvation and to obtain near optimal operation [82]. Note that this output constraint is implemented as a soft constraint in the *MPC* toolbox in order to prevent the infeasible solution.

Simulating different scenarios, it is found that the compressor voltage variations from the steady-state value to obtain the same control performance regarding the control of the oxygen excess ratio are smaller in the two actuator case than in the one actuator case. These smaller compressor voltage variations are compensated by the control of the outlet valve area: Fig. 5.6(b) shows the comparison of the oxygen excess ratio and the compressor voltage in case of using one actuator and two actuator control architectures when a series of step changes in the stack current are applied (Fig. 5.6(a)).

This current is considered a measured disturbance for *MPC* controller. From this figure it can be clearly seen that for the same quality of regulation of the oxygen excess ratio, providing a maintained set point of 2.3, the two actuator architecture requires smaller voltage variations in the compressor.

Besides, two other basic variables of the fuel cell performance are also shown in Fig. 5.6(c): the stack voltage and the oxygen partial pressure in the cathode. Even though these variables are not controlled in this analysis, their behavior must be checked in order to avoid high degradation of the efficiency or dangerous responses.

The simulation results show different trade-offs: the control architecture with one actuator maintains the stack voltage close to the nominal value and drives the oxygen partial pressure to higher variations while the control structure with two actuators maintains the oxygen partial pressure closer to the nominal value and drives the stack voltage to higher variations.

5.2.4 Fault-Tolerance of the two considered *MPC* control architectures

In this section, the advisability of implementing an active fault-tolerant scheme using the two actuators *MPC* control architecture is shown. As explained in previous sections, the *MPC* formulation allows to easily include active fault-tolerant control capabilities in the control law. In this section, the case of actuator faults in the *PEM* fuel cell system is addressed. In a preliminary manner, the compressor faults are modelled through a reduction of the compressor voltage range. According to Section 5.2.3, the *FDI* module should provide the *MPC* controller the new limits of the compressor voltage range, once the fault has been detected, isolated and estimated. The active *FTC* control architecture is showed in Figure 5.7, where the actuator operating range limits are estimated by the *FDI* module.

The *FDI* module (drawn in dashed line) is not implemented in this section and it is assumed that it is available and working perfectly. In order to take into account changes in the compressor voltage range due to the fault (actuator limits), the linear model for *MPC* design is modified by including the actuator limits as new states that will be estimated by the *FDI* module and can be written as
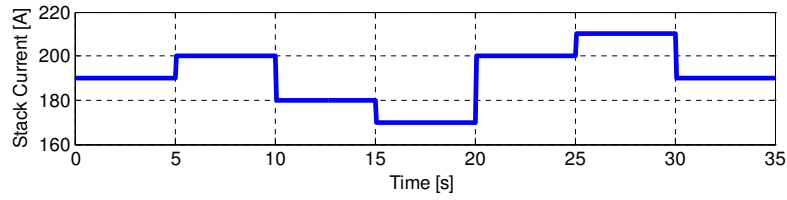
(a) Step changes in the stack current.
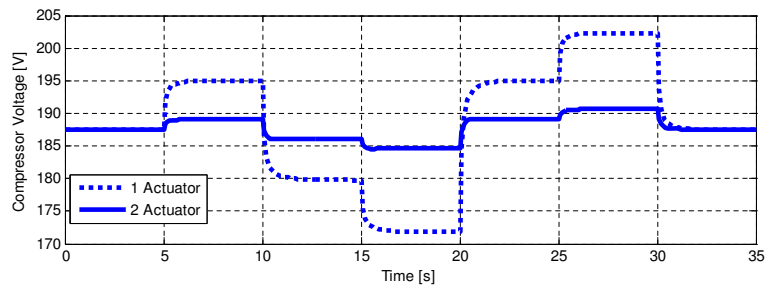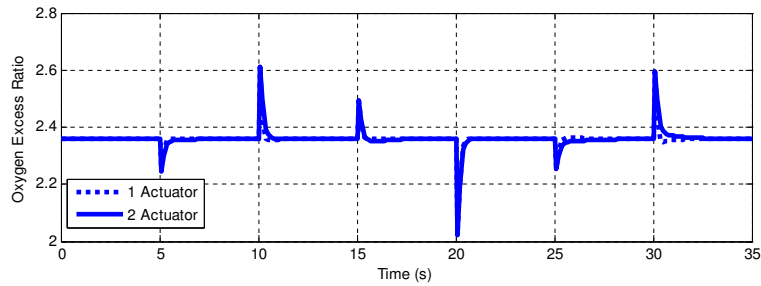
(b) Evolution of the oxygen excess ratio and the compressor voltage.
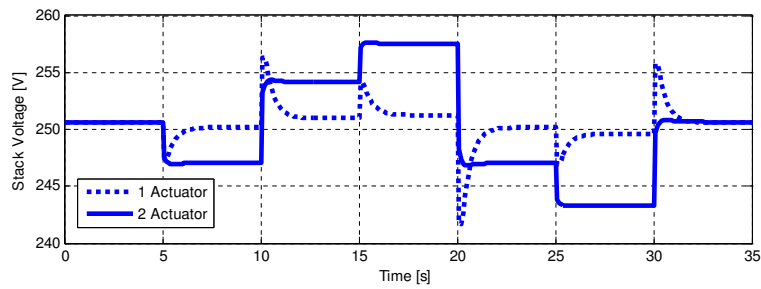
(c) Evolution of the stack voltage and the partial pressure of oxygen.

Figure 5.6: Comparison of control results using both architectures.
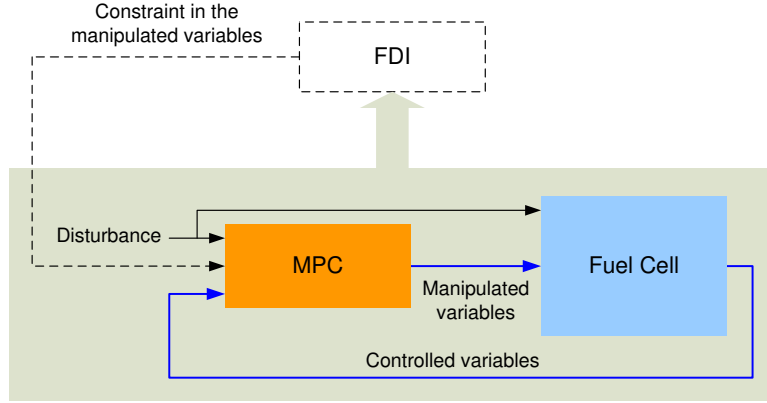
Figure 5.7: Fault-tolerant *MPC* scheme for air compressor faults

$$
\begin{bmatrix} x_1(k+1) \\ \vdots \\ x_n(k+1) \\ \hline x_{n+2}(k+1) \\ x_{n+2}(k+1) \end{bmatrix} = \begin{bmatrix} A & 0 \\ \hline 0 & I \end{bmatrix} \begin{bmatrix} x_1(k) \\ \vdo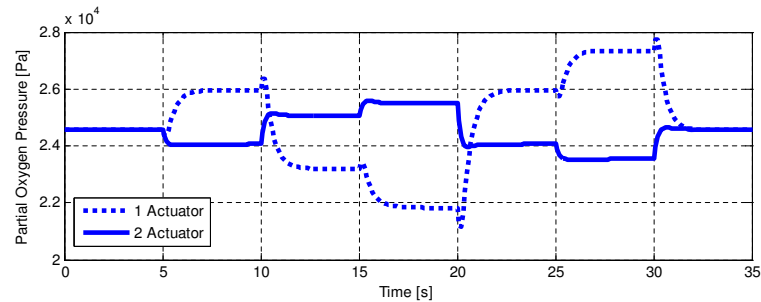ts \\ x_n(k) \\ \hline x_{n+1}(k) \\ x_{n+2}(k) \end{bmatrix} + \begin{bmatrix} B \\ \hline 0 \end{bmatrix} \begin{bmatrix} u_1(k) \\ u_2(k) \end{bmatrix} \qquad (5.23)
$$

$$
\begin{bmatrix} y_1(k) \\ \vdots \\ y_m(k) \\ \hline y_{m+1}(k) \\ y_{m+2}(k) \end{bmatrix} = \begin{bmatrix} C & 0 \\ \hline 0 & I \end{bmatrix} \begin{bmatrix} x_1(k) \\ \vdots \\ x_n(k) \\ \hline x_{n+1}(k) \\ x_{n+2}(k) \end{bmatrix} + \begin{bmatrix} D \\ \hline D' \end{bmatrix} \begin{bmatrix} u_1(k) \\ u_2(k) \end{bmatrix}, \qquad (5.24)
$$

where x_i, $i = 1, \cdots, n$ and y_i, $i = 1, \cdots, m$ are the original states and outputs, respectively, and A, B, C, and D are the original matrices of the linearized fuel cell system model described in Section 4.1. Vector D' is defined as $D' = [\ -1 \quad -1\ ]^T$ and I is the identity matrix of suitable dimensions.

In (5.23), x_{n+1} corresponds to the upper limit while x_{n+2} corresponds to the lower limit, and $x_{n+1}(k + 1) = x_{n+1}(k)$ and $x_{n+2}(k + 1) = x_{n+2}(k)$ means that the upper limit and the lower limit remains constant during the prediction horizon, respectively. Besides, additional output constraints have been added to the *MPC* controller: $y_{m+1}(k) \geq 0$ and $y_{m+2}(k) \leq 0 \ \forall k$ to ensure that the computed control variable $u(k)$

will be into the range estimated by *FDI* module. Thus,

$$y_{m+1}(k) = x_{n+1}(k) - u(k) \geq 0 \Rightarrow u(k) \leq x_{n+1}(k) \quad (5.25)$$

$$y_{m+2}(k) = x_{n+2}(k) - u(k) \leq 0 \Rightarrow u(k) \geq x_{n+2}(k). \quad (5.26)$$

5.2.5 Results

Figures 5.8 to 5.10 show the simulation results of *FTC* scheme for several fault actuator scenarios considering the two control structures presented in Section 5.2.3. The current applied to the stack is the same than in the non-faulty scenario presented in Fig. 5.6(a). The control action is shown in Fig. 5.8 when the actuator (air compressor) fault causes a range reduction such that the upper limit of the range is reduced to 75% of the original one. In this case, there is no control degradation since the compressor voltage does not reach the upper range limit in any of the two considered controller architectures. Figure 5.9 shows the case corresponding to a reduction of the upper limit of 50% with respect to the original one. Now, the control degradation is visible in case of the controller architecture that uses only one actuator (the compressor) when the values of stack current are high. In the case of the two actuator architecture, since the voltage excursion of the controller does not reach the upper limit of the operating range, the controlled variable is not affected. Finally, the upper limit range is reduced to be 25% of the original one in Fig. 5.10. In this case, the control goal is highly affected in the case of using the one actuator architecture while in the case of the two actuators architecture the control results are still unaffected.

The results presented in the previous section show that the control architecture that uses two actuators offers a better fault tolerance against compressor faults. This is because to achieve the same control results, the compressor voltage changes are smaller. The inclusion of the cathode outlet valve opening adds additional degree of freedom to the system that can be exploited in case of non severe faults in the compressor.

5.3 Conclusions

In the first section of this chapter, a new model-based fault diagnosis methodology based on the relative fault sensitivity has been presented and tested. An advantage of
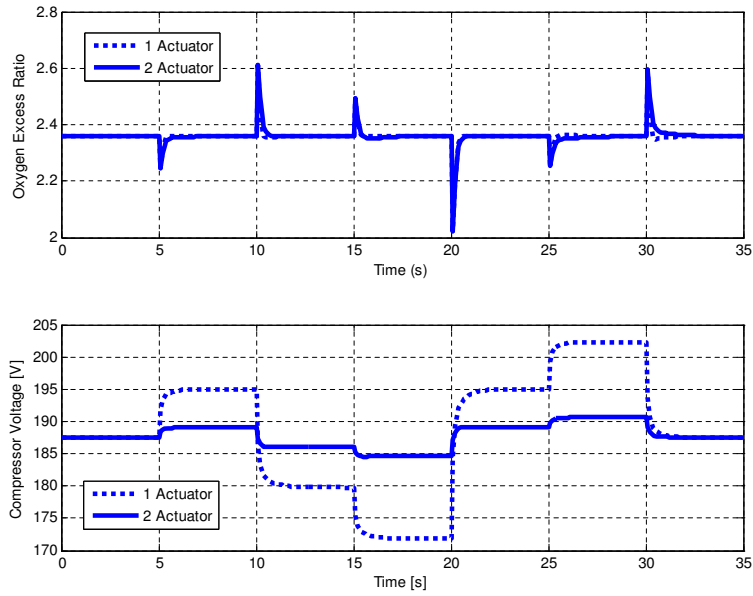
Figure 5.8: Fault-tolerant *MPC* results in case of an actuator fault that limits the operating range to $0 - 75\%$ of the original range.
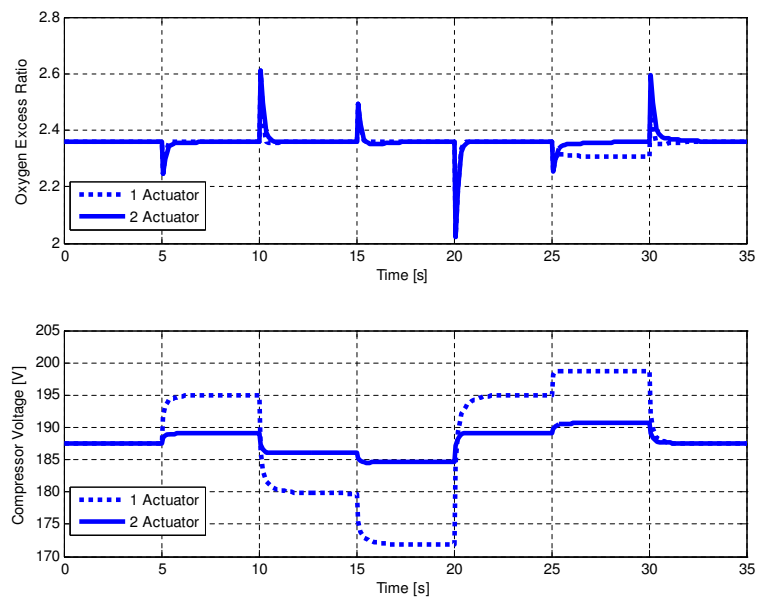
Figure 5.9: Fault-tolerant *MPC* results in case of an actuator fault that limits the operating range to $0 - 50\%$ of the original range.
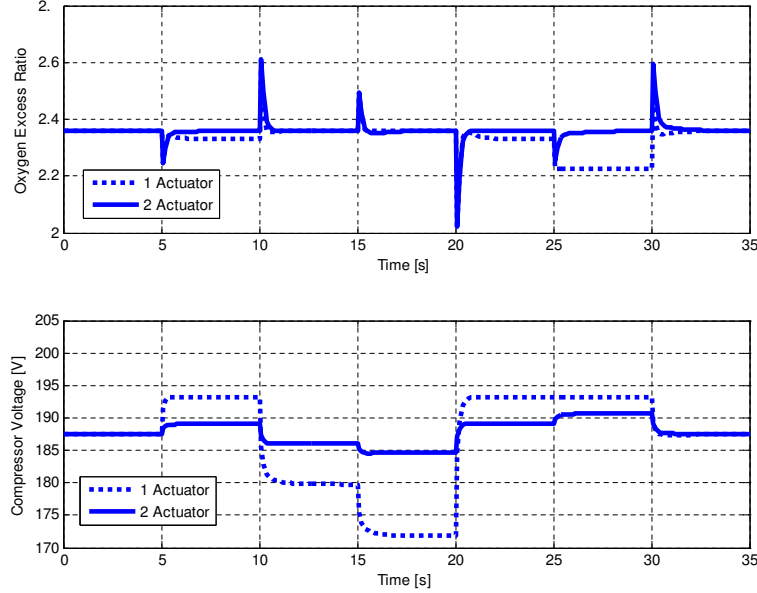
Figure 5.10: Fault-tolerant *MPC* results in case of an actuator fault that limits the operating range to $0 - 25\%$ of the original range.

this new methodology is that it does not require the knowledge of the fault magnitude to provide a diagnostic. Furthermore, it allows to isolate faults although all the considered faults affect all the residuals, whenever the sensitivities are different.

To prove this methodology, a *PEM* fuel cell simulator based on a model presented in the literature has been developed. The simulator was modified to include a set of possible fault scenarios proposed in this thesis work. This modified simulator allows imposing a determined fault scenario, within the considered set of faults, and analyzing its behavior. All the simulated faults have been tested with the new diagnosis methodology, which has diagnosed correctly the simulated faults in contrast with other well known methodologies using binary signature matrix of analytical residuals and faults, which do not permit to isolate the complete set of faults.

In the second section, fault-tolerance of *MPC* control for fuel cell systems has been addressed. *MPC* is a suitable control methodology to control fuel cell systems because of their multivariable and complex behavior. At the same time, *MPC* is one of the control methodologies that can introduce more easily fault-tolerance. However, the problem of including actuator fault-tolerance in the control loop of *FCS* had not been

already addressed in the literature for those systems.

Here, a new control structure that not only uses the compressor voltage as a control variable but also the cathode outlet valve area has been proposed. It is shown that using this new control structure allows improving the control performance and at the same time allows introducing fault-tolerance against compressor faults. This result reinforces the idea of inclusion of the cathode output valve, which is a debatable aspect in the design of *PEMFC*. Finally, the proposed approach has been assessed on a simulation test bench based on a known *PEM* fuel cell model.

Chapter 6

Design and analysis of Fuel Cell Hybrid Power Systems

The control of *Fuel Cell Systems* was studied in Chapter 4 and Chapter 5, analyzing the system composed by the fuel cell stack and its auxiliary subsystems (e.g., compressor, valves, etc.), with the following objectives: to achieve high efficiency, reducing the hydrogen consumption, to improve the dynamic behavior, and to guarantee its safe operation. We continue in this chapter and Chapter 7 with the study of fuel cell-based systems approaching the fuel cell hybrid systems with some energy storage. The objectives remain the same.

In a *Fuel Cell Hybrid System (FCHS)*, an *Energy Storage System (ESS)*, e.g., a battery or a supercapacitor bank, is added to the fuel cell system in order to increase the efficiency and performance of the power generation system as it was explained in Section 2.2. Hybridization has important advantages in *Fuel Cell Hybrid Vehicles* (*FCHV*), a fuel cell application that is central in this thesis.

Therefore, the process of designing a hybrid system, or methodology of design, is addressed in this chapter. We concentrate our attention on *FCHVs* because this application is particularly attractive, although some general aspects studied in this chapter also apply to other applications such as stand-alone residential *PEMFC* power systems.

6.1 Outline of the Chapter

The design process of *FCHVs* according to drivability conditions includes the determination of the electrical topology and the determination of the hybridization degree. With the selected design, the optimal hydrogen consumption for different driving cycles and the energy flows in the hybrid vehicle are analyzed. The entire study is performed with a detailed model of the *FCHV* in *ADVISOR*: the determination of the hybridization degree according to drivability requirements, the analysis of the energy flows, and the computation of the optimal hydrogen consumption.

The different tasks of this chapter are deeply interrelated and regardless of being presented separately, each one is considering the global context. Besides, in order to operate a *FCHV* efficiently, it is also necessary to implement a control strategy to coordinate the power split between the *FCS* and the *ESS*: the *Energy Management Strategies (EMS)*. This issue is covered in detail in Chapter 7.

6.2 Advantages of hybridization in *FCHVs*

The hybridization in fuel cell-based systems should produce an increase in the efficiency over a large operating range. In *FCHVs*, three different mechanisms allow this efficiency improvement:

Regenerative braking In automotive applications, it is possible to recover energy from regenerative braking, allowing a considerable improvement in the hydrogen economy. The recovered energy from regenerative braking may represent an important fraction of the economy improvement. However, the amount of energy that is possible to recover is strongly dependent on the driving profile. In urban driving cycles, in which there are abundant backings, the percentage of regenerable energy is much greater than in non-urban cycles where this percentage is quite small.

Energy management strategy The efficiency of a *FCS* is maximum at a fraction of the rated power. Therefore, it is convenient to operate the fuel cell in its maximum efficiency zone. Thus, taking advantage of an auxiliary power source

and an adequate energy strategy, it is possible to maintain the fuel cell operating at its maximum efficiency region most of the time and reduce the hydrogen consumption.

Fuel cell downsizing In a pure fuel cell-based power generation system, the *FCS* must be sized to meet the maximum load. When the load is strongly variable (e.g., in automotive applications or stand-alone residential applications), the *FCS* is working, in average, well below its rated power. One important advantage of hybridization is that it allows a diminution of the rated power of the fuel cell stack in these type of applications. Therefore, it is possible to meet the demand with a smaller *FCS* in combination with an energy storage system. In addition to this advantage, downsizing the *FCS* has an impact on the hydrogen economy in three ways: downsizing leads to *i*) improvements in the hydrogen economy when the peak efficiency of the *FC* stack is shifted to better match with the power requirements from a given driving cycle, *ii*) a smaller compressor, reducing the parasitic losses, and *iii*) a diminution in the fuel cell system mass, reducing the total mass.

Although the main motivation for introducing hybridization in fuel cell systems is to improve the hydrogen economy, the benefits are not limited to that. In fact, hybridization is useful to solve two important problems in fuel cell control:

Improvement of the transient response The dynamics of *FCS* are relatively slow, mainly because of the dynamics of the air compressor and the manifold-filling dynamics [25]. In this context, an additional energy flow from an energy storage device with high specific power[1] is useful to compensate this drawback. In the literature, this issue is not completely resolved. In [83], it is concluded that it is feasible to use a *FCS* in a load-following mode without any storage device. In that work, the conclusions are based on results obtained from experimental data taken from a scaled-down *FCS* and a particular Standard Driving Cycle. It is remarked that it is possible to take out short bursts of power from the stack, due

---

[1]The specific power is defined as power per unit of mass ($W \ kg^{-1}$).

to the *"charge double layer"*[1] *(CDL)* capacitance. However, other publications, for example [58], [34] or [18], conclude that the use of energy storage devices is beneficial from both the system dynamics and the hydrogen economy.

Prevention of "Oxygen Starvation" Oxygen Starvation is a complicated phenomenon that occurs when the oxygen partial pressure falls below a critical level at any point in the cathode. It can be produced by an abrupt increase in the current demand (that causes a rapid increase in the oxygen consumption due to the cathode electrochemical reaction) and an insufficient air supply. This phenomenon can be observed trough a rapid decrease in the cell voltage although in severe cases can produce a short circuit and a hot spot on the surface of the membrane cell [35]. The phenomenon is not well described in the literature and more information from electrochemical studies is needed to be able to quantify the critical level of oxygen concentration below which permanent damage is produced or, perhaps more probably, the combination of level and time. Nevertheless, hybridization can help avoiding oxygen starvation by means of the additional energy supply from the energy storage elements. with this elements, the peaks of actual current demand to the fuel cell in a hybrid system are lower than in the pure fuel cell case where no auxiliary power source is present.

6.3 Electrical structure for Fuel Cell Hybrid Vehicles

The electrical structure of a *fuel cell-based vehicle* involves, essentially, a fuel cell stack with its auxiliary systems and the load, which is generally an alternating current (AC) electrical motor. The *FCS* by itself is an electrical power source, whose direct current (DC) output voltage drops with the current according to the polarization curve. Thus, it is necessary to incorporate power converters to convert the voltage from DC to AC with the appropriate frequency and voltage level.

The electrical structure for a *FCHV* also includes an energy storage system (e.g., a battery bank, asupercapacitor bank or a combiantion of battery and supercapacitors),

---

[1]The *"charge double layer"* (*CDL*) is an electrode phenomenon: when two different materials are in contact there is a build-up of charge on the surfaces or a charge transfer from one to the other. The effect is that if the current suddenly changes, the voltage shows an immediate change due to the internal resistance, but moves fairly slow due to this accumulated charge. One way of modelling this if by using an equivalent circuit, with the *CDL* represented by an electrical capacitor [5].

with the possibility of stocking energy recovered from braking and energy from the fuel cell. This feature requires that the converter that connects the *ESS* is a bidirectional converter to allow the charge and discharge of the *ESS*.

In this section, we approach the design of the electrical structure for a *FCHV* focusing in the determination of the electrical topology (Section 6.3.1) and the selection of the *Energy Storage System* (Section 6.3.2). The detailed design of the power converters and their control is beyond the scope of this work.

6.3.1 Topology of the electrical structure

The topology of an electric system is given by the interconnections of the system components. The selection of the most adequate topology is discussed in [9, 45, 46, 48], where different structures and their appropriate control are analyzed, also the advantages and disadvantages of each case are shown. Thus, several topologies are considered in the literature to connect the *ESS* and the *FCS* to the load, depending on the following issues:

- Characteristics of the load (*DC* or *AC* voltage, single-phase or three-phase, and range of voltage).

- Possibility of energy recovering from the load (e.g., regenerative braking).

- Range of voltage in the *ESS*.

- Output voltage of the *FCS*

In this work, we analyzed the better option for a *FCHV* and a number of options, represented by the decision tree shown in Fig. 6.1, were considered before choosing the topology of the electrical system, which is shown in Fig. 6.2

The main decision was if the vehicle has regenerative braking. This electrical topology is used as frame of reference for the rest of this chapter and for the study of the energy management strategies for *FCHVs* in Chapter 7.

In this topology, the *FCS* is connected to the *DC* bus through a step-up power converter (*Boost* converter) because the *DC* voltage bus is normally high voltage, whereas the *ESS* is connected to the *DC* through a bi-directional power converter (*Buck-Boost*
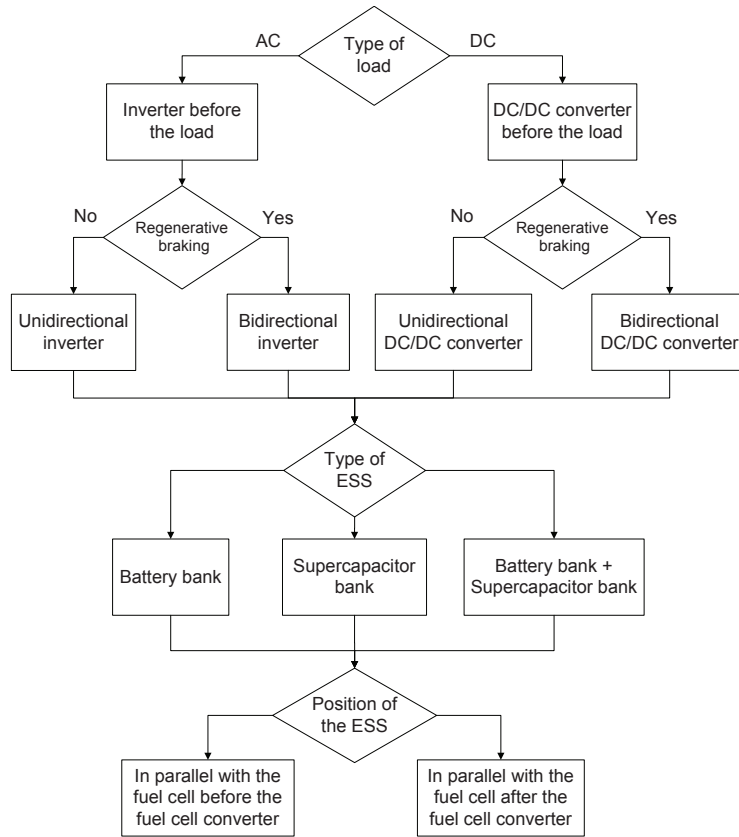
Figure 6.1: Decision tree for the selection of the electrical structure for the *FCVH*.

converter) allowing the charge and discharge of the *ESS*. With regard to the load, which is an *AC* induction motor, it is fed through a *DC-AC* inverter.

The power converter that connects the *ESS* to the *DC* bus is fundamental to implement the energy management strategy in the hybrid system: this converter acts as a *"switch"* that allows to regulate the energy flow between the *ESS* and the *DC* bus. In the same way, the converter that connects the *FCS* to the *DC* bus allows the regulation of the power flow from the *FCS* and, besides, has to cope with the variations in the *FCS* output voltage since the *FCS* does not act as an ideal voltage source.

6.3.2 Energy Storage System: Batteries vs. Supercapacitors

The *Energy Storage System (ESS)* in the fuel cell hybrid system can be implemented either by a high specific energy device like batteries or by a high specific power device
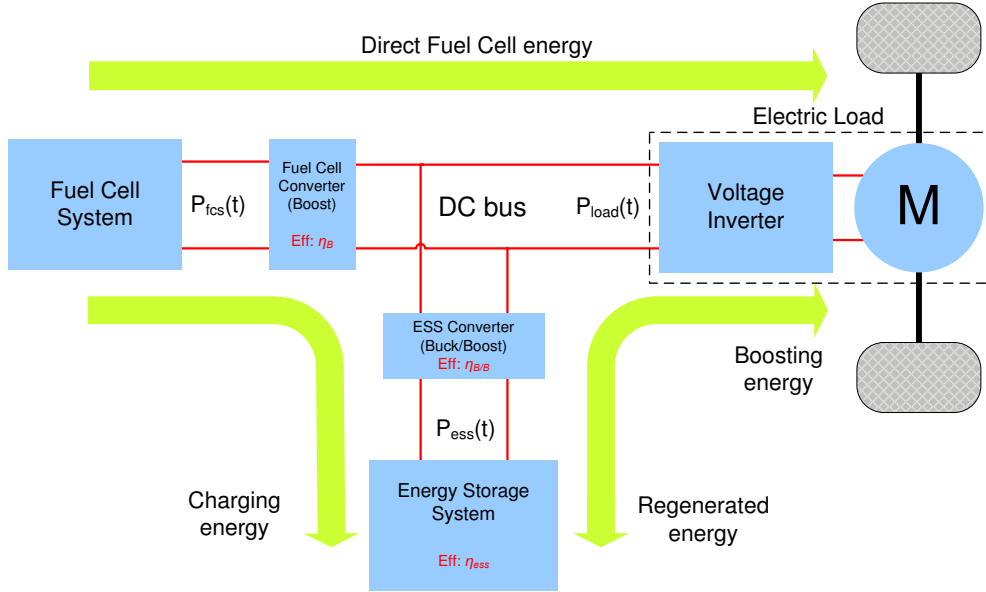
Figure 6.2: Diagram showing the electrical topology and the energy and power flows in a *FCHV*.

like supercapacitors (*SCs*). There is also the possibility of a combined storage bank composed of batteries and capacitors [84]. The supercapacitors present significantly better specific energy than conventional capacitors and much better specific power than conventional batteries. The capacitance of *SCs* may vary from a few Farads to several thousand Farads per cell [85].

Before dealing with this analysis, two meaningful parameters concerning the *ESS*, are introduced:

Hybridization Degree (HD) The *Hybridization Degree* is defined by a relationship between two installed power: the *maximum FCS power* ($P_{fcs,\ max}$) and the *maximum ESS power* ($P_{ess,\ max}$). We use the following expression:

$$HD = \frac{P_{ess,max}}{P_{fcs,\ max} + P_{ess,\ max}} \times 100 \qquad [\%]. \qquad (6.1)$$

With this definition a 100% *HD* indicates a vehicle without *FC* (only storage bank), and 0% *HD* indicates a pure fuel cell vehicle (no storage bank).

Power/Energy storage system ratio (P/E) The *Power/Energy storage system ratio* is defined as the relationship between the *Specific Power (P)* and the *Specific*

Energy (E) of the storage system [86]:

$$P/E = \frac{P\,[W\ kg^{-1}]}{E\,[Wh\ kg^{-1}]} \qquad [W\ Wh^{-1}]. \tag{6.2}$$

Some relevant examples are collected from the literature [86] and reported in Table 6.1. Actually, for some supercapacitors on the market, such the model BCAP0350 from Maxwell Technologies [87], the specific power is $3900\,W\ kg^{-1}$ and a recent study with asymetric double-layer supercapacitor reports advances in specific energy, approaching $40\,Wh\ kg^{-1}$ [88].

Table 6.1: Characteristics of some relevant Energy Storage Systems examples

	P/E $[W\,Wh^{-1}]$	Specific power $[W\,kg^{-1}]$	Specific energy $[Wh\,kg^{-1}]$
High power lead-acid batteries	10	300	30
Ni-Mh batteries	10	$4-500$	$50-70$
Supercapacitors	>100	up to 1000	up to 5

We choose supercapacitors (*SCs*) in this work because they are more attractive for applications with low energy and high power demand, particularly at low temperatures, although cost may remain an obstacle. *SCs* can be deeply charged and discharged at high rates for $500.000 - 1.000.000$ cycles with a relatively small change in characteristics ($10 - 20\%$ of degradation in capacitance and resistance) and with high charge/discharge efficiency [85]. However, batteries and supercapacitors do not compete but are complementary in the development of *Hybrid Electric Vehicles (HEVs)* because of the high-specific energy of the former and the high-specific power of the latter, notwithstanding the significantly longer cycle-life of *SCs* (more than two order of magnitude [89]).

Different types of *HEV* require energy storage systems characterized by different specific power and energy, P/E ratio and cycle-life. In the work of Gao [90], two *Fuel Cell Hybrid Vehicles (FCHVs)* are studied, comparing a fuel cell-battery hybrid powertrain and a fuel cell-supercapacitor hybrid powertrain. The conclusion is that the second option is better since *SCs* can more effectively assist fuel cell to meet transient power demand. Since *SCs* have high specific power, they can supply great quantities of instantaneous power, allowing to boost the fuel cell in power-demanding situations, such as fast accelerations or climbing. Although the study of Gao is done with a fuel

cell-battery hybrid powertrain composed of lead-acid batteries instead of other type of batteries with higher specific power (e.g., *Li-ion* or *Ni-MH*), the general conclusion still is valid because of the exceptional specific power of *SCs*. In [91], analyzing the requirements of batteries for city hybrid buses, it is remarked that to get a really significant fuel consumption improvement it is essential to be able to recover a good percentage of the available energy during braking and, for that end, devices with high power recharge capability are required.

With regard to the lifetime, it is concluded that actual batteries are not good for automotive applications. However, some modifications in the chemistry of conventional lead-acid batteries are being analyzed in order to operate in high-rate partial-state-of-charge mode with acceptable performance [92]. There are also *ultrabatteries* in development which are hybrid energy-storage devices combining an asymmetric super-capacitor[1] and a lead-acid battery in one unit taking advantage of the best from both technologies without the need for extra electronic controls [93].

6.4   Fuel Cell Hybrid Vehicle model

In order to study *Fuel Cell Hybrid Vehicles (FCHV)* it is necessary to rely on accurate and practical models to describe the system behavior. *ADVISOR* is a system analysis tool for vehicle modelling created by the National Renewable Energy Laboratory (USA) in the *MATLAB/Simulink* environment [26, 27]. It provides a flexible and robust set of models, data, and script text files, which are used to quantify the fuel economy, the performance, and the emissions of vehicles that use alternative technologies including fuel cells, batteries, supercapacitors, electric motors, and internal combustion engines in hybrid configurations.

In this platform, the vehicle is modelled in detail taking into account the several components that compose the vehicle drivetrain (i.e., vehicle, wheel and axle, final drive, gearbox, clutch, fuel converter, etc.). For example, (6.3) determines the mechanical power that is necessary to meet the desired speed v, with road slope α and acceleration $\dot{v}(t)$:

$$P_{mec}(t) = \left(m_T \, g \, f_r + \frac{1}{2} \, \rho_a \, C_d \, A_f \, v(t)^2 + m_T \, g \, \sin(\alpha(t)) + m_T \, \dot{v}(t) \right) v(t). \quad (6.3)$$

---

[1]The term *asymmetric supercapacitors* stands for supercapacitors with different types of electrodes.

Table 6.2: Vehicle specifications in the case of study.

Specification	Symbol	Value	Unit
Vehicle total mass	m_T	1380	kg
Vehicle mass[a]	m_{veh}	882	kg
Frontal area	A_f	2	m^2
Drag coefficient	C_d	0.335	-
Coefficient of rolling friction	f_r	0.009	-
Air density	ρ_a	1.2	$kg\,m^{-3}$
Gravity	g	9.8	$m\,s^{-2}$

[a] Vehicle mass without taking into account the FCS mass and the ESS mass.

This equation performs the force balance among the rolling resistance force, the aerodynamic drag force, the force of gravity that must be overcome to climb a grade and the force required to accelerate, respectively. The meaning of the constants in (6.3) are explained in Table 6.2. Actually, the necessary power supplied by the fuel cell is greater than the determined in (6.3) because of the power losses in the final drive, the gearbox, and the motor. These losses depend on the efficiencies of the components and *ADVISOR* utilizes efficiency maps to compute the power losses according to the present speed.

In this work, we consider the performance of a *FCHV* based on a small car and the entire system being modelled in *ADVISOR* according with the principal parameters listed in Table 6.2. This model is used as a case of study in Section 6.5 and Section 6.6 to exemplify the methodologies proposed.

6.4.1 Fuel Cell System model

The *FCS* consists of the fuel cell stack, which is a serially layered pack of fuel cells, and the auxiliary system, a set of devices necessary for the *FCS* operation that include a compressor, cooling/heating devices, and a water management system. Among the auxiliary components, the compressor is the one with larger power consumption (up to 93.5% of the total auxiliary power consumption [60]). Therefore, the *FCS* is a complex and nonlinear system whose dynamical model, like the one developed by Pukrushpan *et al.* [13], is too sophisticated to be used in an energy management strategy. Even a much simpler model, like the one developed by Correa *et al.* [22], which does not contemplate

the filling dynamics of cathode and anode and the compressor dynamics, is not suitable for that purpose. Moreover, the standard driving cycles in *ADVISOR* are defined every 1 *s* and the transient response of the *FCS* generated power is shorter than 1 *s*. Thus, a static model as the one employed in the *ADVISOR* platform is adequate to represent the *FCS* when the objective is to implement adequate management strategies.

The most relevant characteristic of the *FCS*, with major impact in its performance, is the hydrogen consumption: the relation between the delivered power and the hydrogen consumption (see Fig. 6.3). This consumption map constitutes a static characteristic of the *FCS* and it does not take into account any others. It is assumed that the *FCS* is controlled by its own controller, a control algorithm that deals with the *FCS* control variables to maintain the system operating properly with the load changes. This issue has been covered in Chapter 4.

Given that in the hybridization degree analysis it is necessary to account with models representing *FCS* of different sizes, it is needed to scale the original model to represent *FCSs* with different rated power. In the work of Kim et al. [60], it is concluded that it is possible to linearly scale the efficiency map of the *FCS*. This conclusion is reinforced by the work of Ahluwalia *et al.* [94], where four *FCSs* with different rated power in study are also linearly scaled, and also is the way in that *ADVISOR* toolbox works.

This consideration of a linear relationship between different scaled *FCS* is possible because of the followings reasons. Firstly, the rated power of the *FCS* depends on the number of cells and the active area of each cell of the fuel cell stack. The polarization curve is practically unaffected by the cell number in contrast to the active area of the cells, which affects the design of the reactant flow channels, influencing the humidity and thermal characteristics of the stack and, consequently, changing the polarization curve [60]. Thus, it is possible to account with fuel cell stacks of different rated power and polarization curve linearly scalable by changing the cell number. Secondly, it is also possible to linearly scale the efficiency map of the compressor, which is, as already said, the auxiliary component with major consumption.

A set of hydrogen consumption maps and a set of efficiency maps are plotted in Fig. 6.3 for different *FCS* rated powers, using data from *ADVISOR*. The efficiency

maps are derived from the consumption maps:

$$\eta_{fcs} \; [\%] = \frac{360 \times 10^3}{Cons_{H_2} \cdot LHV_{H2}}, \tag{6.4}$$

where the hydrogen consumption $Cons_{H_2}$ is expressed in $g \; kWh^{-1}$ and LHV_{H2} is $120 \; kJ \; g^{-1}$. In the four efficiency maps, the efficiency at rated power is 50% and the the maximum efficiency (60%) is at 25% of the rated power.

6.4.2 Energy Storage System model

The energy storage system, either if it is based on batteries or supercapacitors, can be modelled with two subsystems. One subsystem takes into account the system efficiency, both during charging and discharging, and the other subsystem computes the actual energy level. The energy stored in the storage system, $E_{ess}(t)$, results integrating $P_{ess}(t)$:

$$E_{ess}(t) = E_{ess}(0) + \int_0^{t_c} P_{ess}(t)dt. \tag{6.5}$$

It is useful to define a parameter that indicates the relative amount of energy in the *ESS*. The *State of Energy, SoE(t)*, is defined as

$$SoE(t) = \frac{E_{ess}(t)}{E_{cap}} \times 100 \qquad [\%], \tag{6.6}$$

where E_{cap} is the maximum energy that the storage system is capable to store. In discrete time the storage system energy, at the time instant k, is

$$E_{ess}(k) = E_{ess}(0) + \sum_{k=1}^{N_c} P_{ess}(k)\Delta t, \tag{6.7}$$

where $N_c = t_c/\Delta t$, t_c is the duration of the driving cycle, and Δt is the sampling time. The *SoE(k)* results

$$SoE(k) = \frac{E_{ess}(k)}{E_{cap}} \times 100 \qquad [\%]. \tag{6.8}$$

Figure 6.4 shows an electrical equivalent model for an *ESS* composed of supercapacitors. Actually, the equivalent circuit is more complex, like the one used in [95], but for the purpose of designing and analyzing the performance of the system, the model in Fig. 6.4 is a good approximation. In fact, this model is similar to the one employed in [61] for these purposes.
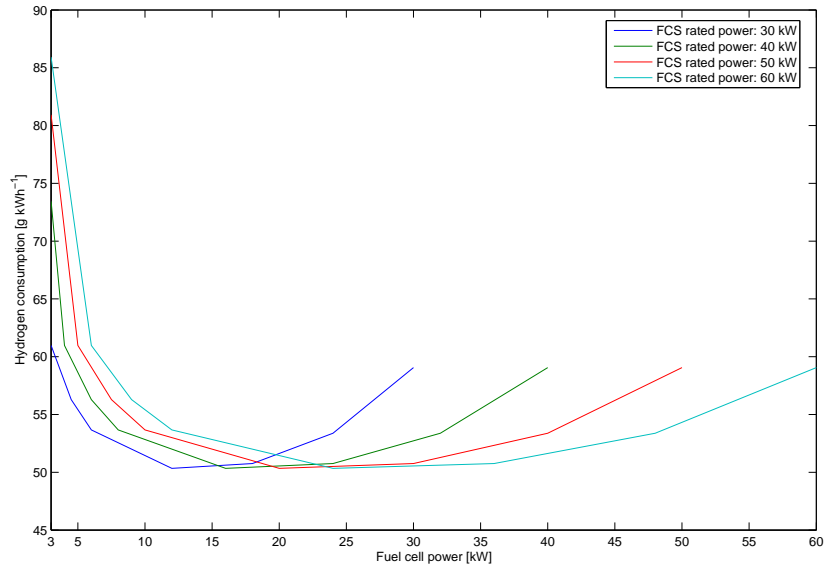
(a) Hydrogen consumption maps.
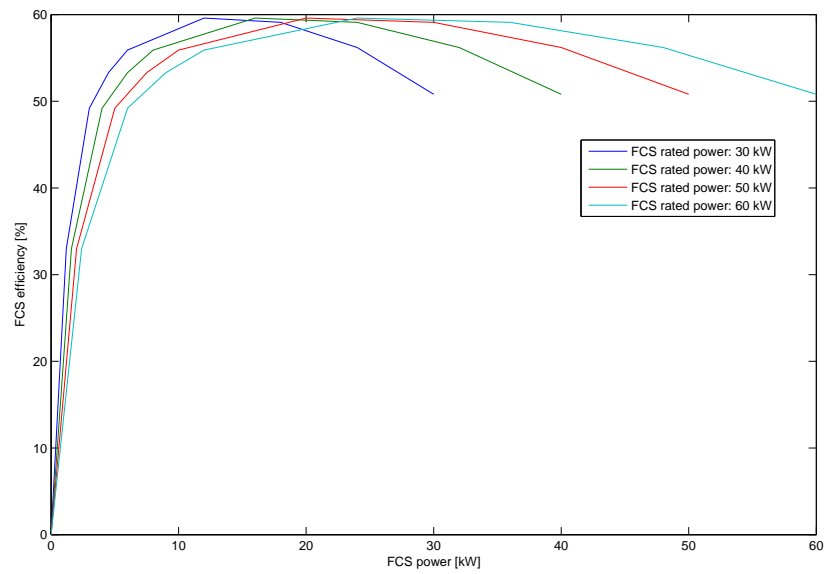
(b) Efficiency maps.

Figure 6.3: Hydrogen consumption and efficiency maps for different rated powers.

Figure 6.4: Equivalent model for the supercapacitor unit

The *ESS* efficiency, in this case a supercapacitor bank, is related with the equivalent series resistance (*ESR*). For a pure capacitor, having zero *ESR*, the efficiency of charge or discharge would be 100%. However, in a real capacitor, having nonzero *ESR*, the irreversible dissipation of power is $E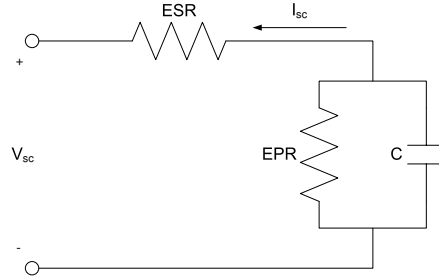SR \cdot I_{sc}^2$, giving efficiencies lower than 100%. The equivalent parallel resistance (*EPR*) represents the self-discharge losses and only impacts long-term energy storage performance of the *SC* and is extremely high [33]. Thus, the time constant of the period of charge/discharge can be expressed by $ESR \cdot C$. Since *ESR* is as low as $0.019\,\Omega$ and C is 58 F [96], it is possible to charge and discharge the *SC* in a very short time. The energy stored in the *SC* is directly proportional to the capacitance and the squared voltage:

$$E_{SC}(t) = \frac{1}{2}C\,V_{sc}^2(t). \tag{6.9}$$

Besides, the power that the *SC* is capable to deliver or to store is inversely proportional to the internal resistance and directly proportional to the squared voltage:

$$P_{SC}(t) = \frac{k_{SC}\,V_{sc}^2(t)}{ESR}, \tag{6.10}$$

where k_{SC} is a constant depending on the particular device. Thus, it is possible to express the power as a function of the energy in the *SC*, instead of $V_{sc}^2(t)$:

$$P_{SC}(t) = \frac{2\,k\,E_{SC}(t)}{ESR \cdot C}, \tag{6.11}$$

an expression that is more convenient, because the proportional relationship between power and energy. In this way, we work with the state of energy, $SoE(t)$, instead of the state of charge, $SoC(t)$.[1]

---

[1]The state of charge, $SoC(t)$, is defined as the relation between the actual charge voltage and the maximum charge voltage in a capacitor, whereas the $SoE(t)$ is defined as the relation between the actual energy and the maximum charge energy.
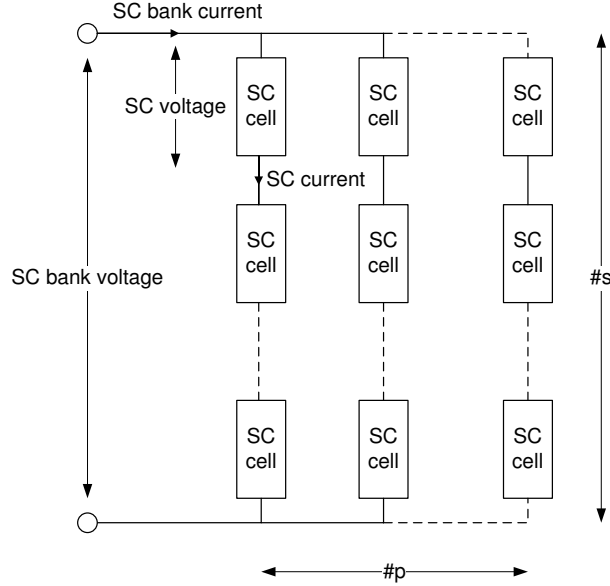
Figure 6.5: Distribution of supercapacitors in a *SC* bank

The *ESS* can be conformed using several equal *SCs* and connecting them in series and parallel. The total capacitance and total resistance of the bank are calculated as

$$R_{ess,\,total} \quad = \quad \#s\frac{ESR}{\#p} \tag{6.12}$$

$$C_{ess,\,total} \quad = \quad \#p\frac{C}{\#s}, \tag{6.13}$$

where $\#s$ is the number of *SCs* connected in series and $\#p$ is the number of series string connected in parallel (see Fig. 6.5).

The *SC* bank voltage is

$$V_{SC,\,total} = \#s \cdot V_{SC,\,max} \tag{6.14}$$

and the total system energy results

$$E_{SC,\,total} = \#_{SC} \cdot E_{SC}, \tag{6.15}$$

where $\#_{SC} = \#p \cdot \#s$ is the total number of *SCs* connected in the bank.

6.4.3 Characteristic load demand

In order to evaluate the performance of a given *FCHV*, standard drive cycles are widely utilized in the literature. These standardized speed profiles, representing urban and

101

Table 6.3: Key statistics of driving cycles

	NEDC	UDDS	FTP	HWFET
Distance $[km]$	10.93	11.99	17.77	16.51
Maximum speed $[km\ h^{-1}]$	120	91.25	91.25	96.4
Average speed $[km\ h^{-1}]$	33.21	31.51	25.82	77.58
Maximum acceleration $[m\ s^{-2}]$	1.06	1.48	1.48	1.43
Maximum deceleration $[m\ s^{-2}]$	-1.39	-1.48	-1.48	-1.48
Average acceleration $[m\ s^{-2}]$	0.54	0.50	0.51	0.19
Average deceleration $[m\ s^{-2}]$	-0.79	-0.58	-0.58	-0.22

highway scenarios, were originally stated for measuring pollutant emissions and gasoline economy of engines [97]. Four standard driving cycles are plotted in Fig. 6.6 and Fig. 6.7: the *New European Driving Cycle (NEDC)*, the *Urban Dynamometer Driving Schedule (UDDS)*[1], the *Federal Test Procedure (FTP)*, and the *Highway Fuel Economy Cycle (HWFET)*.

In each figure, two magnitudes are plotted: the speed profile and the demanded power to fulfill the profile. The calculation of the power demand is done exploiting the model developed in *ADVISOR* according to the parameter of the small vehicle described in Table 6.2 (vehicle total mass of $1380\,kg$).

The *NEDC* cycle includes four intervals representing urban driving conditions, repeated without interruption, followed by one interval representing extra urban driving conditions with a more aggressive, high speed, profile. The *UDDS* cycle and the *FTP* represent city driving conditions whereas the *HWFET* cycle represents highway driving conditions. In Table 6.3, the key statistics about the driving cycles are showed concerning speed, acceleration and deceleration.

The power histogram corresponding to the four driving cycles are plotted in Fig. 6.8. It is observed that most of the time the *FCS* is operating in an unfavorable zone. This fact reaffirms the idea of implementing an adequate energy management strategy to overcome this drawback. This issue is studied in Chapter 7.

During a driving cycle, the power required by the vehicle varies strongly from very

---

[1]It is also known as *Federal Urban Driving Schedule (FUDS)*.
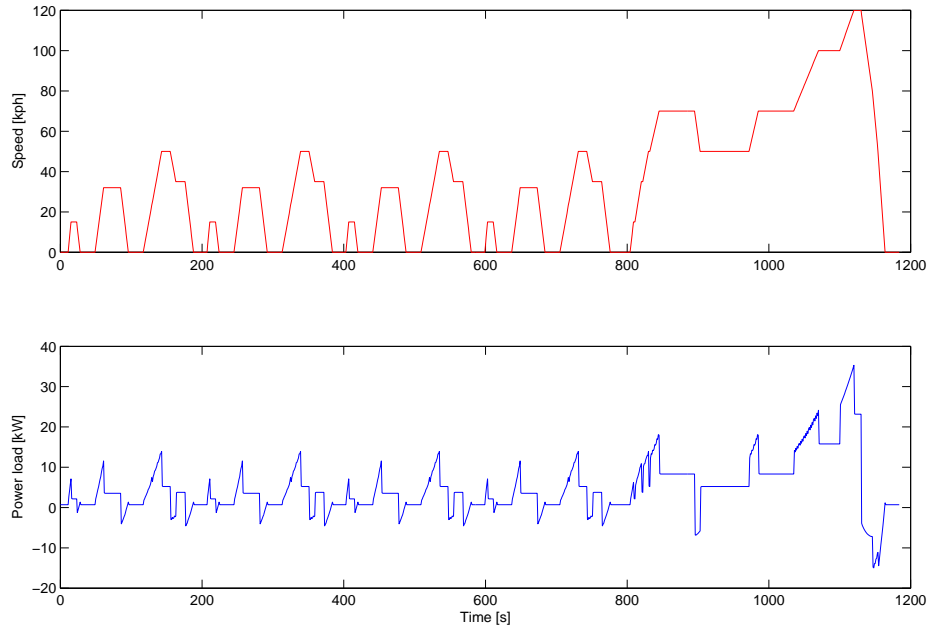
(a) New European Driving Cycle (NEDC)
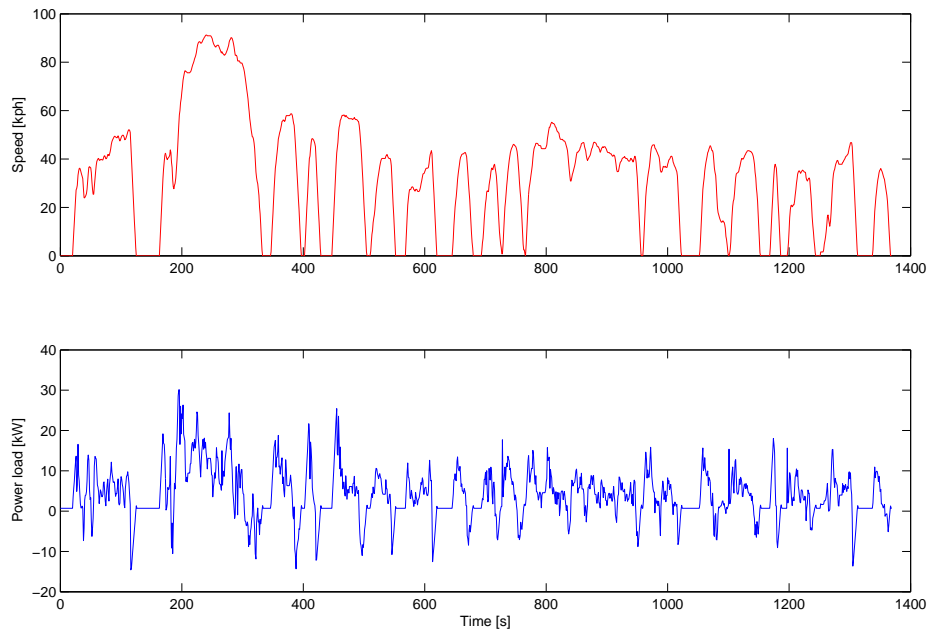
(b) Urban Dynamometer Driving Schedule (UDDS)

Figure 6.6: Speed and power profiles for the *NEDC* and the *UDDS* standard driving cycles for a vehicle of total mass 1380 *kg*.
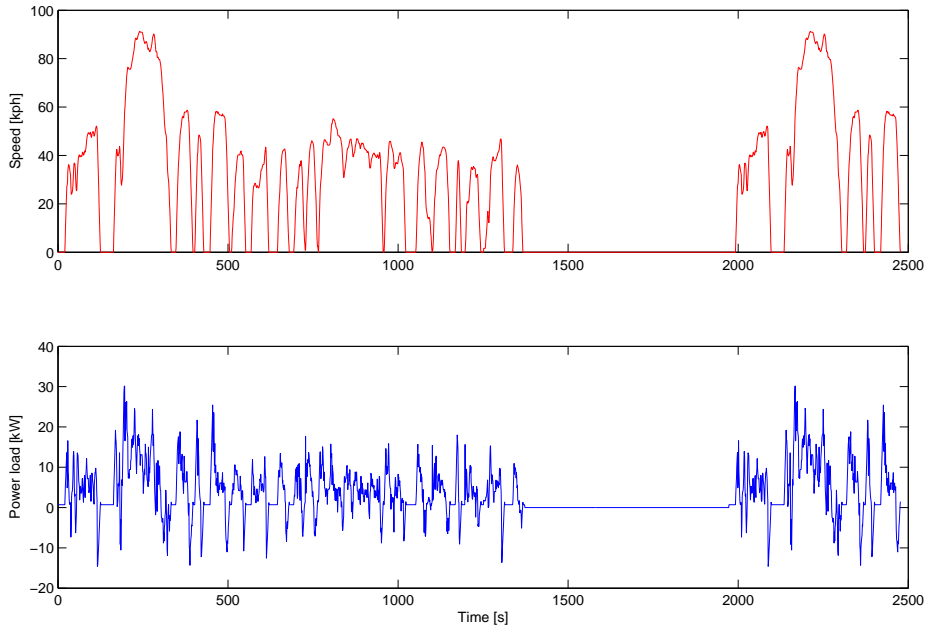
(a) Federal Test Procedure (FTP)
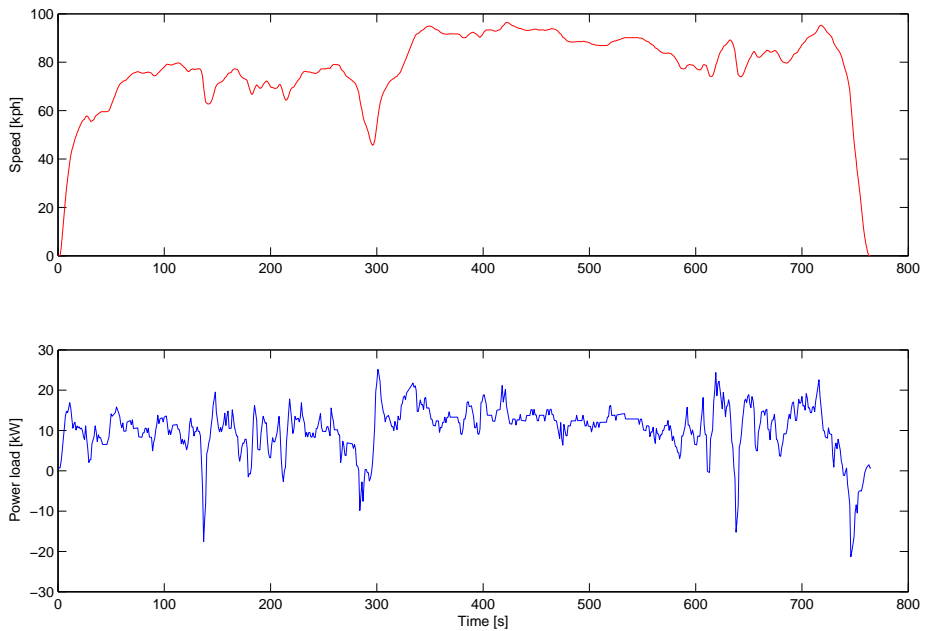
(b) Highway Fuel Economy Cycle (HWFET)

Figure 6.7: Speed and power profiles for the *FTP* and the *HWFET* standard driving cycles for a vehicle of total mass 1380 *kg*.
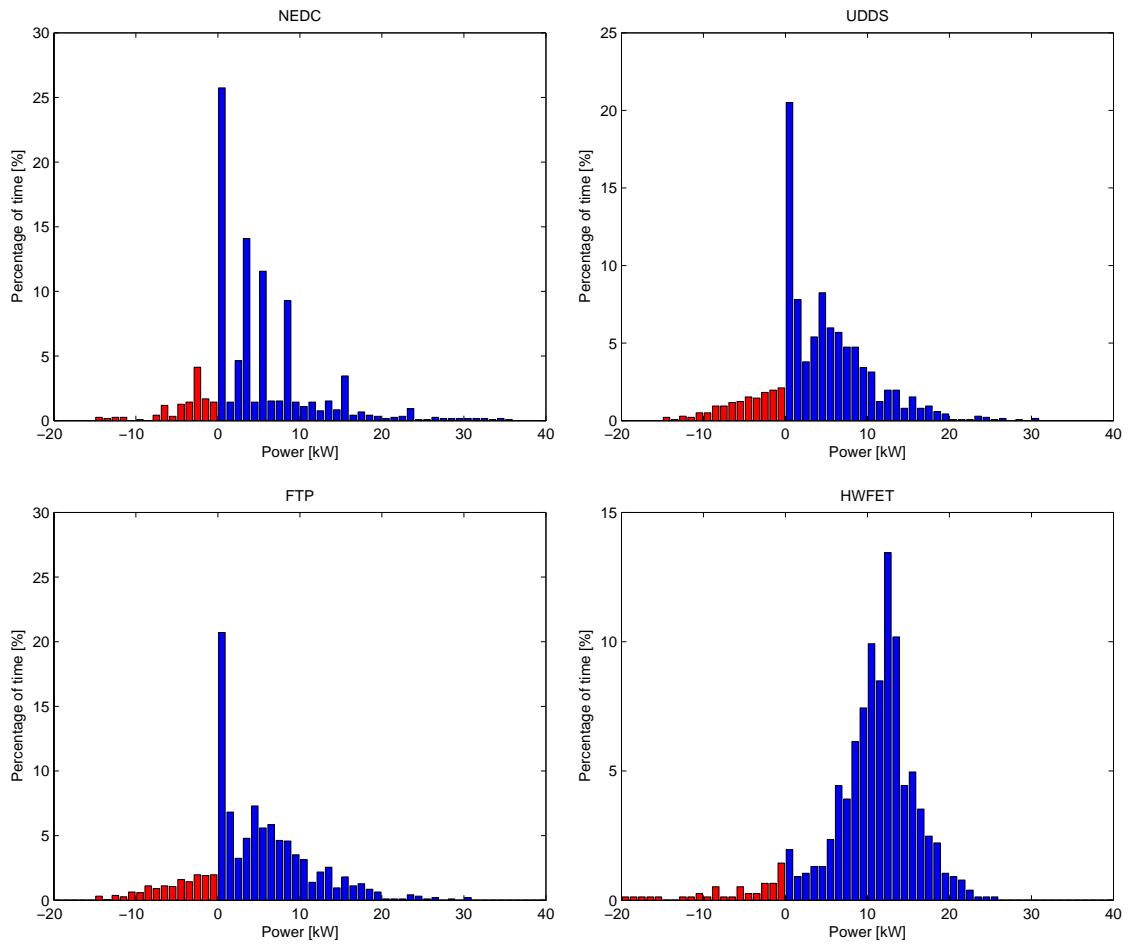
Figure 6.8: Power histogram for the vehicle in study of total mass 1380 kg running in different standard cycles.
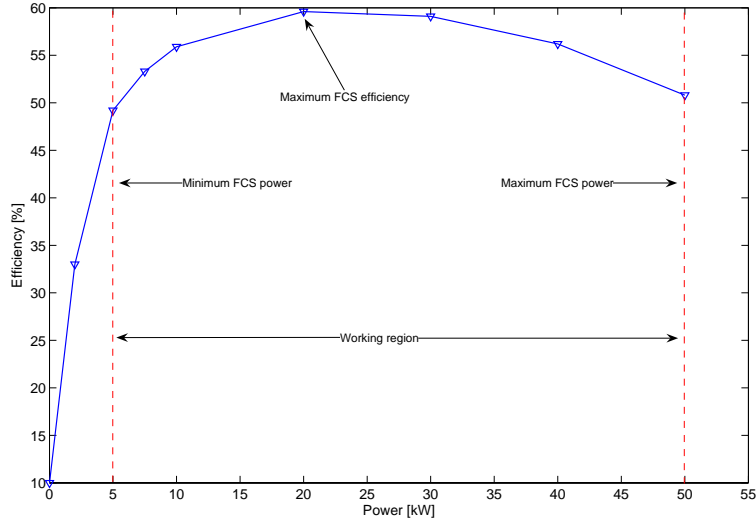
Figure 6.9: Efficiency curve for a *50-kW FCS* from *ADVISOR* model.

low powers to relatively high powers. High power requirements take place during a relatively short fraction of time. If there is no energy storage, the *FCS* must meet the highest peak power and, therefore, the *FCS* is oversized most of the time. In addition, the efficiency of a *FCS* is strongly degraded at low powers (see Fig. 6.9). Thus, if no hybridization is present, the *FCS* has to work in large periods of time at a low efficiency zone. On the contrary, with an additional power source and a suitable energy management strategy it is possible to avoid these unfavorable operating zones. Thus, the hydrogen economy can be improved through hybridization.

Analyzing a typical efficiency curve for a *50-kW FCS* according to *ADVISOR* model (see Fig. 6.9), it is concluded that the energy management strategy has to avoid the *FCS* operation at powers smaller than 5 *kW* because the efficiency is strongly degraded below 50%. With this model (Fig. 6.9) of *FCS* the maximum efficiency is obtained operating at 20 *kW*. In this case, the *FCS* efficiency is approximately 60%. Within the range of 5 to 50 *kW*, the efficiency is high enough, close to the maximum value. Therefore, a good strategy would be one that allows the *FCHS* to work most the longest possible periods of time close to the point of maximum efficiency. This strategy would depend on the *ESS* state-of-energy. For example, if the load power is greater than the maximum efficiency power and there is no sufficient stored energy to meet the power balance,

then, the strategy has to move the operating point toward the zone of higher power although the *FCS* efficiency is worse. The opposite situation takes place if the load power is lower than the maximum efficiency power and there is no sufficient capacity of storage in the *ESS*.

The question is how to determine the most convenient operating point at every time. It is necessary to formulate a functional cost that quantifies the increase of the hydrogen consumption produced by the displacement from the maximum efficiency point. But in addition, it is necessary to relate this functional to the state of energy in the *ESS*, not only considering if at the present time the state of energy is suitable to meet the power balance, but also considering the more foresighted point of view of the future power requirements. This is difficult to achieve because the driving cycle is not known a priori. This point is studied in Chapter 7.

6.5 Analysis of the energy flows in the *FCHV*

In Section 2.2.1, it was stated that in a *FCHV* there are four principal energy flows between the fuel cell system, the energy storage system, and the electric load. Entering more into detail, the energy flow from the hydrogen tank towards the wheels through the power bus, the electric motor and the gearbox can be seen in Fig. 6.10 for the case of study with the main parameters listed in Table 6.2, running on the *NEDC*. The number in the arrows corresponds to the total energy transferred between components or the total losses in the components along the load profile in study. Each component has its own losses, except the power bus which is considered ideal. Thus, the initial amount of energy from the hydrogen tank is degraded. Besides, the vehicle employs energy to overcome the rolling resistance and the aerodynamics drag force. In the same figure, it is also represented the wheel-to-ESS flow, the energy flow from regenerative braking to the *ESS*, which also diminishes due to the losses in the components.

As it was mentioned in Section 2.2.2, the amount of energy that it is possible to recover from regenerative braking depends on the particular driving cycle. Our results show that for a *FCHV* according to the parameters of Table 6.2 (total mass of 1380 kg), the maximum recoverable energy represents the 7.6% of the hydrogen energy that is spent to fulfill the *NEDC* cycle, whereas, in the case of *UDDS* and *FTP*, it represents
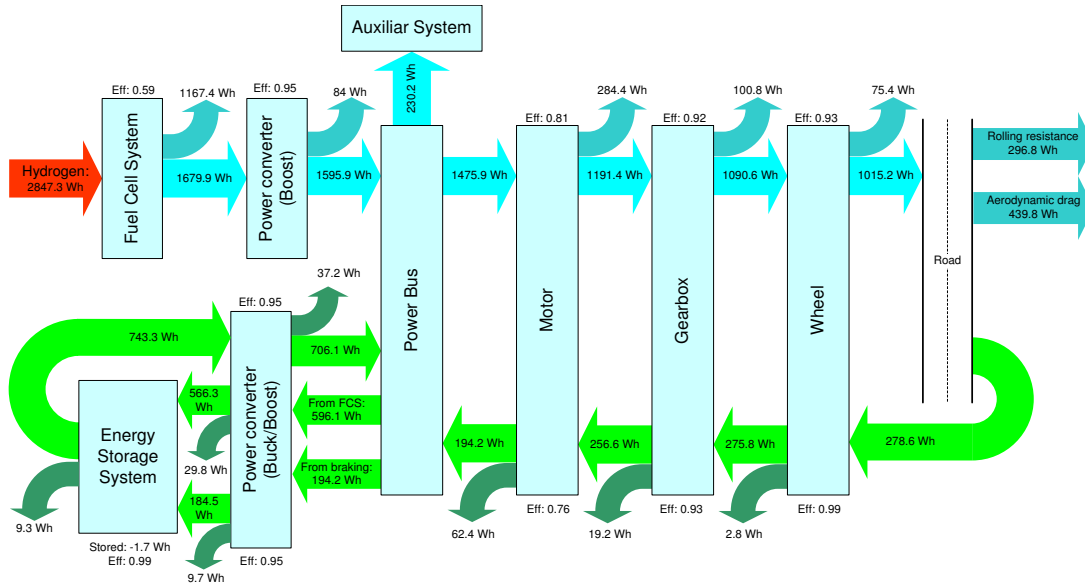
Figure 6.10: Energy flow in the *FCHV* running on *NEDC*.

the 11.7% and 11.4%, respectively. On the other hand, in a highway cycle like *HWFET*, the regenerative braking energy only represents the 2.3% of the hydrogen energy. Some works report greater ratios of energy recovery. For example, in [98], it is reported that in *NEDC* cycle with a similar vehicle, the braking energy is 35% of the traction energy, meanwhile with the *UDDS* cycle the braking energy ups to 50%. Nevertheless, theses ratios only account for the energy available at the wheel. If the losses in the internal components where the energy passes through are taken in account, the braking energy available at the storage system is much lower. It is also important to note that all these ratios are calculated in the limit situation where no friction brake is used and assuming that in the *ESS* there is always sufficient capacity to store the available energy, allowing the maximum energy recuperation. Thus, these ratios only represent a superior limit and in real situations the available energy to store may be lower. Table 6.4 summarizes the main values of the energy flow analysis for the four cycles in study.

Table 6.4: Energy flow summary in a 1380-kg *FCHV*.

	NEDC		UDDS		FTP		HWFET	
	$[Wh]$	$[\%]^a$	$[Wh]$	$[\%]^a$	$[Wh]$	$[\%]^a$	$[Wh]$	$[\%]^a$
Hydrogen energy	2847	100	2957	100	4416	100	4141	100
FCS energy out	1680	59.0	1744	59.0	2605	59.0	2442	59.0
FCS losses	1167	41.0	1213	41.0	1811	41.0	1699	41.0
Motor energy in	1476	51.8	1611	54.5	2419	54.8	2148	51.8
Total losses in power mode[b]	461	16.2	538	18.2	775	17.5	622	15.0
Total losses[c] in regenerative mode	84	3.0	144	4.9	202	4.6	39	0.9
Recovered energy from braking	194	6.8	310	10.5	452	10.2	86	2.1
Rolling resistance energy	297	9.4	326	11.0	482	10.9	448	10.8
Aerodynamic drag energy	444	15.4	293	9.9	508	11.5	953	23.0

[a] The % column refers to the percentage of energy with respect to the hydrogen energy.
[b] The total losses in power mode is the summation of the losses in the direct path from the *FCS* to the wheels.
[c] The total losses in regenerative mode is the summation of the losses in the path from the wheels to the *ESS*.

6.6 Determination of the Hybridization Degree according to drivability conditions

In order to be competitive with conventional vehicles, *FCHVs* must satisfy different types of driving conditions. This means that, both in transitory and sustained driving conditions, the power balance between the load and the power sources must be satisfied. In the case of time sustained driving conditions, the fuel cell must be able to meet situations such as high speed driving or overcoming a certain gradient. On the other hand, the combined *FCS* and storage system must be able to meet transitory conditions such as accelerations. In this sense, in the work of Ahluwalia *et al.* [98] it is stated that the hybrid system must satisfy the following requirements. Firstly, the FCS by itself must be capable of supporting time sustained driving conditions. This requirement
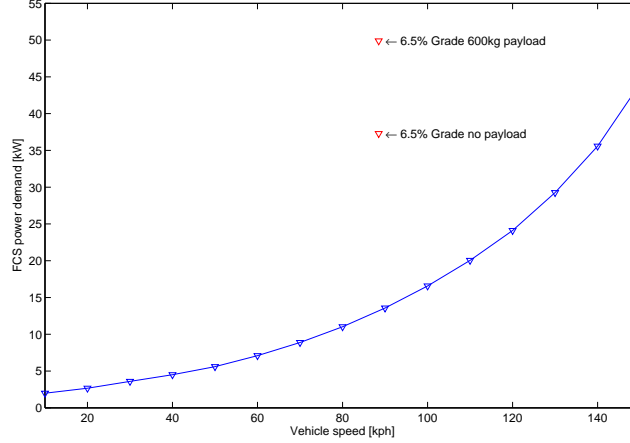
Figure 6.11: Power demand vs. vehicle speed for a vehicle of 1380 kg.

includes two different tests: a top speed test where a specified speed is maintained and a grade test where the vehicle must maintain a determined speed with a determined grade and a certain overweight. Secondly, with the assistance of *ESS*, the hybrid system must be able to fulfill a certain acceleration requirement.

Assuming the drivability requirements and exploiting the *FCHV* model developed in the *ADVISOR* environment, it is possible to quantify the amount of power that the powertrain needs to supply to fulfill the traction requirements. In Table 6.5, the power demands to fulfill each traction power requirement is presented. These powers correspond to a vehicle with total mass of 1380 kg. Besides, the power demand to maintain different sustained speeds and the power demand to maintain a sustained speed of 88.5 kph with a grade of 6.5% are shown in Fig. 6.11.

The hybridization degree analysis according to drivability conditions consists in determining the *FCS* rated power and the amount of supercapacitors in the *ESS* necessary in order to fulfill the requirements stated in Table 6.5. Once these two design variables are determined, it is possible to calculate the total mass of the vehicle as the summation of the mass of the *FCS*, m_{FCS}, the mass of the *ESS*, m_{ESS}, and the mass of the basic vehicle, $m_{veh,\ basic}$:

$$m_{veh,\ total} = m_{ESS} + m_{FCS} + m_{veh,\ basic}. \tag{6.16}$$

Table 6.5: Power demand to fulfill the traction power requirements for a 1380 kg vehicle.

Traction power requirements	Power [kW]
Sustained driving conditions	
Top speed (150 kph)	44.1
88.5 kph at 6.5 % grade without overweight	37.3
88.5 kph at 6.5 % grade with overweight (600 kg)	49.9
Transitory driving conditions	
Acceleration (0 to 96.5 kph in 10 s)	93.1

The mass of the basic vehicle is the mass of the vehicle without the *FCS* and the *ESS* (i.e., without the powertrain), but it is not a constant mass. It depends on the chosen *FCS* because the mass of the auxiliary system in the vehicle depends on the rated power of the *FCS*.

The procedure followed for dimensioning the hybridization degree is represented in Fig. 6.12. The first step of this dimensioning process concerns the time sustained conditions. The dimensioning process starts with the calculation of the minimum necessary *FCS* that a vehicle of 1380kg, according with the case of study defined in Section 6.4, needs to meet the top sustained speed requirement. Then, the process continues with the calculation of the minimum necessary *FCS* that the vehicle needs to meet the grade requirement. Both estimations are done using only the *FCS* to power the vehicle because it is a sustained power and because it is sustained, it can only be supported by the *FCS*. The *FCS* that fulfills the two requirements is the maximum value between the two results. Then, the vehicle mass is calculated according to the mass of this *FCS* using (6.16). In this step, m_{ess} is assumed to be null.

The second step is related to the acceleration test and consists in the determination of the minimum amount of supercapacitors in the *ESS* that is necessary to add to the previous *FCS* to reach the acceleration requirement. Once this step is done, the total mass is recalculated according to the determined number of supercapacitors using (6.16).
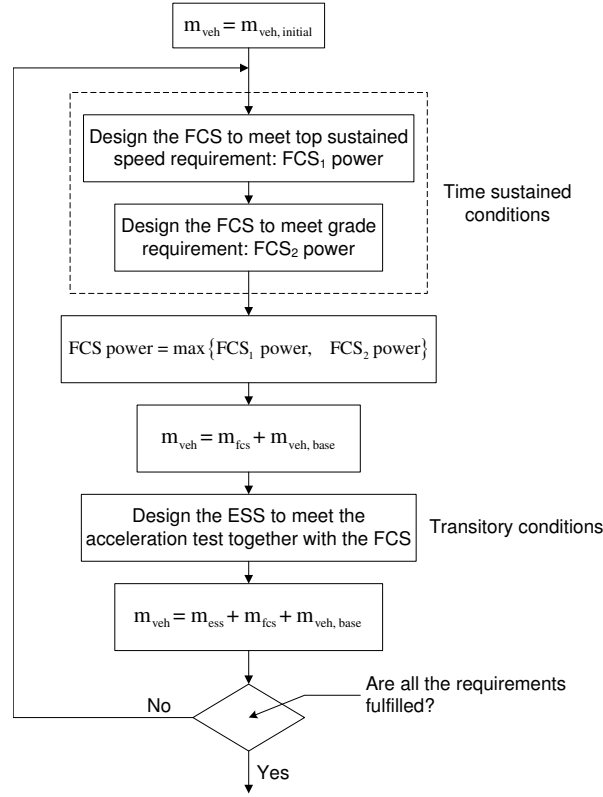
Figure 6.12: Schematic diagram of the hybridization degree analysis according to drivability conditions.

The procedure is repeated from the first step using the vehicle mass calculated in the last step until the results converge in a combination of FCS and ESS such the vehicle is capable to meet both the sustained and the transitory driving conditions.

The results show that the minimum FCS is $35\,kW$ and the minimum supercapacitor bank is 130 modules. Each module in the ADVISOR model has a specific power of $2.5\,kW\,kg^{-1}$ and a specific energy of $6\,Wh\,kg^{-1}$ with a mass of $0.408\,kg$. Thus, the maximum energy in the bank is $318.2\,Wh$ and the final total mass of the vehicle results in $1109\,kg$.

However, this is the minimum value of FCS and there is still a degree of freedom in the final selection between two extreme cases: the case with *35-kW FCS* and *130-module* bank, and the pure FCS case (with a larger FCS and no ESS) where all the power needed is supplied by the FCS. Therefore, an analysis is performed varying the
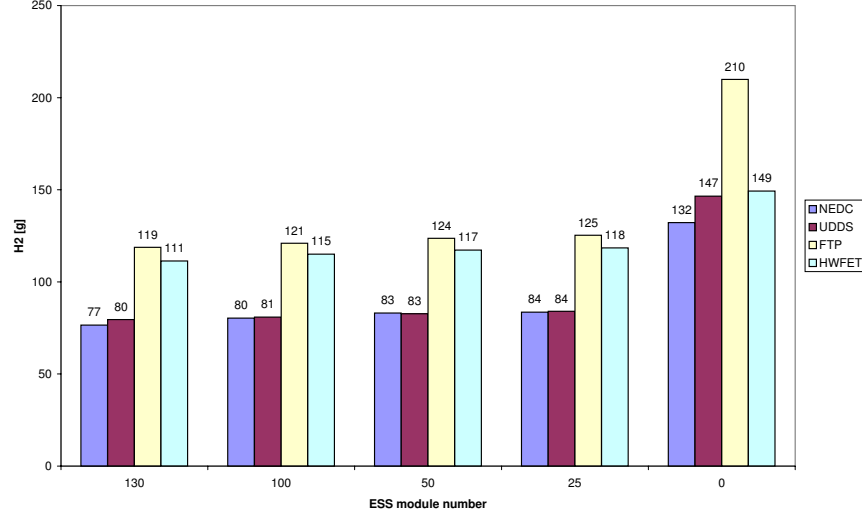
Figure 6.13: Hydrogen consumption for different Hybridization Degrees (*FCS* power and *ESS* module number).

ESS module number (i.e., varying the hybridization degree), and for different driving cycles, to find the combination with the lowest hydrogen consumption.

The results of hydrogen economy and total mass, shown in Fig. 6.13 and Fig. 6.14, reveal that the best option, with lower mass and lower hydrogen consumption is the vehicle consisting in a *FCS* of 35 *kW* and an *ESS* bank of 130 modules. In this case, the total vehicle mass results to be 1109 *kg* and the hybridization degree is 79%. With regard to Fig. 6.13, the hydrogen consumption is the optimal. It is remarkable the relatively insensitive of the hydrogen consumption varying the *ESS* module number. This is because the increase of the optimal consumption in this analysis is only produced by the increase in the vehicle mass. On the contrary, in the case of *ESS* module number null, the increase in the optimal hydrogen consumption is high because there is no possibility of energy recovery. The computation of these hydrogen optimal consumptions are done using the analysis formulated in the following section.
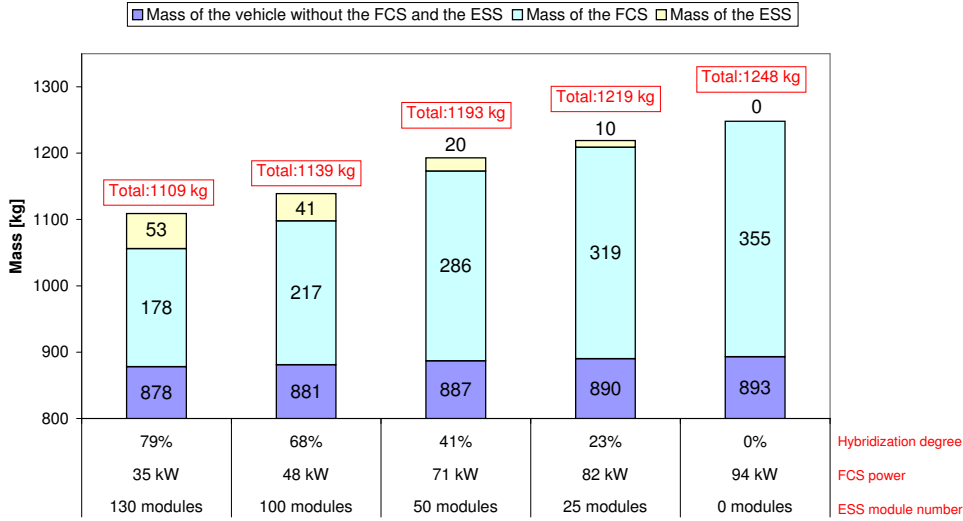
Figure 6.14: Total vehicle mass for different Hybridization Degrees (*FCS* power and *ESS* module number).

6.7   Computation of the optimal hydrogen consumption in the *FCHV*

In the previous section, the optimal hydrogen consumption is indicated for different profiles. In order to evaluate the performance of the Energy Management Strategies *EMSs*, which are developed in Chapter 7, in terms of hydrogen consumption, it is also useful to determine the minimum amount of hydrogen that a specified vehicle needs to achieve a given driving speed profile. Thus, each *EMS* will be evaluated comparing its hydrogen consumption with respect to the consumption in optimal conditions, a reference context that represents the minimum amount of hydrogen necessary to achieve the load profile. In some works, e.g., [99, 100, 101], this analysis is performed through the use of the *Dynamic Programming* (*DP*) technique, a procedure that allows to determine a global optimal operation of the system for a given load profile by evaluating all possible control sequences in a systematic way [99]. However, a disadvantage of this technique is the relative long computation time due to the large required grid density. The grid is the result of the discretization of time and the state variables in appropriate grid-levels. The grid density should be taken high, because it influences the accuracy of the result.

In this work, we propose a method to analyze the minimum hydrogen consumption

with reduced computational cost because it avoids the discretization of the state variables. Only the time is discretized because the standard driving cycles in _ADVISOR_ are defined every $1\,s$. The procedure is based on the following assumptions:

- The capacity of storage in the _ESS_ is sufficient to recover all the available energy from regenerative braking

- The friction brake is not employed during the entire cycle

- When the power consumption is null the _FCS_ is turned off

- The _FCS_ is already hot at the nominal operating temperature when the cycle starts

- The total vehicle mass is known and in our case of study it is $m_{veh} = 1109\,kg$

A simulation is performed for each driving cycle in such a way that the _FCS_ works alternately in two operating points, namely _"On"_ and _"Off"_, according to the actual $SoE(k)$:

- When $SoE(k) \leq SoE(0)$, the _FCS_ is operated at its point of maximum efficiency (the _"On"_ point).

- When $SoE(k) > SoE(0)$, the _FCS_ is turned off (the _"Off"_ point).

As a result, the final state of energy $(SoE(N))$ is into a reduced range around the initial state of energy $(SoE(0))$.

Thus, the hydrogen consumption only accounts the necessary hydrogen to fulfill the cycle of duration N. The main advantage of this method is that, unlike the usual methodology used in the literature, which is based on _Dynamic Programming_, it avoids the discretization of the state variables and only the time is discretized because the standard driving cycles that are utilized in _ADVISOR_ are defined every $1\,s$. Therefore, this methodology allows the calculation of optimal hydrogen consumption in the _FCHV_ with low computational time, maintaining a high accuracy. Figure 6.15 shows a scheme with the _FCS_ operation to perform the calculation previously described and the results are collected in Table 6.6, where the _braking/hydrogen ratio_ is defined as the ratio
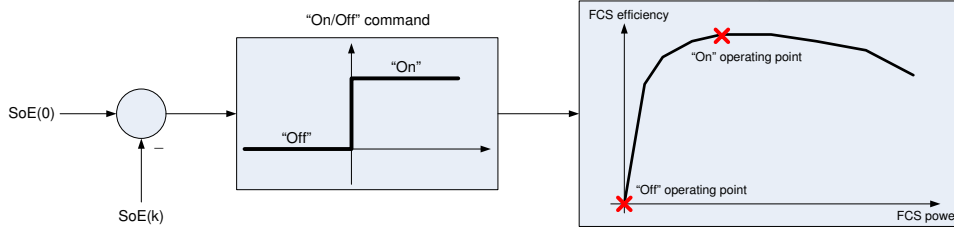
Figure 6.15: Scheme showing the *On/Off* operation of the *FCS* model to perform the analysis of the minimum hydrogen consumption.

between the energy recovered from braking in the *ESS* and the energy of the hydrogen, calculated from the *Lower Heating Value* (ΔH_{LHV}) of hydrogen, consumed in the *FCS* during the cycle. Since the *FCS* is either working at the point of maximum efficiency or it is turned off (with the assumption that when the *FCS* is turned off the power consumption is null), the calculation of the minimum consumption is guaranteed.

Table 6.6: Results from the analysis of the optimal hydrogen economy for a vehicle of 1109 *kg*.

	NEDC	UDDS	FTP	HWFET
Hydrogen consumption [g]	77	80	119	111
Hydrogen consumption [$g\ km^{-1}$]	7.0	6.6	6.7	6.7
Braking recovery [Wh]	194.2	310.4	452.4	85.8
Braking/hydrogen ratio[a] [%]	7.6	11.7	11.4	2.3

[a] The braking/hydrogen ratio is defined as the ratio between the energy recovered from braking in the *ESS* and the energy of the Lower Heating Value energy of the hydrogen consumed in the *FCS*.

6.8 Discussion

From the design process explained in Section 6.6 it is remarkable that despite the rated power of the resulting *FCS* is 35 *kW*, the power demand is quite lower in the standard driving cycles most of the time. In fact, in *NEDC*, *FTP*, and *UDDS*, the most common demand is in the range from 0 to 15 *kW*, whereas in *HWFET* the power demand is concentrated around 12.5 *kW*. Thus, the *FCS* is often working disadvantageously, specially in *NEDC* and *UDDS*, since the efficiency is low in this range. Consequently, there is a conflict between drivability and efficiency because the minimum *FCS* size to

accomplish drivability is too high and does not permit to operate at the more efficient FCS range for the most common demands.

From the analysis of Section 6.5 and Section 6.7, it is noticeable the high percentage of recoverable energy from braking in the urban driving cycles (*NEDC*, *UDDS*, and *FTP*) assessed by the braking/hydrogen ratio in Table 6.6. This ratio is a good indicator of the amount of energy that is actually reused since the model is developed into a great detail and all the losses in the components of the vehicle are taken into account. In contrast, the parameter that is used to indicate the recovered braking energy in [98] is a fraction of the traction energy and, consequently, is much higher. However, this parameter does not indicate the fraction of the energy from hydrogen that is really regenerated.

6.9 Conclusions

In this chapter, the design of *Fuel Cell Hybrid Systems* oriented to auto- motive applications is approached and some relevant aspects related to the hydrogen economy are analysed. First, the advantages of this kind of power systems are analyzed focusing in the mechanism that allows the improvement of the efficiency of *FCHVs*. Then, the electrical structures for *FCHVs* are addressed, analyzing the electrical topology, comparing two types of energy storage devices (i.e., batteries vs. supercapacitors) and concluding that supercapacitors seem the best technical alternative nowadays , analyzing the requirements of *HEVs* concerning the storage system, and, finally, modelling the energy storage system. The main conclusions of this chapter are:

- Using a detailed model in *ADVISOR* to perform a precise study of the system, the results show that through hybridization it is possible to improve the hydrogen economy in *FCHVs* significantly, compared with the pure fuel cell case without supercapacitors (Fig. 6.13): 41.7% on *NEDC*, 45.6% on *UDDS*, 43.3% on *FTP*, and 22.5% on *HWFET*. This is possible because of the reduction on the total mass of the vehicle, the more efficient operation of the *FCS*, and the energy recovery from braking.

- In the determination of the hybridization degree there is a conflict between driv-ability and efficiency, which means that the design necessary to fulfill drivability requirements is not the most efficient in terms of hydrogen economy.

- The braking/hydrogen ratio defined in Section 6.7 is a more realistic indicator than other parameters used in the literature to analyze the reduction of the hydrogen consumption due to regenerative braking. It shows that is possible to recover up to 7.6% of the hydrogen energy on *NEDC*, 11.7% on *UDDS*, 11.4% on *FTP*, and 2.3% on *HWFET*.

The main contributions of this chapter stem from three methodologies proposed to design and analyze *FCHS*. Firstly, an iterative and systematic methodology to determine the hybridization degree to fulfill drivability requirements. Secondly, a new method to assess the optimal hydrogen consumption with low computational cost that avoids the discretization of the state variables. This method demonstrated to be useful to evaluate the performance of any energy management strategy because it provides a benchmark to compare the hydrogen consumptions of each strategy. Thirdly, a proce-dure to analyze the energy flows inside the *FCHV* was done. This procedure allows the calculation energy flows for a given *FCHV*, including the calculation of the fraction of energy from regenerative braking.

Chapter 7

Energy Management Strategies in Fuel Cell Hybrid Systems

The *Energy Management Strategies* (*EMS*) are algorithms which determine at each sampling time the power generation split between the *Fuel Cell System* (*FCS*) and the *Energy Storage System* (*ESS*) in order to fulfill the power balance between the load power and the source power. Depending on how the power split is done a minimization of the hydrogen consumption can be obtained. To find a global optimal solution, control techniques where a minimization problem is resolved have been studied [99]. In general, these techniques do not offer a causal solution, and, in consequence, are not feasible because it is assumed that the future driving cycle is entirely known a priori. Nevertheless, their results can be used to evaluate the performance of new strategies in study. On the other hand, strategies which deal with local optimization are convenient for real implementation.

Another approach, particularly convenient to work in real time operation, is the type of strategies where the system operation is based on heuristic rules from the knowledge of the performance of the components of the system. These strategies can achieve a comparable performance to those strategies where some optimization technique is utilized. In this way, two strategy based on the knowledge of the fuel-cell efficiency map are presented in this chapter.

In this chapter, the *EMS* in *FCHVs* are approached. Despite the *FCHS* have other applications, in this chapter we concentrate our attention in automotive applications. The objective is to improve the performance of the hybrid vehicle in terms of hydro-
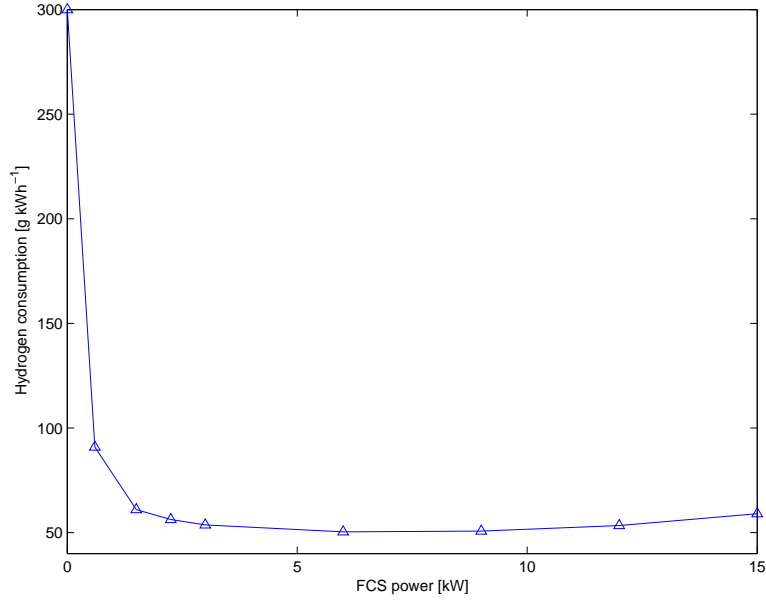
Figure 7.1: Hydrogen consumption map as a function of the *FCS* power.

gen economy and transient response. The distribution of the chapter is as follow: in Section 7.1, the objective of the *EMSs* are formalized. Secondly, in Section 7.2, three new different strategies are proposed: two of them are based on the *FCS* efficiency map and the third is based on constrained nonlinear programming. In Section 7.3, the simulation results, showing the temporal response of the strategies and the performance comparative between them, are presented. In Section 7.4, the experimental results to validate the strategies are presented. Finally, in Section 7.5, the conclusions on *EMS* in *FCHS* close the chapter.

7.1 Objectives of *EMS* in *FCHS*

The hydrogen consumption map of a *FCS* clearly reveals a zone, below a limit power, where the hydrogen consumption is very high meanwhile the zone above this limit power has a significative lower consumption as can be seen in Fig. 7.1. Thus, the principal objective of the energy management strategy is to minimize a cost function J, a mathematical expression that represents the cumulative hydrogen consumption

during the time:

$$\min_{X} J(X) \qquad \text{subject to} \qquad H(X) = 0 \qquad \text{and} \qquad G(X) \leq 0, \qquad (7.1)$$

where the vector X is

$$X = \begin{bmatrix} P_{fcs}(t) \\ P_{ess}(t) \end{bmatrix}. \qquad (7.2)$$

This means that the *EMS* has to determine the optimal value of the *Fuel Cell System* power, $P_{fcs}(t)$, and the *Energy Storage System* power, $P_{ess}(t)$, in order to minimize the cost function *J(X)*:

$$J(X) = \int_{0}^{t_c} F(X)dt, \qquad (7.3)$$

where t_c is the duration of driving cycle and $F(X)$ is the hydrogen consumption according to the hydrogen consumption map of the *FCS*:

$$F(X) = Cons_{H_2}\left(P_{fcs}(t)\right). \qquad (7.4)$$

The constraint $H(X) = 0$ in (7.1) means that at every time the power balance in the *DC* bus must be satisfied:

$$P_{fcs}(t) \cdot \eta_B + P_{ess}(t) \cdot \eta_{B/B} \cdot \eta_{ess} = P_{load}(t) \qquad \forall t \in [0, t_c]. \qquad (7.5)$$

On the other hand, the constraint $G(X) \leq 0$ in (7.1) states the constraints in the *FCS* power and the *ESS* power:

$$P_{fcs,min} \leq P_{fcs}(t) \leq P_{fcs,max} \qquad (7.6)$$

$$\Delta P_{fcs,min} = \Delta P_{fcs,fall\ rate} \leq \frac{dP_{fcs}(t)}{dt} \leq \Delta P_{fcs,rise\ rate} = \Delta P_{fcs,max} \qquad (7.7)$$

$$P_{ess,min}\left(SoE(t)\right) \leq P_{ess}(t) \leq P_{ess,max}\left(SoE(t)\right) \qquad (7.8)$$

$$SoE_{min} \leq SoE(t) \leq SoE_{max} \qquad (7.9)$$

$$\forall t \in [0, t_c].$$

The restrictions in the *FCS* power are stated in (7.6): the maximum power is limited by the *FCS* rated power, whereas the minimum *FCS* power command must be limited to a value below which it is not suitable to operate because the parasitic load is too large, reducing the system net power.

7. Energy Management Strategies in Fuel Cell Hybrid Systems

There is a phenomenon of delay between the onset of the load on the *FCS* and the response of the reactant supply system results which may lead in a "starvation" of reactants in the *FCS*. This may be avoided by restricting the dynamics required by the load [28]. The same approach is followed in [102] and [28] where the maximum positive rise is limited to avoid damage in the stack. Therefore, in our work, the *FCS* power load is increased no faster than a certain power rise rate ($\Delta P_{fcs,max}$). Besides, we propose to operate the *FCS* in such a way that the power is decreased no faster than a certain power fall rate ($\Delta P_{fcs,min}$) to prevent overpressure into the stack. Both situations can be managed by using the *ESS* as a power buffer. These restrictions are formulated in (7.7).

With regard to the *ESS*, the maximum and minimum power flow are also limited, as is formulated in (7.8). The maximum power that the *ESS* can supply or store depends on the actual voltage in the *ESS*, $V_{ess}(t)$, the maximum voltage $V_{ess,\,max}(t)$, and the minimum voltage $V_{ess,\,min}(t)$:

$$
\begin{aligned}
P_{ess,\ chrg\ max} &= \frac{(V_{ess}(t) - V_{ess,\,max}) \cdot V_{ess}(t)}{R_d} &\quad \text{during charging} \\
P_{ess,\ disch\ max} &= \frac{(V_{ess}(t) - V_{ess,\,min}) \cdot V_{ess}(t)}{R_d} &\quad \text{during discharging,}
\end{aligned}
\tag{7.10}
$$

where R_d is the *ESS* internal resistance. The charge voltage is related with the *ESS* energy, so that, it is possible to express (7.10) as a function of the *State of Energy* in the *ESS*, $SoE(t)$ (defined in (6.6)):

$$
P_{ess}(t) = \frac{k \cdot E_{cap}}{R_d \cdot C_R} \cdot SoE(t),
\tag{7.11}
$$

where E_{cap} is the maximum energy that the *ESS* is capable to store, R_d and C_R are the internal resistance and the capacitance of the supercapacitors, and k is a constant depending in the particular technology. Therefore,

$$
P_{ess,\ chrg\ max}(t) = k_{ess} \cdot (SoE(t) - SoE_{max})
\tag{7.12}
$$

$$
P_{ess,\ dischrg\ max}(t) = k_{ess} \cdot (SoE(t) - SoE_{min}),
\tag{7.13}
$$

where

$$
k_{ess} = \frac{k \cdot E_{cap}}{R_d \cdot C_R}
\tag{7.14}
$$

is the constant that relates the actual *SoE* and the power that the device can supply or store. Thus, $P_{ess,\ chrg\ max}(t)$ is the maximum power that the *ESS* is capable to store

at the instant t (charging mode) and the $P_{ess,\ dischrg\ max}(t)$ is the maximum power that the ESS is capable to supply at instant t (discharging mode). According to the sign convention employed, the power is negative when the ESS is in charging mode, meanwhile it is positive when the ESS is discharging mode. The k_{ess} constant depends on the DC internal resistance R_d, the supercapacitor capacitance C_R, and the constant k depending on the particular supercapacitor technology. The internal resistance of supercapacitors is extremely low and the capacitance is exceptionally high, allowing a very fast operation both during charging and discharging. In the supercapacitors employed in this work, they are $R_d = 0.019\ \Omega$ and $C_R = 58\ F$, thus, $k_{ess} = 479\ kW$.

Besides the previous objective, another important objective of EMS is the improvement in the transient response of the $FCHS$. As it was mentioned before in Section 4.2.3, the temporal behavior is fundamentally conditioned by the compressor dynamics. This drawback can be overcome by means of an adequate energy management strategy. In fact, it is possible to improve the transient response of the $FCHS$ by means of the ESS energy contribution. In that sense, the energy management strategy acts as follows: if the power requested to the FCS exceeds a determined maximum rise rate, then the power rise rate that the FCS actually gives is limited and the rest of power is supplied by the ESS if it is possible according to the present value of $SoE(t)$. If, on the contrary, the power requested to the FCS exceeds the maximum fall rate, then the actual power fall rate is limited and the surplus power is absorbed by the ESS whenever there is sufficient storage capacity.

7.2 Energy Management Strategies

In this section, three energy management strategies for $FCHVs$ are presented. Two of them are based on the knowledge of the fuel cell efficiency map and the third strategy is based on constrained nonlinear programming. The electrical topology previously established in Section 6.3.1 is represented in Fig. 7.2, which is common in the three strategies. In this figure, they are also represented the energy flows in the $FCHS$: the regenerated energy from load to the ESS bank, the charging energy from the FCS to the ESS, the boosting energy from the ESS to the load, and the fuel cell energy that directly supplies the load from FCS.
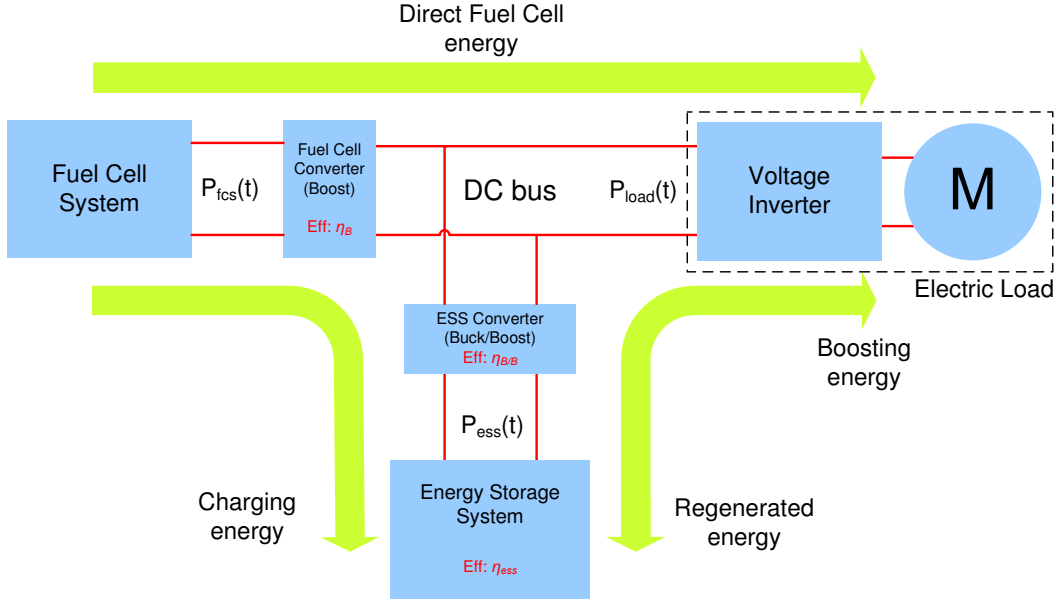
Figure 7.2: Energy-flow scheme in the strategy based on efficiency map.

Table 7.1: Efficiency values assumed in hybrid-modelling process.

Efficiency values		
Boost power converter efficiency	η_B	0.95
Buck/Boost power converter efficiency	$\eta_{B/B}$	0.95
Supercapacitor bank efficiency	η_{ess}	0.9

The efficiency of the *Boost* power converter (η_B), that connects the *FCS* with the power bus, the efficiency of the *Buck/Boost* converter ($\eta_{B/B}$), that connects the *ESS* with the bus and the efficiency of the *ESS* itself, and the efficiency of the *ESS* (the charging and the discharging efficiency), are assumed as constants (see Table 7.1). The *FCS* efficiency is represented with an efficiency map as a function of the power . In this way, the power that the *FCS* supplies to the bus is affected by the *Boost* converter efficiency; the power that the *ESS* supplies is affected by the *Buck/Boost* efficiency and the *ESS*-discharging efficiency; whereas the power that the *ESS* stores from the bus is affected by the *Buck/Boost* converter efficiency and the *ESS*-charging efficiency.

7.2.1 Strategy based on the *FCS* efficiency map

One of the most relevant characteristic of a *FCS* is the efficiency map (see Fig. 2.4), a chart that shows how the efficiency changes with the load power and is related to the consumption map through (6.4). It is supposed that the *FCS* operating point is controlled and, thus, external parameters such the ambient temperature have no influence in the efficiency map.

The first strategy proposed in this thesis work is a *quasi-load-following*[1] strategy where the *FCS* is operated in an advantageous zone where the efficiency is high. In this case, the operating zone is constrained between an inferior limit ($P_{fcs,lo}$) and a superior limit ($P_{fcs,hi}$). The superior limit is imposed by the maximum power that the fuel cell can deliver (i.e., $P_{fcs,hi} = P_{fcs,max}$), whereas the inferior limit is determined according to the efficiency curve. As we mentioned before, the efficiency of a *FCS* at low power is very poor due to the parasitic power. Thanks to the inferior limit, the energy management strategy avoids this unfavorable zone (see Fig. 6.9).

Considering that the losses in the power converters (η_B and $\eta_{B/B}$) and the *ESS* efficiency η_{ess} are constants, the power balance in the *DC* bus previously defined in (7.5), can be rewritten as

$$P_{fcs}(k) \cdot \eta_B + P_{ess}(k) \cdot \eta_{B/B} \cdot \eta_{ess} = P_{load}(k) \qquad k = 1,\, 2\,,\ldots,\, N_c, \qquad (7.15)$$

where $N_c = t_c/\Delta T$ is the cycle duration, assuming a constant sampling period $\Delta T = 1\ s$.

This *EMS* gives priority to the *FCS*-power supply since the *FCS* is the primary power source and the direct power flow to the *DC* bus through the *FCS* power converter has lower losses than the indirectly way through the *ESS* power converter, the *ESS* itself and back to the load. Consequently, given the present $P_{load}(k)$, if

$$P_{fcs,lo} \cdot \eta_B \leq P_{load}(k) \leq P_{fcs,max} \cdot \eta_B \qquad (7.16)$$

and

$$\Delta P_{fcs,fall\ rate} \leq \Delta P_{load}(k) \leq \Delta P_{fcs,rise\ rate}, \qquad (7.17)$$

where

$$\Delta P_{load}(k) = P_{load}(k) - P_{load}(k-1). \qquad (7.18)$$

---

[1]A load-following strategy is a strategy that adjusts the power output of the fuel cell according to the load requirement.

Then, the *FCS* operates in load-following mode:

$$P_{fcs}(k) = P_{load}(k)/\eta_B \tag{7.19}$$

and

$$P_{ess}(k) = 0. \tag{7.20}$$

If, on the contrary

$$P_{load}(k) \leq P_{fcs,lo}(k) \cdot \eta_B, \tag{7.21}$$

then

$$P_{fcs}(k) = P_{fcs,lo}(k) \tag{7.22}$$

and, the *ESS* stores the rest of generated power, if the *ESS* is not too charged:

$$P_{ess}(k) = -min\left\{|P_{load}(k) - P_{fcs}(k) \cdot \eta_B| \cdot \eta_{ess} \cdot \eta_{B/B}, \quad |SoE(k) - SoE_{max}| \cdot k_{ess}\right\}. \tag{7.23}$$

Conversely, if

$$P_{load}(k) \geq P_{fcs,hi}(k) \cdot \eta_B, \tag{7.24}$$

then

$$P_{fcs}(k) = P_{fcs,max} \tag{7.25}$$

and, the *ESS* supplies the rest of load power, if there is enough energy in *ESS*:

$$P_{ess}(k) = min\left\{\frac{(P_{load}(k) - P_{fcs}(k) \cdot \eta_B)}{\eta_{B/B} \cdot \eta_{ess}}, \quad (SoE(k) - SoE_{min}) \cdot k_{ess}\right\}. \tag{7.26}$$

The representation of how is determined the *FCS* operating point is shown in Fig. 7.3. However, the transition between operating points is limited by the maximum rates, thus, finally

$$P_{fcs}(k) = \begin{cases} P_{fcs}(k-1) + \Delta P_{fcs,fall\,rate} \cdot \Delta T, & \text{if } \Delta P_{fcs}(k) \leq \Delta P_{fcs,fall\,rate} \\ P_{fcs}(k-1) + \Delta P_{fcs,rise\,rate} \cdot \Delta T, & \text{if } \Delta P_{fcs}(k) \geq \Delta P_{fcs,rise\,rate}, \end{cases} \tag{7.27}$$

where $\Delta P_{fcs} = P_{fcs}(k) - P_{fcs}(k-1)$, with $P_{fcs}(k)$ as it was previously calculated in 7.19, 7.22 or 7.25, according to the conditions 7.16, 7.21 or 7.24, respectively. The power $P_{ess}(k)$ is calculated as in indicated in 7.23 and 7.26.
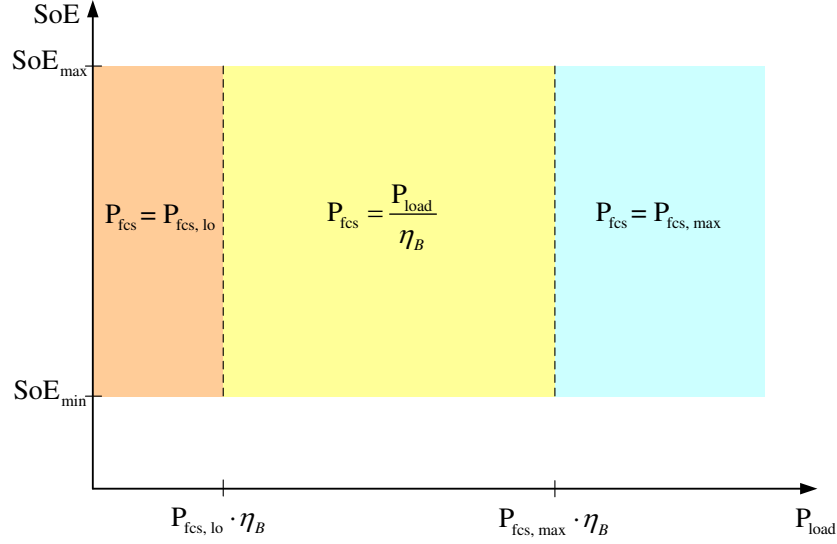
Figure 7.3: *FCS* operating point as a function of the *SoE* in the *ESS* and the load power P_{load} for the strategy based on efficiency map.

7.2.2 Improved strategy based on the *FCS* efficiency map

The second strategy based on the *FCS* efficiency map is a strategy which operates the *FCS* preferably in its point of maximum efficiency in order to improve the hydrogen economy. The operating point of the *FCS* is determined based on the the actual power demand and the state of energy of the *ESS*. The *FCS* power command is determined according to the following rules. If the load power is

$$P_{fcs, \, lo} \cdot \eta_B \leq P_{load}(k) \leq P_{fcs, \, hi} \cdot \eta_B \tag{7.28}$$

and, the *SoE* is

$$SoE_{lo} \leq SoE(k) \leq SoE_{hi}, \tag{7.29}$$

where $P_{fcs,hi}$ is

$$P_{fcs,hi} = P_{fcs,max} \cdot \eta_B \cdot X_{fcs,hi}, \tag{7.30}$$

and $X_{fcs,hi}$ is a fraction of the maximum *FCS* power; then, the *FCS* is operated in its point of maximum efficiency:

$$P_{fcs}(k) = P_{fcs, \, max \, eff}. \tag{7.31}$$

The remaining power to achieve the load demand flows from or to the *ESS* according to the 7.26 if $P_{load}(k) > P_{fcs,\,max\,eff}$ (discharging mode), or 7.23 if $P_{load}(k) < P_{fcs,\,max\,eff}$ (charging mode).

If the load power is

$$P_{fcs,\,hi} \cdot \eta_B \leq P_{load}(k) \leq P_{fcs,\,max} \cdot \eta_B, \tag{7.32}$$

and the *SoE* is

$$SoE_{lo} \leq SoE(k) \leq SoE_{hi}, \tag{7.33}$$

then, the *FCS* is operated in load following mode:

$$P_{fcs}(k) = P_{load}(k)/\eta_B \tag{7.34}$$

and $P_{ess}(k)$ is as indicated in (7.23) or (7.26).

On the other hand, if

$$P_{load}(k) \geq P_{fcs,\,max} \cdot \eta_B \quad \text{and} \quad SoE(k) \leq SoE_{hi} \tag{7.35}$$

or

$$SoE(k) \leq SoE_{lo}, \tag{7.36}$$

then, the *FCS* is operated at its maximum power:

$$P_{fcs}(k) = P_{fcs,\,max}, \tag{7.37}$$

and $P_{ess}(k)$ is as indicated in (7.26). If, on the contrary

$$P_{load}(k) \leq P_{fcs,\,lo} \cdot \eta_B \quad \text{and} \quad SoE(k) \geq SoE_{lo}, \tag{7.38}$$

or

$$SoE(k) \geq SoE_{hi} \tag{7.39}$$

then, the *FCS* is operated at its lower operating point:

$$P_{fcs}(k) = P_{fcs,\,lo}, \tag{7.40}$$

and $P_{ess}(k)$ is as in 7.23. Additionally, if $P_{load}(k) = 0 \,\forall t \in [k_1,\,k_2]$ with $(k_2 - k_1) > T_{off}$, and, $SoE(k) > SoE_{hi}$ with $k > k_2$, then, the *FCS* is turned off to avoid unnecessary hydrogen consumption because the parasitic losses in the *FCS*. Figure 7.4 indicates
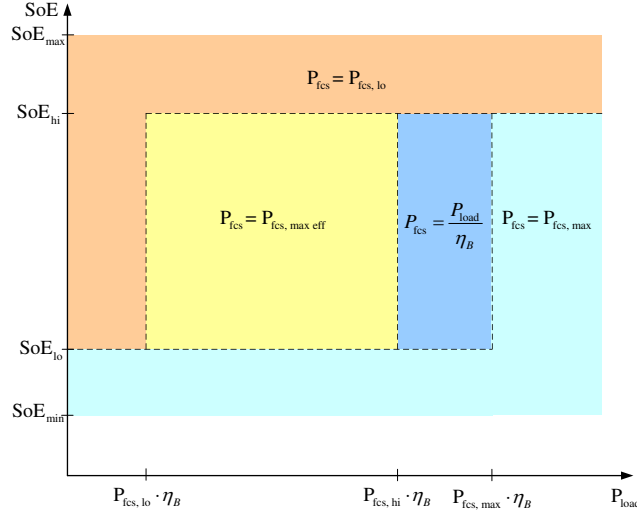
Figure 7.4: *FCS* operating point as a function of the *SoE* in the *ESS* and the load power P_{load} for the improved strategy based on efficiency map.

the *FCS* operating point as a function of the $SoE(k)$ in the *ESS* and the load power $P_load(k)$. In the same way that in the previous strategy, the transition between operating points is realized according to the constraints concerning the maximum fall power rate and the maximum power rate as indicated in (7.27).

7.2.3   Strategy based on constrained nonlinear programming

In this strategy, an optimization problem with linear constraints is resolved at each sampling period ΔT where a nonlinear cost function, which represents the hydrogen consumption, is minimized. The problem can be put into the following form [103]:

$$\min_{X} J(X) \qquad \text{subject to} \quad H(X) = 0 \quad \text{and} \quad G(X) \leq 0, \tag{7.41}$$

where the vector X is

$$X = \left[\begin{array}{c} P_{fcs} \\ P_{ess} \end{array} \right]. \tag{7.42}$$

The cost function $J(X)$ represents the hydrogen consumption in the *FCS*:

$$J(X) = F(P_{fcs}(k)), \tag{7.43}$$

where

$$F(P_{fcs}(k)) = Cons\, H_2(P_{fcs}(k)) \cdot P_{fcs}(k) \cdot \Delta T, \tag{7.44}$$

129

and $Cons\,H_2(P_{fcs}(k))$ is the hydrogen consumption $(g\,Wh^{-1})$ as a function of $P_{fcs}(k)$. This relationship is shown in the form of a consumption map in Fig. 7.1.

The set of constraints $H(X) = 0$ represents the power balance in the DC bus:

$$P_{fcs}(k) \cdot \eta_B + P_{ess}\,(k) \cdot \eta_{B/B} \cdot \eta_{ess} = P_{load}(k) \qquad k = 1,\,2\,,\ldots,\,N_c \qquad (7.45)$$

and the set of constraints $G(X) \leq 0$ represents the limitations in $P_{fcs}(k)$ and $P_{ess}(k)$. The $P_{fcs}(k)$ is limited in its maximum and minimum value, and in the maximum rise rate and fall rate:

$$P_{fcs,\,lo} \leq P_{fcs}(k) \leq P_{fcs,\,hi}, \qquad (7.46)$$

and

$$P_{fcs}(k-1) + \Delta P_{fcs,\,fall\,rate} \cdot \Delta T \leq P_{fcs}(k) \leq P_{fcs}(k-1) + \Delta P_{fcs,\,rise\,rate} \cdot \Delta T. \quad (7.47)$$

This can be rewritten as

$$P_{fcs,\,min} \leq P_{fcs}(k) \leq P_{fcs,\,max}, \qquad (7.48)$$

where

$$P_{fcs,\,max}(k) = max\,[P_{fcs,\,hi}; \quad P_{fcs}(k-1) + \Delta P_{fcs,\,fall\,rate} \cdot \Delta T] \qquad (7.49)$$

$$P_{fcs,\,min}(k) = min\,[P_{fcs,\,lo}; \quad P_{fcs}(k-1) + \Delta P_{fcs,\,rise\,rate} \cdot \Delta T]. \qquad (7.50)$$

On the other hand, $P_{ess}(k)$ is limited to its maximum or minimum value depending on the actual $SoE(k)$. The $SoE(k)$ is limited:

$$SoE_{min} \leq SoE(k) \leq SoE_{max}, \qquad (7.51)$$

thus,

$$k_{ess} \cdot (SoE(k) - SoE_{max}) \leq P_{ess}(k) \leq k_{ess} \cdot (SoE(k) - SoE_{min})\,, \qquad (7.52)$$

where k_{ess} is the constant defined in (7.14).

Table 7.2: Simulation parameters used to test the energy management strategies.

Parameter	Symbol	Value	Unit
Number of supercapacitors	N_{cap}	250	-
ESS specific energy	$E_{ess,\ spec}$	6	$Wh\ kg^{-1}$
Maximum ESS energy	$E_{ess,\ max}$	612	Wh
Maximum SoE	SoE_{max}	1	-
Minimum SoE	SoE_{min}	0.2	-
High limit of SoE	SoE_{hi}	0.9	-
Low limit of SoE	SoE_{lo}	0.3	-
Maximum ESS power	$P_{ess,\ max}$	255	kW
Maximum FCS power	$P_{fcs,\ max}$	15	kW
Maximum FCS rise rate power	$\Delta P_{fcs,\ rise\ rate}$	600	Ws^{-1}
Maximum FCS fall rate power	$\Delta P_{fcs,\ fall\ rate}$	-900	Ws^{-1}
Maximum FCS efficiency	$\eta_{fcs,\ max}$	0.6	-
FCS power of maximum efficiency	$P_{fcs,\ max\ eff}$	6	kW
Energy storage efficiency	η_{ess}	0.99	-
Boost converter efficiency	η_B	0.95	-
Buck/Boost converter efficiency	$\eta_{B/B}$	0.95	-

7.3 Simulation results

The enunciated strategies were tested in a hybrid system consisting in the vehicle described in Table 6.2, provided with a *FCS* and a supercapacitors-based *ESS* with the principal parameters listed in Table 7.2. The supercapacitors bank is modelled according to the Section 6.4.2. The *ESS* can store a total of $612\,Wh$. The parameters $P_{fcs,\ lo}$ and $P_{fcs,\ hi}$ act as adjustment parameters, allowing to improve the fuel economy and performance according to the particular strategy and cycle. These parameters are shown in Table 7.3.

The strategies are tested on the four driving cycles described in Section 6.4.3: the *New European Driving Cycle (NEDC)*, the *Urban Dynamometer Driving Schedule (UDDS)*, the *Federal Test Procedure (FTP)*, and the *Highway Fuel Economy Test (HWFET)*.

Firstly, the simulation results corresponding to the three strategies are shown: the power split between the fuel cell system and the energy storage system, and the evolution of the $SoE(t)$ in the *ESS* are shown in Figs. 7.5 to 7.8 for the first strategy, in

Table 7.3: Values of the parameters $P_{fcs,\,lo}$ and $P_{fcs,\,hi}$ used in the *EMSs*.

	$P_{fcs,\,lo}$ [kW]	$P_{fcs,\,hi}$ [kW]
Strategy based on efficiency map	1	15
Improved strategy based on efficiency map	1	12
Strategy based on nonlinear programming	2	15

Figs. 7.9 to 7.12 for the second strategy and in Fig. 7.13 to 7.16. Secondly, a comparative between the corresponding performances for the four cycles is done.
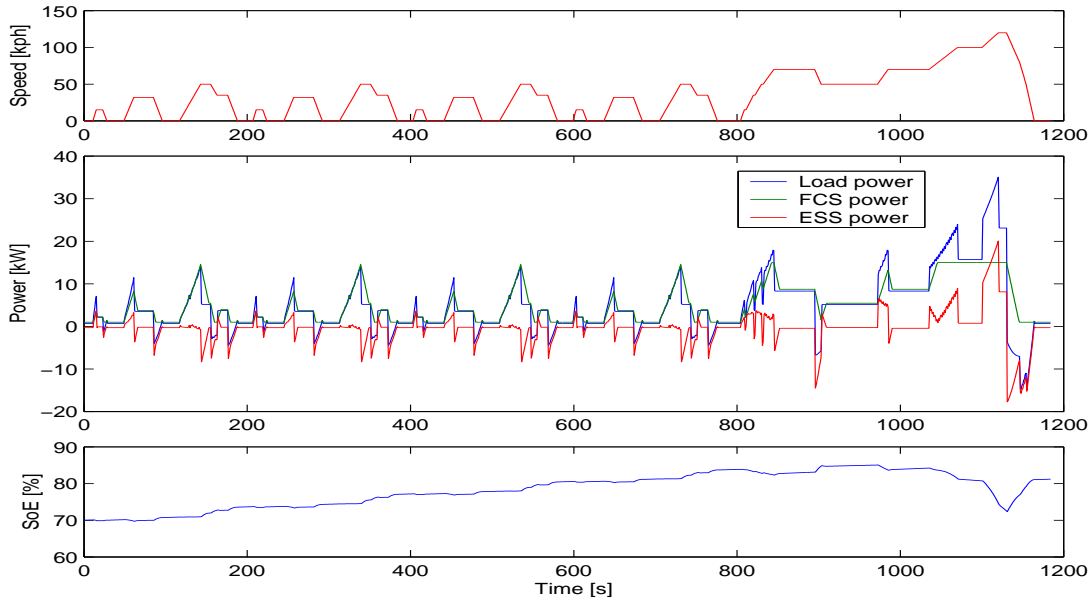

Figure 7.5: Power split running on *NEDC*, and the evolution of the *SoE*, using the strategy based on efficiency map.

The comparative between the performance of the strategies, in terms of hydrogen consumption per kilometer, is done in Fig. 7.17. The comparative is done between the performance of the three strategies with respect to the corresponding to the optimal case where the consumption is minimum; the values in percentage indicate the increment in consumption with respect to the optimal case. The performance of the optimal case was estimated in Section 6.7 assuming that the entirely cycle is known a priori, thus, it is possible to operate the *FCS* during the entirely cycle with maximum efficiency. In addition, the performance corresponding to the *FCS* pure case, where there is no
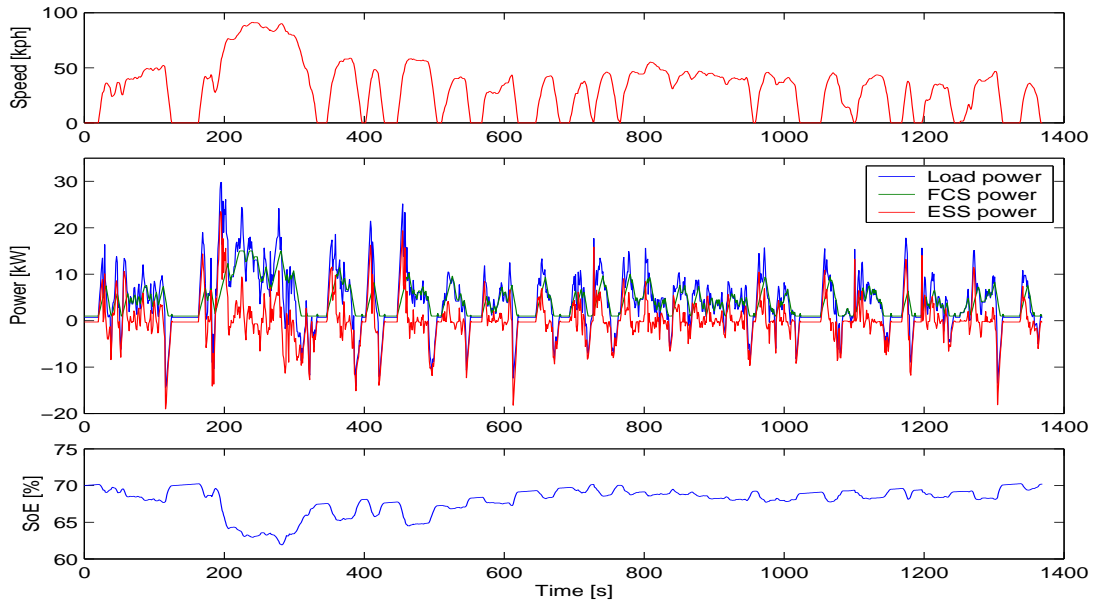
Figure 7.6: Power split running on *UDDS*, and the evolution of the *SoE*, using the strategy based on efficiency map.

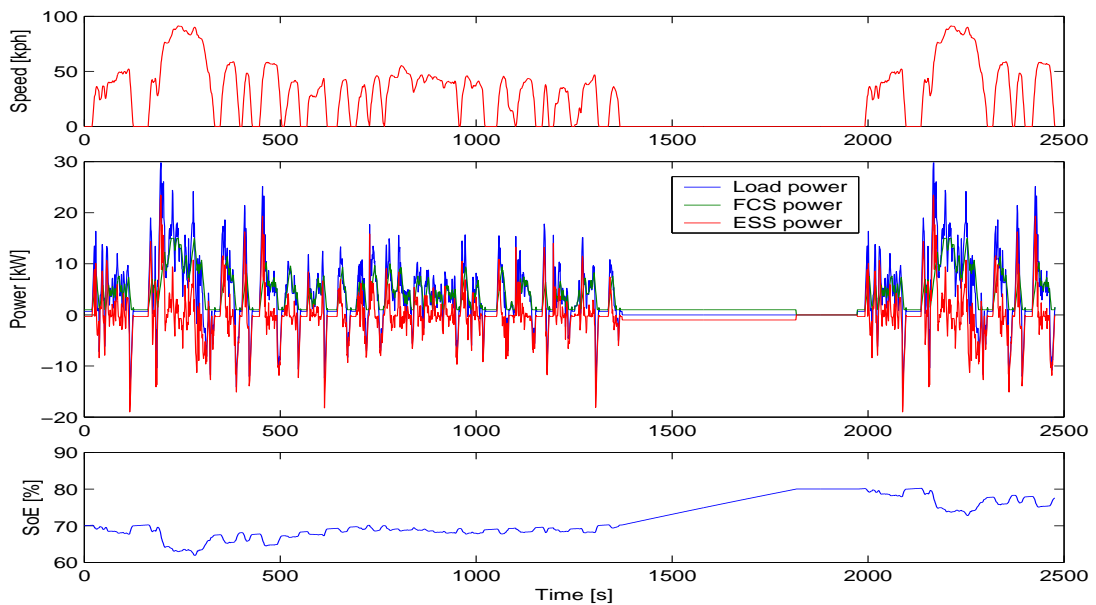Figure 7.7: Power split running on *FTP*, and the evolution of the *SoE*, using the strategy based on efficiency map.
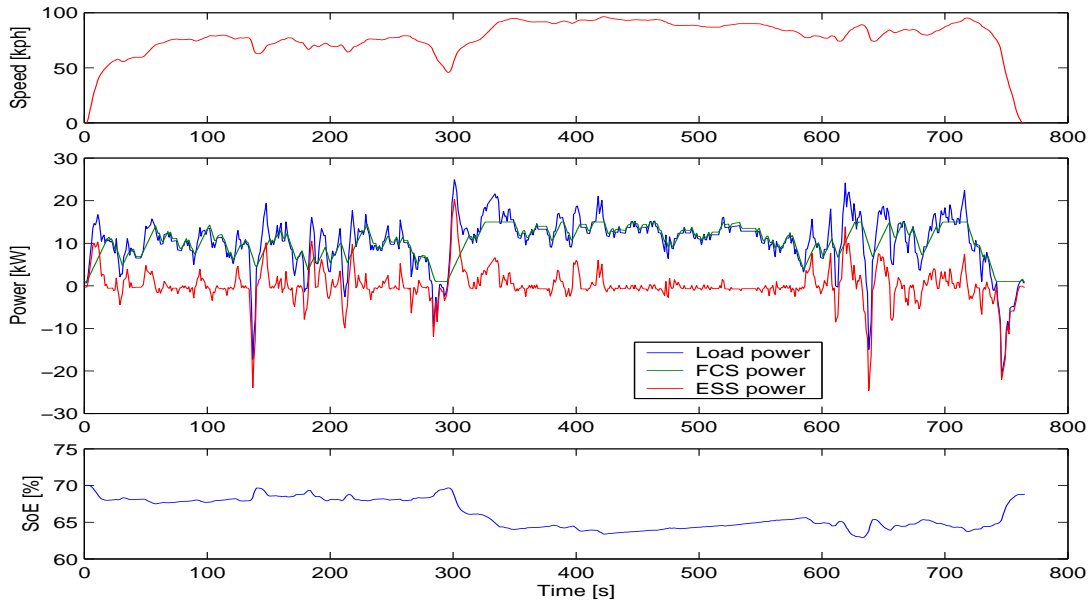
Figure 7.8: Power split running on *HWFET*, and the evolution of the *SoE*, using the strategy based on efficiency map.

Figure 7.9: Power split running on *NEDC*, and the evolution of the *SoE*, using the improved strategy based on efficiency map.

Figure 7.10: Power split running on *UDDS*, and the evolution of the *SoE*, using the improved strategy based on efficiency map.

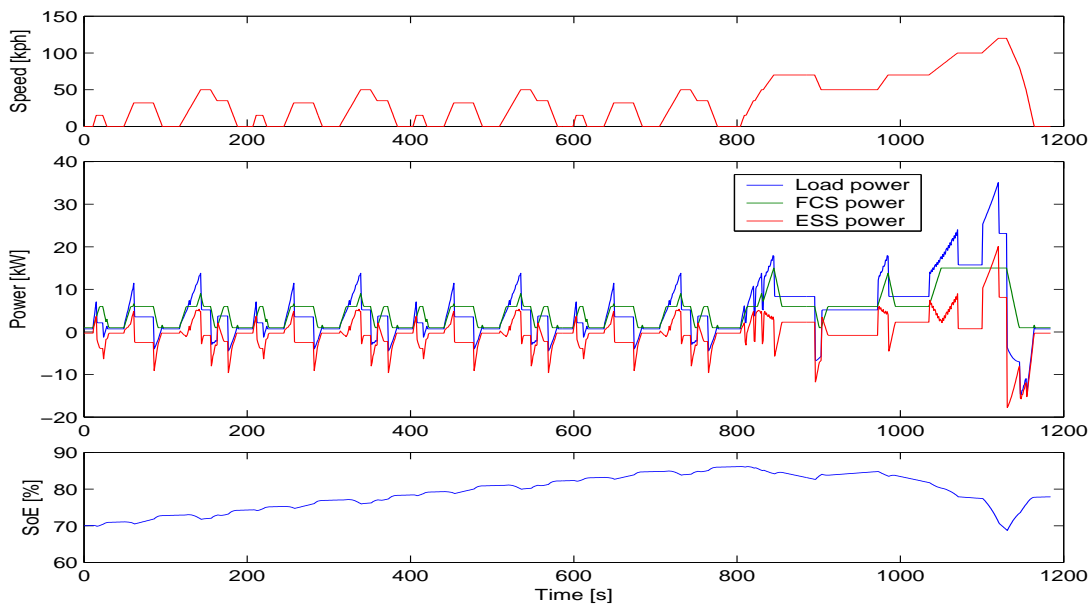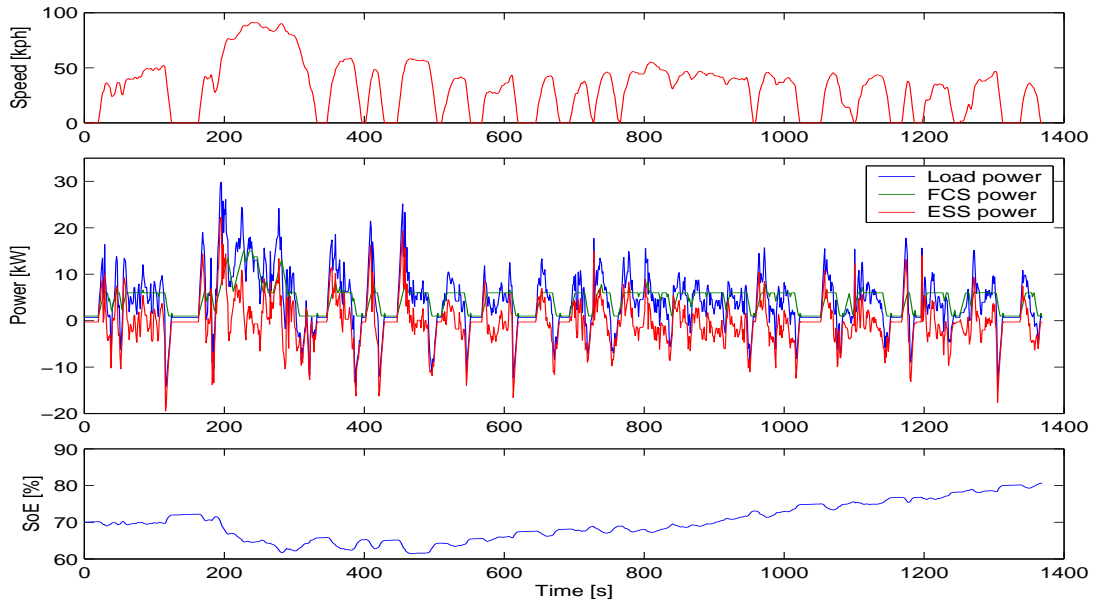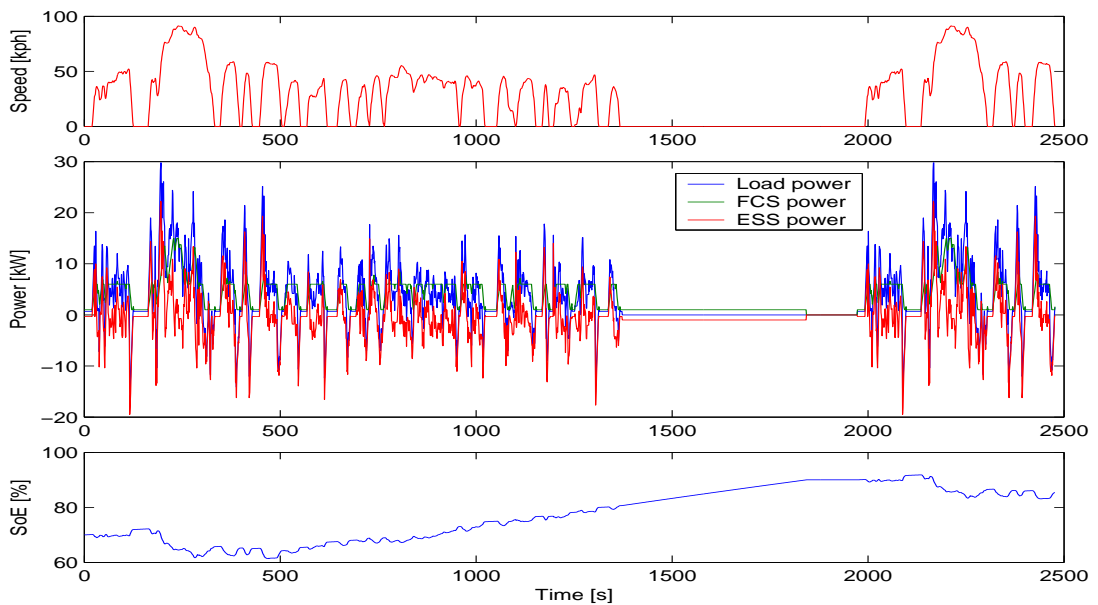Figure 7.11: Power split running on *FTP*, and the evolution of the *SoE*, using the improved strategy based on efficiency map.
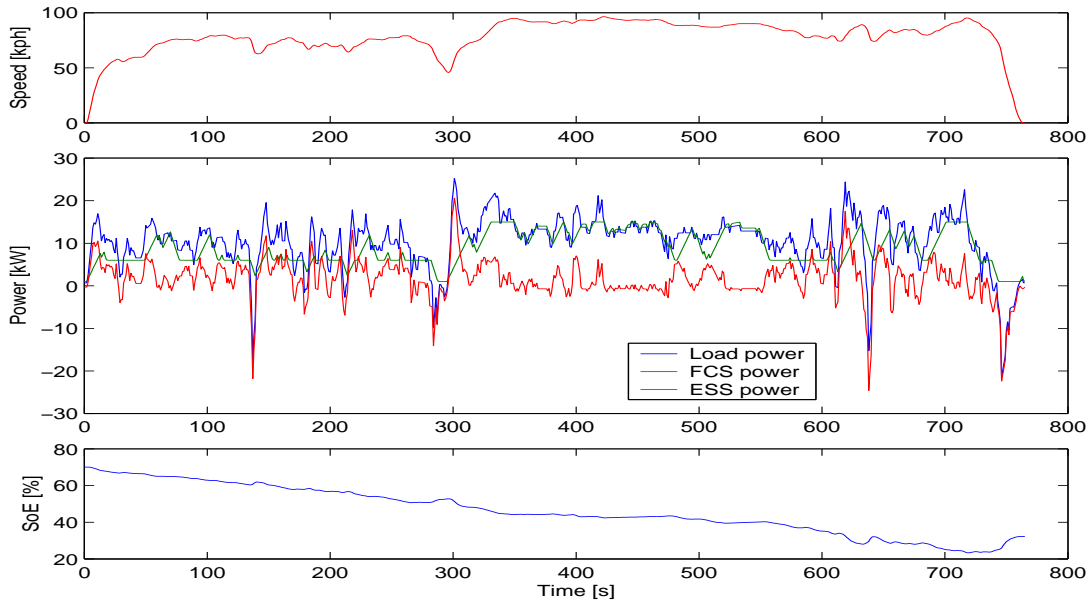
Figure 7.12: Power split running on *HWFET*, and the evolution of the *SoE*, using the improved strategy based on efficiency map.

Figure 7.13: Power split running on *NEDC*, and the evolution of the *SoE*, using the strategy based on constrained nonlinear programming.

Figure 7.14: Power split running on *UDDS*, and the evolution of the *SoE*, using the strategy based on constrained nonlinear programming.

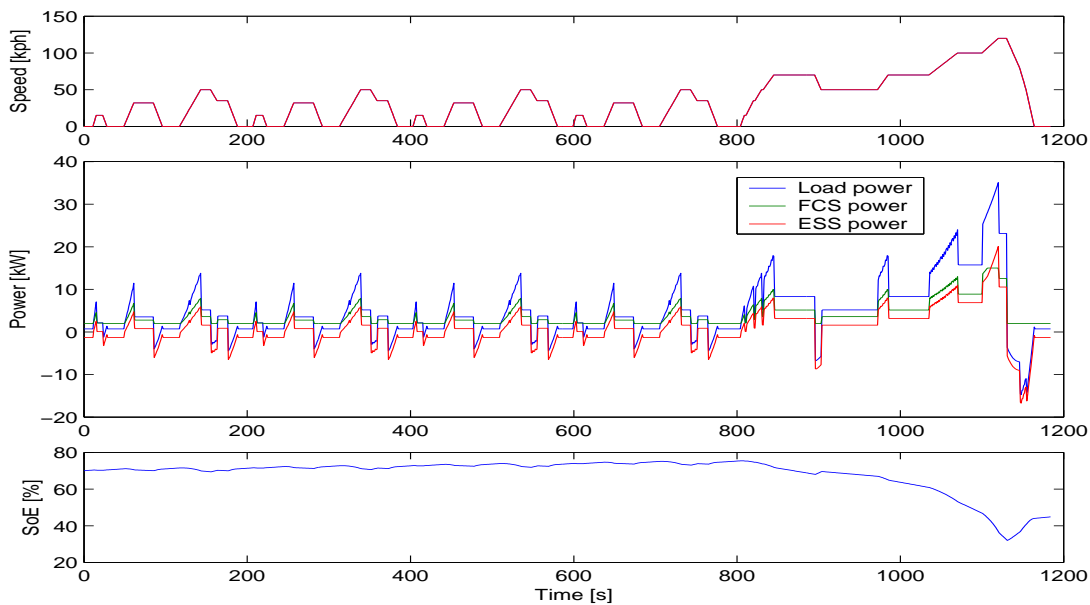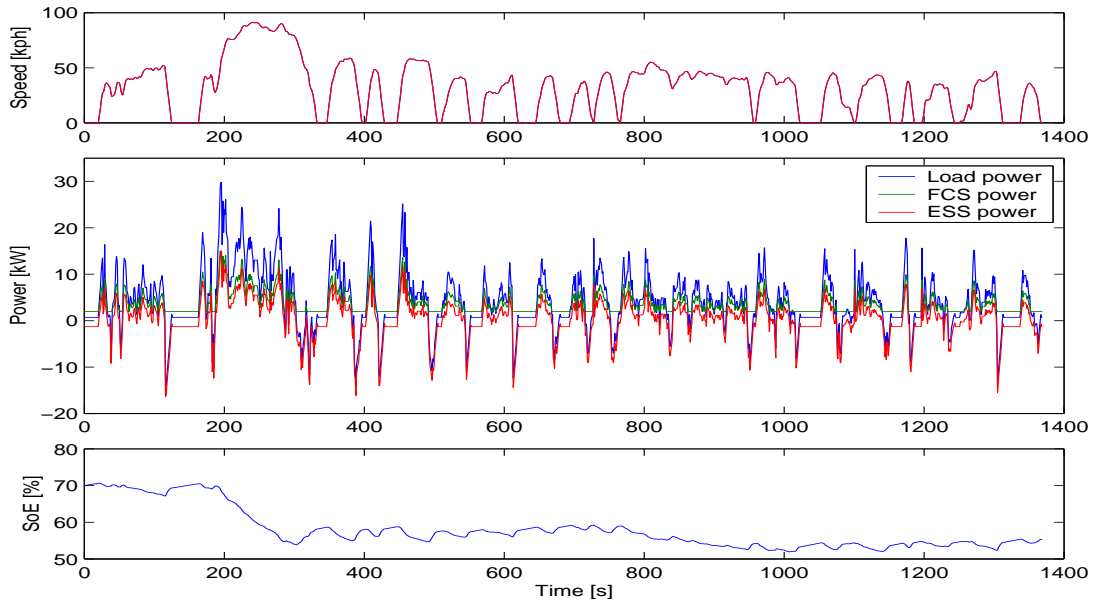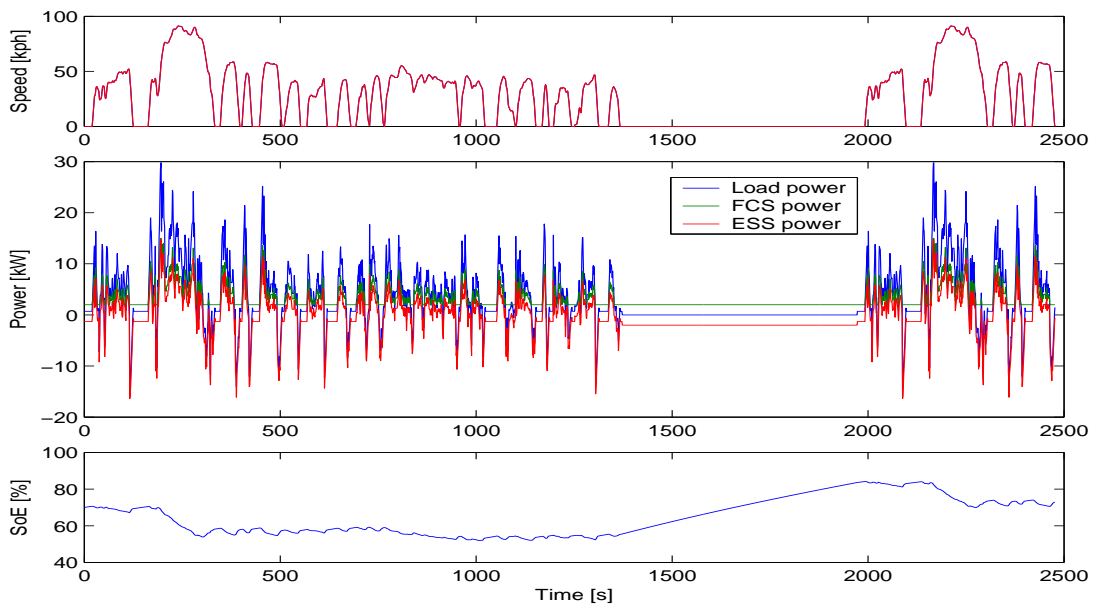Figure 7.15: Power split running on *FTP*, and the evolution of the *SoE*, using the strategy based on constrained nonlinear programming.
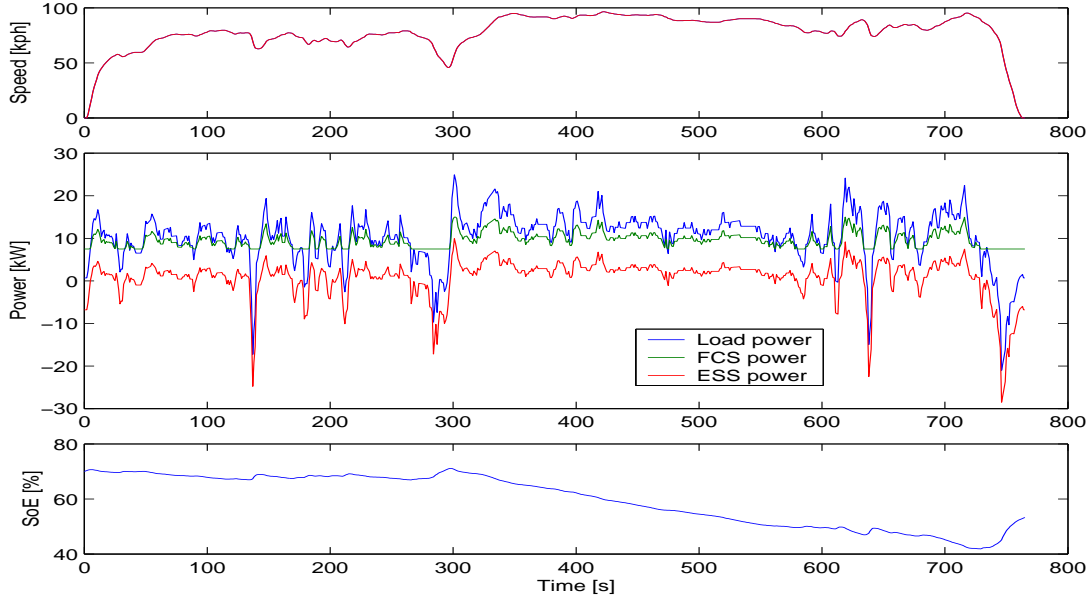
Figure 7.16: Power split running on *HWFET*, and the evolution of the *SoE*, using strategy based on constrained nonlinear programming.

hybridization, is included in Fig. 7.17. The analysis of the *FCS* pure case is performed with a 37.5-*kW FCS*, a power that is sufficient to fulfill the four cycles in study.

In general, the final state of charge $SoE(N_c)$ is different to the initial state of charge $SoE(0)$, resulting in a gain or a loss of energy in the *ESS* over the driving cycle. Because of that, the results are corrected in order to compare the results correctly. The corrected consumption of hydrogen is based on the assumption that after the cycle, the *FCS* is continuing running in its point of maximum efficiency until the *SoE* reaches again the initial value. Thus, the corrected consumption results

$$Cons_{H_2, corrected} = Cons_{H_2} + \frac{\Delta E_{ess, stored}}{\Delta H_{LHV} \cdot \eta_{fcs,\, max} \cdot \eta_B \cdot \eta_{B/B} \cdot \eta_{ess}}, \qquad (7.53)$$

where, $Cons_{H_2}$ is the cumulative consumption of hydrogen over the cycle previous to the correction, $\Delta E_{ess, stored}$ is the difference of the energy stored in the *ESS* at the end of the cycle with the energy at the beginning of the cycle (positive if $SoE(N_c) > SoE(0)$ and negative in the opposite situation), ΔH_{LHV} is the lower heating value of hydrogen, $\eta_{fcs,\, max}$ is the maximum efficiency of the *FCS* and η_{ess} is the *ESS* efficiency.
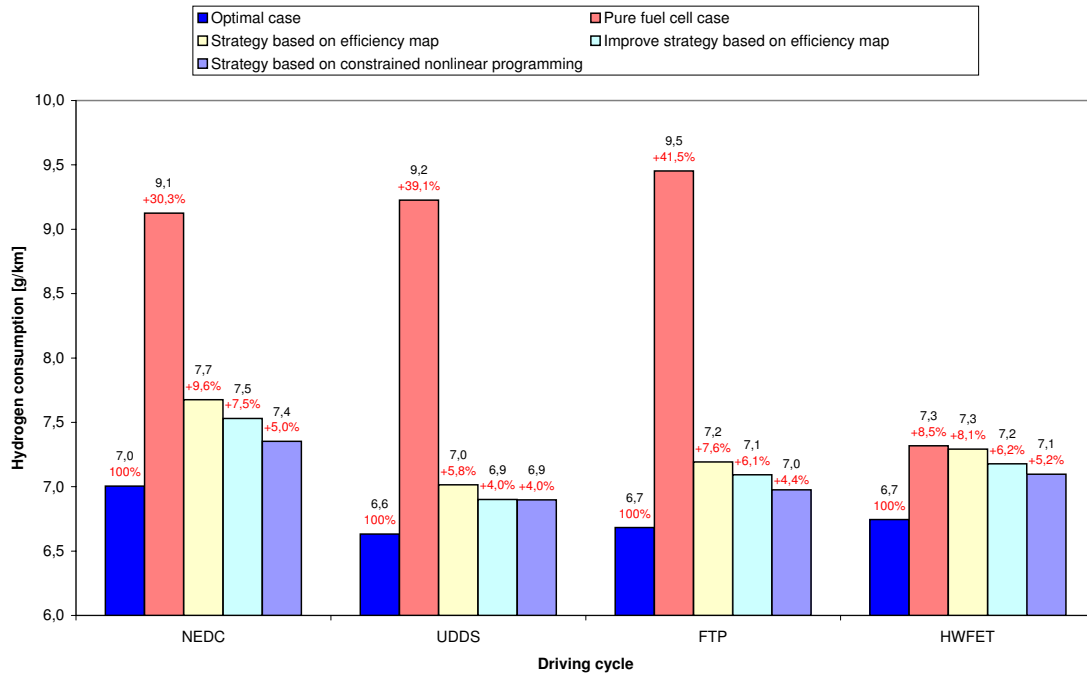
Figure 7.17: Comparative between the hydrogen consumption of the proposed strategies, the optimum case and the *FCS* pure case. The percentages in red indicate the increment in consumption with respect to the optimal case.

7.3.1 Discussion

The analysis of the hydrogen economy in Fig. 7.17 shows that the three strategies have a good performance compared to the optimal case where the entire driving cycle is known a priori, which is not feasible in practice. In fact, the maximum deviation from the optimal case is 9.6% in the strategy based on efficiency map running on *NEDC*. The strategy based on constrained nonlinear programming gives the best performance in all the cases; however, the performance is similar to the two strategies based on efficiency map. On the other hand, compared to the pure fuel cell case in Fig. 7.18, the results show considerable hydrogen savings running on cycles *NEDC*, *UDDS*, and *FTP*. On the contrary, running on *HWFET* the savings is exiguous. This cycle is a highway driving cycle and one of its characteristic is that the average deceleration is significantly lower ($-0.22 \ m \ s^{-2}$) than the corresponding to the other cycles (*NEDC*: $-0.79 \ m \ s^{-2}$; *UDDS*: $-0.58 \ m \ s^{-2}$; *FTP*: $-0.58 \ m \ s^{-2}$). These results suggest that the strategies achieve the objectives satisfactorily when a significant energy is recovered
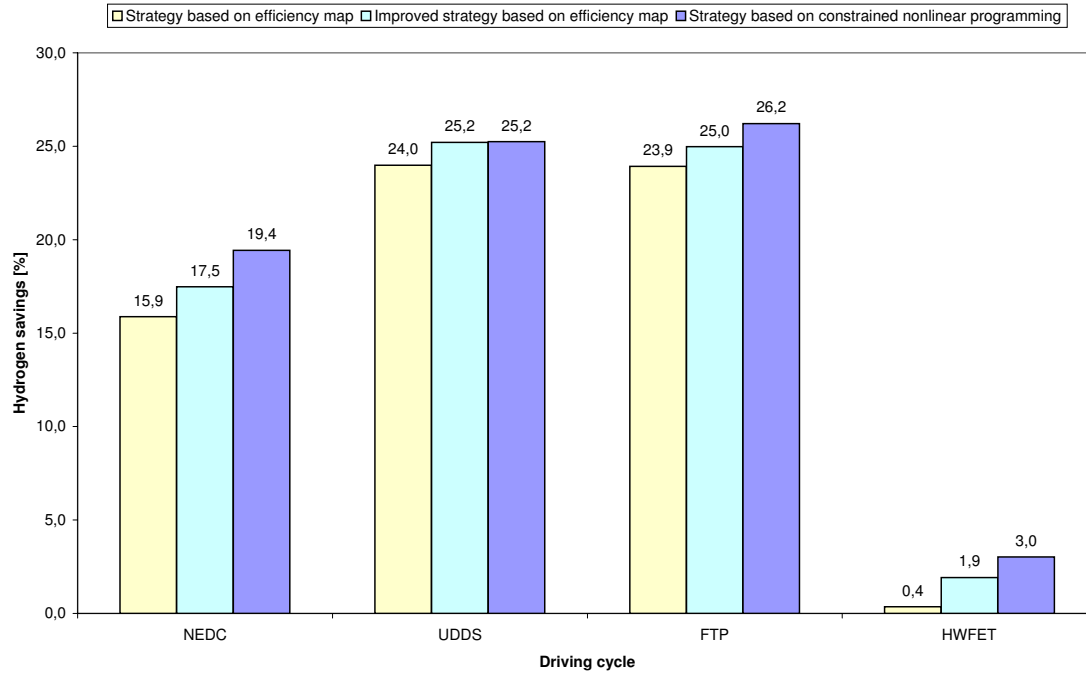
Figure 7.18: Hydrogen savings with respect to the pure fuel cell case.

from braking.

It is remarkable that it is possible to meet the load power in the four driving cycles with a 15-*kW FCS* that is significantly lower to the corresponding in the pure fuel cell case with no hybridization (37.5 *kW*), an advantage that is translated in a reduction in the production costs. This is possible thanks to the *ESS* power assistance in the proposed strategies.

The analysis of the influence of the initial *SoE* on the hydrogen consumption shows that the first strategy and the third strategy have minimal dependence, which denotes robustness to this parameter. On the other hand, the performance of the second strategy is dependent on the initial *SoE*, specially in the *HWFET* cycle. In this case, the performance is worse than in the first strategy if the initial *SoE* is lower than 60%. The results of the influence of the initial *SoE* in the three strategies running on the *UDDS* cycle and the *HWFET* are shown in Fig. 7.19.

140
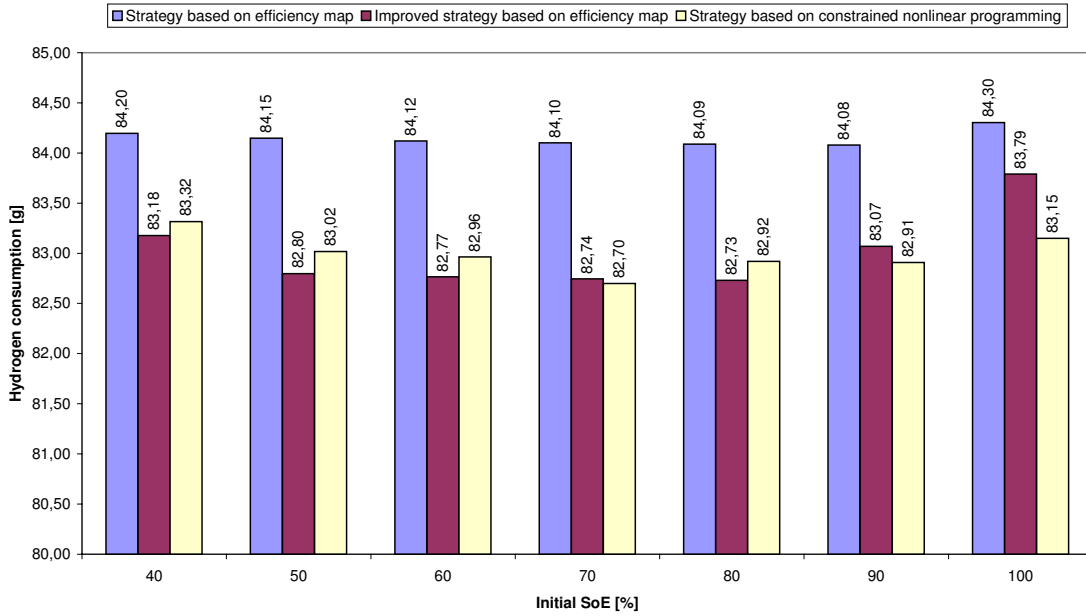
(a) UDDS
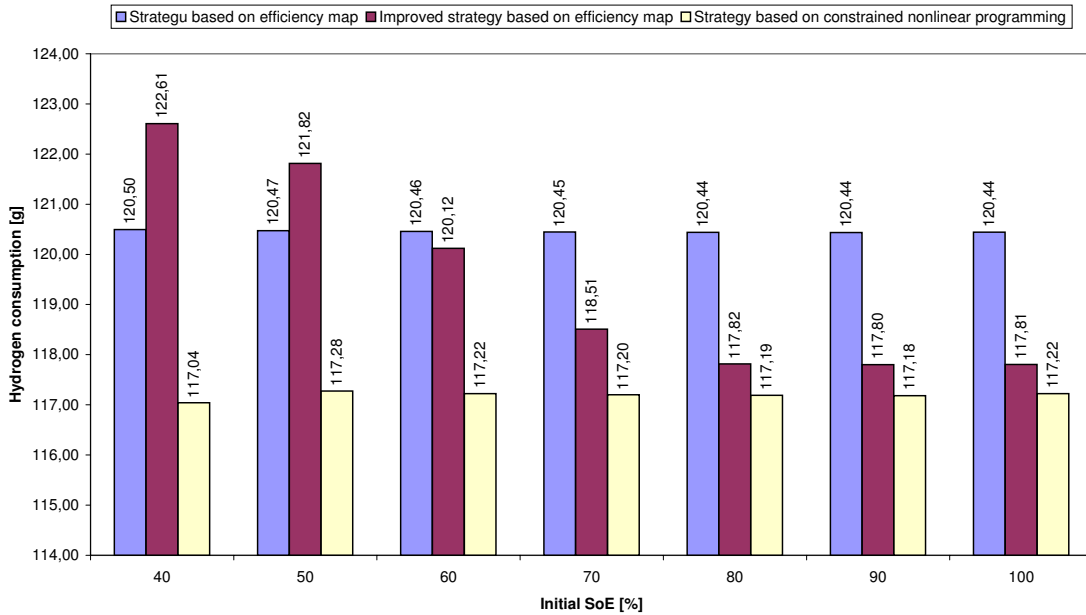
(b) HWFET

Figure 7.19: Influence of the initial *SoE* on the hydrogen consumption in two driving cycles.

7.4 Experimental validation

This section presents the implementation of the previously developed *EMSs* in Section 7.2 on an experimental test setup. The main objective is to show that through the use of these *EMSs* is possible to operate the *FCS* efficiently, reducing the hydrogen consumption, thereby justifying the use of hybrid arrangements (i.e., hybridization) in fuel cell-based vehicles.

The arrangement of this section is as follows. First, the experimental setup is described. Then, the experimental results are presented showing the temporal behavior, the performance in terms of hydrogen consumption, and the comparative between *EMSs*. Finally, the conclusions of this section are presented.

7.4.1 Experimental setup

The experimental setup is a test environment in which some components of the *FCHV* are actually present, some are emulated, and some others are simulated. The objective of this setup is to reproduce, as close as possible, the *FCHV* behavior in order to validate the *EMSs*. In this experimental setup (shown in Fig. 7.20), the *FCS* is a *NEXA* power module made by *Ballard* of 1.2 *kW*. The power module is fed with hydrogen from a pressurized tank and the hydrogen flow is measured with a mass flow meter (*Bronkhorst*, model *F-201AC*), an instrument device with a maximum flow capacity of 50 *SLPM*.

The vehicle power consumption is emulated with a programmable electronic load (*Höcherl & Hackl*, model *ZS1606*), a power device that can support up to *1600 W @ 60 V, 150A*. This load is commanded by the *Host* computer in Fig. 7.20, which is in charge of carrying out the *EMS*. The *ESS* is simulated with a model developed in the *LabVIEW*[1] environment. This model is developed according to real supercapacitors from *Maxwell Technologies*. The main characteristics of these devices are listed in Table B.1. The actual *SoE* is calculated according to this model, which is running in the *Host* computer.

---

[1]LabVIEW is the acronym for *Laboratory Virtual Instrumentation Engineering Workbench* and is a platform and development environment for a visual programming language from National Instruments. This platform is commonly used for data acquisition, instrument control, and industrial automation. For more detail see [104].

The data acquisition and control system is composed by a *Host* computer and a computer running in real time, namely *RTOS* computer. The *RTOS* computer communicates with the input/output (*I/O*) modules, made by *National Instrument*, throughout a *FPGA* target and a *PCI* bus. The two computers are connected via ethernet. The *Host* computer also allows monitoring the evolution of the system variables and commanding the system through a graphical interface developed in *LabVIEW*. The measured variables are the hydrogen flow, the load current and the stack voltage. These variables are measured every $200\,ms$.

The operation of the experimental setup is as follows. First, the *FCS* operation is determined according to the *EMSs* that were described in Section 7.2. To that end, the *EMSs* were programmed in the *LabVIEW* environment. These applications run in the *RTOS* computer and assess a new request to the *FCS*, $P_{fcs}(k)$, every $1\,s$. The $P_{ess}(k)$ value is determined from the power balance in the *DC* bus as in (7.15). Then, the $P_{fcs}(k)$ is required to the *NEXA power module* through the electronic load, which is commanded from the *RTOS* computer. The electronic load is operated in constant power mode, i.e., the load sinks a power in accordance with the external-programming signal from the *RTOS* computer. On the other hand, the $P_{ess}(k)$ is utilized in the *ESS* model, running in the *Host* computer, to actualize the actual $SoE(k)$.

7.4.2 Experimental results

According to the previous explanation, the experimental setup was utilized to validate the enunciated *EMSs* running on the same four driving cycles that in Section 7.3. In the simulation stage, it was utilized a *15-kW FCS* to fulfill the driving cycles. In this stage, all the powers are scaled down with a factor of 12.5 to fit with the rated power of the *NEXA* power module (1.2 kW). In Figs.7.22, 7.23, and 7.24 are shown the experimental results showing the evolution of *FCS* power P_{fcs}, measuring the stack voltage and the stack current; the evolution of *SoE*, from the *ESS* model; and the hydrogen consumption, measured with a mass flow meter.

The comparative of the hydrogen consumption between the strategies in the experimental setup and the strategies in the simulation environment is shown in Fig. 7.25. To do this comparative the experimental results are multiplied by the the same scale factor used to scale down the power. From this comparative, it is possible to draw
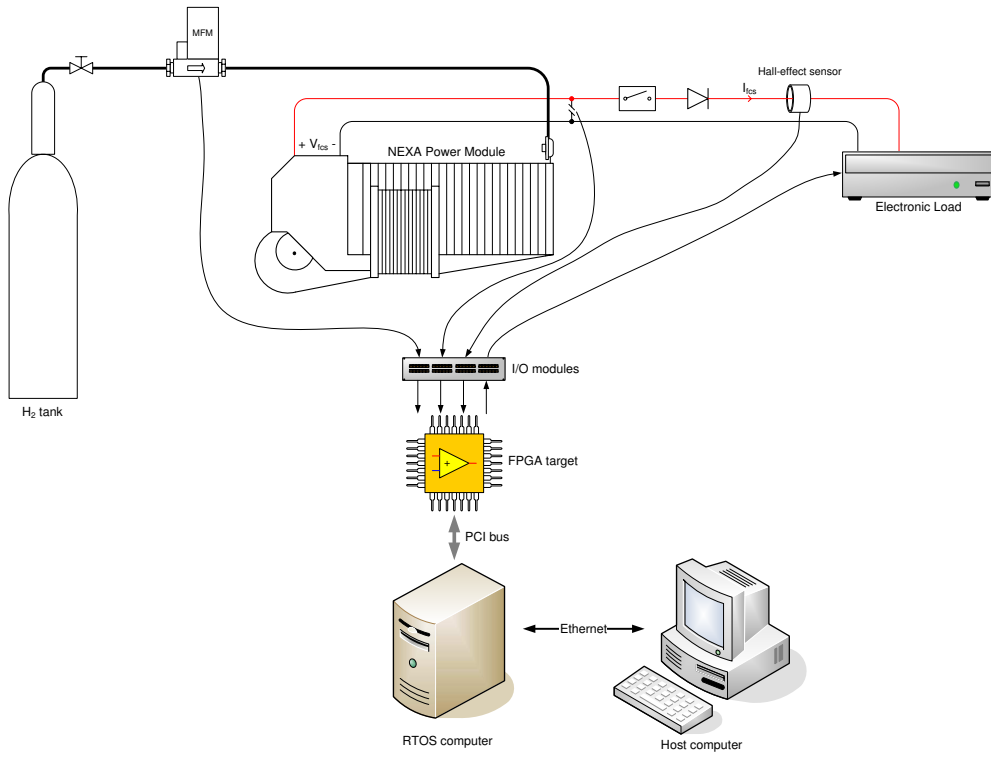
Figure 7.20: Scheme showing the experimental setup to validate the *EMSs*.

some observation. Firstly, the hydrogen consumption corresponding to the experimental setup is higher than the corresponding to the simulation setup. This is owing to the fact that the efficiency of the *NEXA* is lower than the efficiency of the *FCS* model in the simulation setup as can be seen in Fig. 7.21 where it is shown the comparative between the experimental efficiency map of *NEXA* and the efficiency map of the *FCS* model in the *ADVISOR* simulator. The experimental map is obtained measuring the inlet hydrogen flow rate and using (6.4). Secondly, the relative consumptions in the experimental setup are similar to the experimental setup with some differences owing to discrepancies in the modelling and measurement errors.

On the other hand, the hydrogen saving achieved using the *EMSs* with respect to the pure fuel cell case with no hybridization is shown in Fig. 7.26. The results show the interest of hybridization, achieving hydrogen savings up to 33.7%.
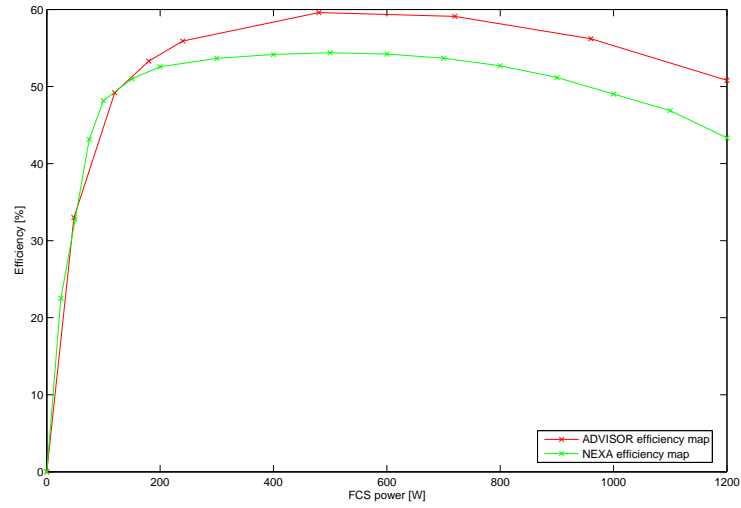
Figure 7.21: Comparative between the experimental efficiency map of *NEXA* and the efficiency map of the *FCS* model in the *ADVISOR* simulator.
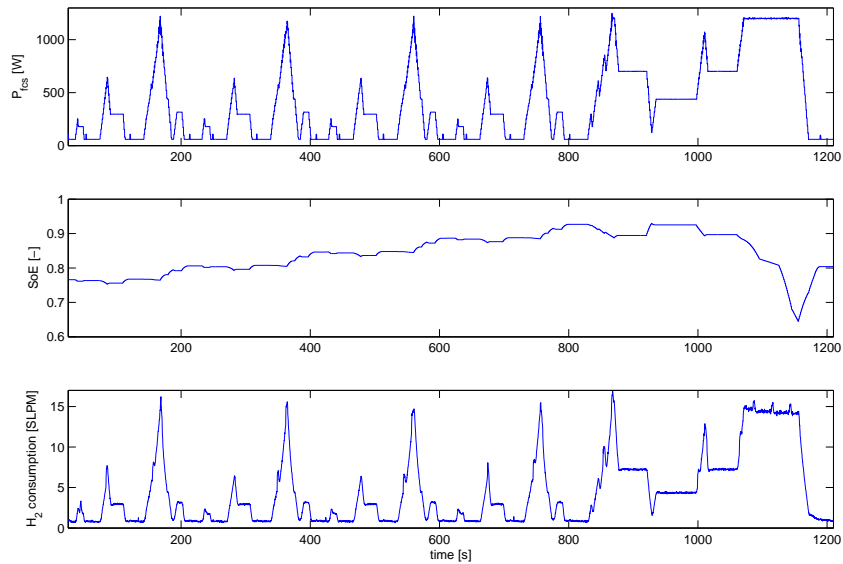
Figure 7.22: Experimental results from the strategy based on efficiency map
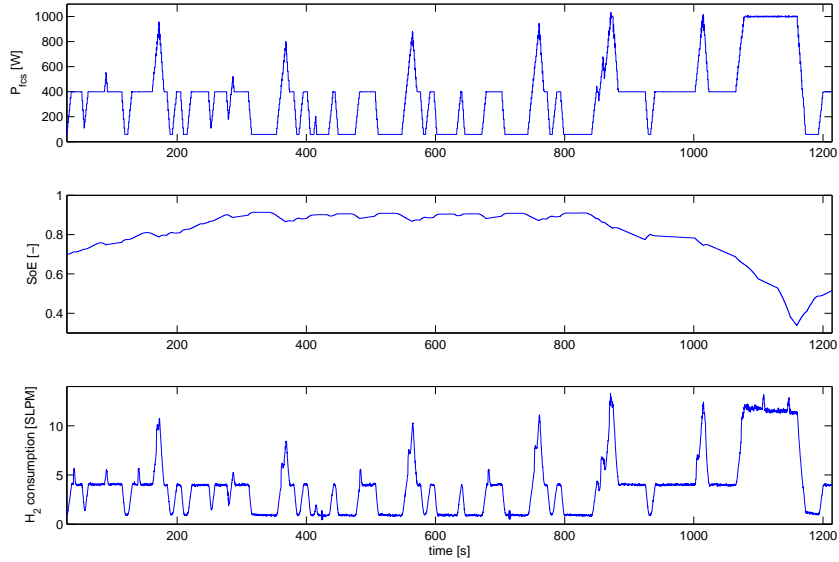
Figure 7.23: Experimental results from the improved strategy based on efficiency map
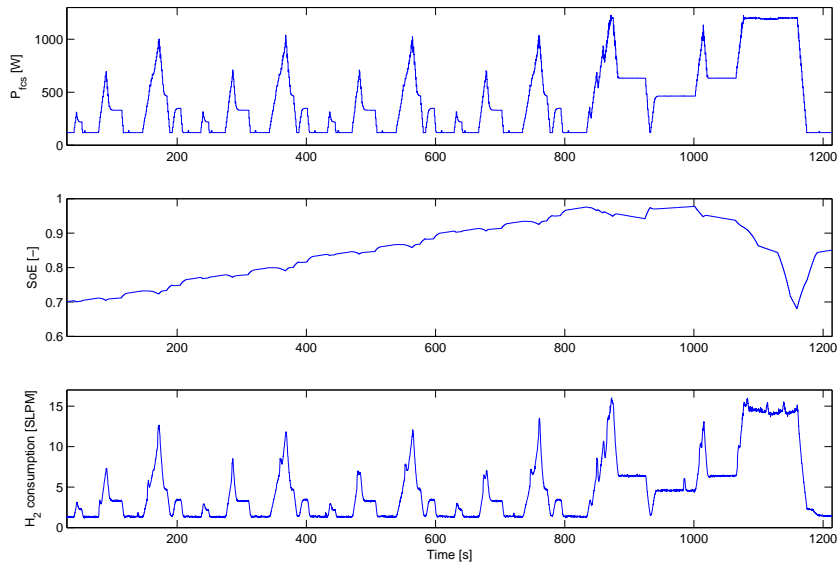
Figure 7.24: Experimental results from the strategy based on constrained nonlinear programming
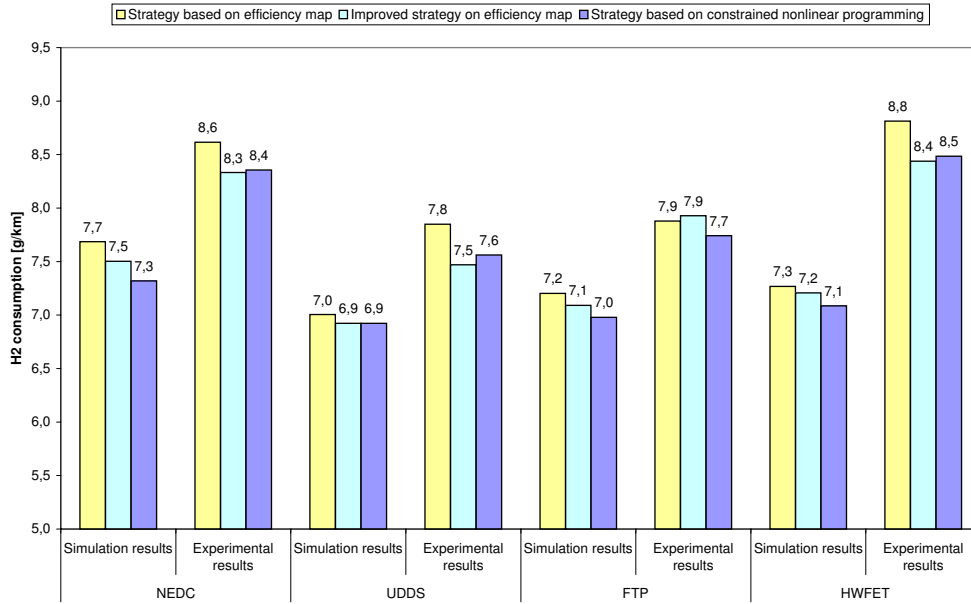
Figure 7.25: Experimental validation of the proposed strategies.
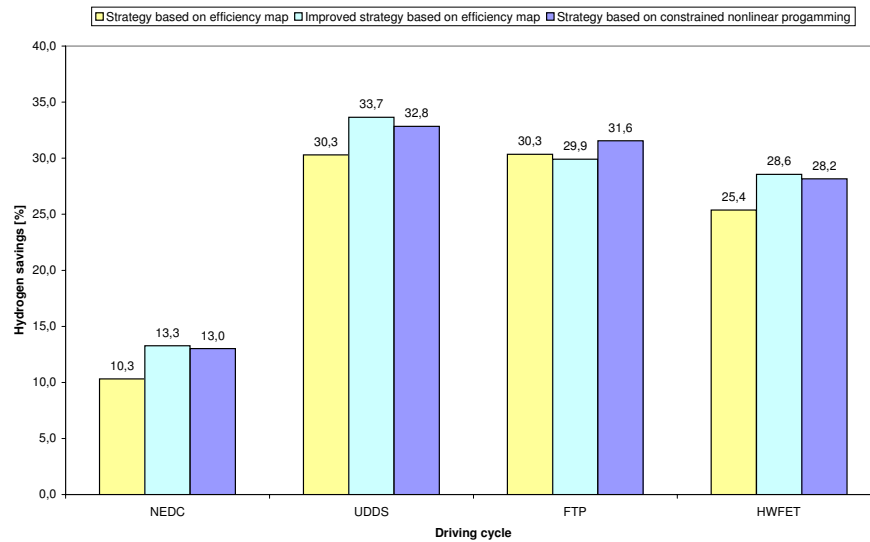
Figure 7.26: Hydrogen savings achieved using the *EMSs* with respect to the pure fuel cell case.

7.5   Conclusions

In this chapter, the Energy Management Strategies for Fuel Cell Hybrid Vehicles were approached. The objectives of the *EMSs* were enunciated and three strategies were proposed. These strategies are based on the knowledge of the efficiency map. The first strategy is a quasi-load-following strategy in which the *FCS* is operated in an advantageous zone where the efficiency is high whereas the second strategy operates the *FCS* preferably in its point of maximum efficiency in order to improve the hydrogen economy. In the third strategy, an optimization problem with linear constraints is resolved at each sampling period where a nonlinear cost function, which represents the hydrogen consumption, is minimized.

First, the *EMSs* were tested in a simulation environment using four standard driving cycles and, then, the *EMSs* were tested in an experimental setup reproducing the *FCVH* behavior were some components are actually present, some are emulated and some others are simulated.

The results show that using the proposed *EMSs* it is possible fulfill the load profiles, achieving a high reduction in the hydrogen consumption, a saving that is achieved operating the *FCS* properly and taking advantage of the energy from regenerative braking. To evaluate the savings, the hydrogen consumptions are compared with two references: the pure fuel cell case with no hybridization and the optimal case with minimum consumption where the driving cycle is known a priori.

Chapter 8

Conclusions and Future Work

In the first part of this chapter, a general perspective of the conclusions of the thesis is presented. In the second part, recommendations for future work are presented. The specific conclusions of each particular subject are at the end of the respective chapter.

8.1   General conclusions

The power generation systems based on hydrogen-fuel cells represent a new technology with great potential to contribute to solve the environmental problem and the shortage of non-renewable energy resources because of the high efficiency in the energy conversion and null emissions.

It is necessary further research to make possible the full insertion of this technology into the society and the research on control and design of electrical generation systems based on fuel cells is one of the fundamental issues. Therefore, an extensive study about the control and design of fuel cell systems oriented to *Fuel Cell Hybrid Vehicles* (*FCHVs*) has been performed in this thesis, covering both the low level control of the system composed of the fuel cell and the air compressor and the high level control of the energy flows between the fuel cell, the energy storage system and the electrical load.

The main focus of this thesis is on the hybrid system composed of a fuel cell and supercapacitors, and the thesis results show the convenience, advantages and limitations of this type of configuration especially in automotive applications. The control and design have been approached with the objectives to improve the efficiency (reducing

the hydrogen consumption) and to support vehicle conductibility requirements similar to a conventional vehicle.

Once the electrical structure for the *FCHV* was adopted, a methodology of design of the vehicle hybrid main parameters was proposed (i.e. the fuel cell size and the number of supercapacitors of the *ESS*). The goal of this design methodology is to obtain a *FCHV* that fulfils conductibility requirements and consumes as little hydrogen as possible. In this design process, it is concluded that there is a trade-off between efficiency and conductibility in the sense that the design that covers a wider drivability condition range is not the more efficient.

The mentioned process design has been performed developing a *FCHV* model in *ADVISOR*, a *MATLAB* toolbox that allows to model in detail hybrid vehicles and analyze their consumption and emissions when they follow a given speed profile. In the thesis, a detailed analysis of the different energy flows into a vehicle when it is running on four different *Standard Driving Cycles* has been performed, including the energy flows from the hydrogen tank toward the wheels and the energy flows from the wheels to the energy storage system during the energy recovery from braking. In this analysis, it is determined how the losses in each component affect the hydrogen economy: the hydrogen energy that is lost in the vehicles components goes from 15.9% in the *HWFET* cycle to 23.1% in the *UDDS*.

With regard to the energy recovery from braking, a parameter has been defined, which quantifies the amount of energy that is recovered: the *braking/hydrogen* ratio. This ratio goes from 2.3% in *HWFET* cycle to 11.7% in *UDDS*, and reveals that the amount of energy that can be effectively recovered is lower than reported in some publications. However, it is concluded that this energy recovery performs a fundamental role in hybrid vehicles helping to improve the economy of hydrogen, allowing to save up to 26.2% of hydrogen in urban scenarios. It is also concluded that the hybridization allows to reduce the size of the fuel cell. In the vehicle considered in the case of study, the reduction is from $94\,kW$ to $35\,kW$ with the consequent benefits: reduction in the total vehicle weight from $1248\,kg$ to $1109\,kg$ and also reduction in the cost of the vehicle.

In this thesis, another important issue that is indispensable to the efficient operation of the hybrid systems has been approached: the development of *Energy Management Strategies* (*EMSs*) that control the flows of energy between the fuel cell, the energy

storage system and the electrical load with the objective to fulfil the demand with the minimum hydrogen consumption.

Three *EMSs* have been proposed, all of them based on the knowledge of the efficiency map. These strategies have been developed exploiting the rigorous model in *ADVISOR* and have been validated through an experimental setup implemented for this purpose. The experimental results show that the operation in real time with high efficiency is possible. The consumption results were evaluated and compared with two references: *i*) the case with no hybridization and *ii*) the case with hybridization with the optimal hydrogen consumption for the proposed vehicle. With regard to the first comparative, it is possible to save up to 26.2% of hydrogen in an urban driving cycle like the *FTP* cycle, using the strategy based on constrained nonlinear programming. However, in a suburban cycle like the *HWFET* the hydrogen savings is only a 3%. With regard to the second comparative, the performance of the three strategies is between 90.9% and 95.7% of the optimal performance.

To compute the optimal hydrogen consumption, a methodology was proposed that, unlike the usual methodology based on *Dynamic Programming*, avoids the discretization of the state variables. In this proposed methodology, only the time is discretized because the standard driving cycles that are utilized in *ADVISOR* are defined every $1\,s$. Therefore, the computational time of this methodology is reduced, maintaining a high accuracy.

EMSs work as high level controllers that command the energy flows in the *DC* bus. However, in order to keep the system in good working order, the fuel cell system must be adequately controlled. With this purpose, the low level control of the system composed of the fuel cell and the air supply system was addressed. An efficient air supply system is important to improve the performance of the generation system because of the power consumption of the compressor.

A control strategy based on *Dynamic Matrix Predictive Control* was proposed, which uses two control variables: the compressor voltage and a new control variable that works together with the aforementioned variable. This new control variable, that is not considered in the literature, is the opening area of a proportional valve at the cathode outlet. Analyzing the simulation results, both in stationary and transient state, it is concluded that using these two variables it is possible to control efficiently

the system, fulfilling the two proposed objectives: the control of the oxygen excess ratio and the control of the generated voltage in the fuel cell. Changing the valve area, it is also possible to improve the efficiency. For example, from 38.4% to 40.5% reducing the valve area from $40\,cm^2$ to $20\,cm^2$ for a certain compressor voltage. Finally, with regard to the temporal behavior, it is concluded that is possible to reduce the time response of the controlled variables from $0.6\,s$ to $0.4\,s$.

On the other hand, the power generation systems based on fuel cell are complex devices prone to failures. For this reason, a diagnosis and fault-tolerant control was addressed. A simulation environment, based on a well known fuel cell model of the literature, that allows to simulate a set of proposed faults, was elaborated in order to develop and evaluate a methodology of diagnosis based on the relative sensibilities of the faults.

With respect to the fault-tolerant control, it was demonstrated that the control structure with two manipulated variables has fault-tolerant capability to face up faults in the compressor: the fault-tolerant control is able to cope with the control of the oxygen excess ratio in the cathode when the operating range of the compressor voltage is reduced up to 25% of the original range.

8.2 Future work

In the course of this dissertation a wide study for the control of fuel cell-based systems has been carried out. However, there are several extensions that can be explored. This include:

Control of the fuel cell system in a wide range of operation

The control of the fuel cell air supply and the fuel cell voltage performed in Chapter 4 was committed using a linearized model of the fuel cell system in a determined operating point and the controller was evaluated with disturbances in the fuel cell current around the nominal value. However, in applications such as *Fuel Cell Vehicles* the power demand varies strongly and, thus, the fuel cell must operate in a wide range of operating points. With hybridization, this range will be minimized. However, we still think that the control technique based on predictive control developed in Chapter 4 should be

extended for a wider range of operating conditions similar to those found in the driving cycles.

Since the fuel cell system is nonlinear, the controller must rely on several models and commutate from one model to another according to the operating zone. Besides, the reference value of λ_{O_2} must be modified according to the fuel cell current since there is an optimal value of λ_{O_2} for each current [38].

Experimental validation of the control strategy based on *DMC*

The control strategy based on *DMC* proposed in Section 4.2.5 was evaluated in a simulation environment exploiting a detailed nonlinear model of the fuel cell system. However, it would be interesting to evaluate the performance of the proposed controller in a real fuel cell system. With this objective, some advances have been achieved: a experimental setup with a 50-*W* fuel cell, an air compressor, a proportional valve at the cathode outlet, and the data acquisition and control system with sensors and actuators was assembled; some experimental test for the identification of the system to determine the *Dynamic Matrix* were performed, and the controller was developed in the *LabVIEW* environment. However, some experimentation is still necessary to show relevant results.

Fault-tolerant control for failure in the cathode output valve

In Section 5.2, the fault-tolerant control for failures in the compressor motor was addressed and it was concluded that the control structure with two actuators has fault tolerant capability to face up faults in the compressor motor. This study could be extended to consider failures in the other actuator: the cathode output valve, as well as other failures that can be foreseeable in a *FCS*.

Appendix A

Principal equations in the Fuel Cell System model

As it was mentioned in Section 4.1, the model used to describe the fuel cell system behavior is based on the model proposed by Pukrushpan et al. [13]. In this appendix, the governing equations of the model are reproduced from [38] where a clear summary of the model is done. For more details see [13] or [25].

The governing equations for the mass of air in the supply manifold, for the masses of oxygen, nitrogen and water in the cathode and for the masses of hydrogen and water in the anode are respectively defined using the principle of mass conservation [38]:

$$\frac{dm_{sm}}{dt} = W_{cp} - W_{sm,out} \tag{A.1}$$

$$\frac{dm_{O2}}{dt} = W_{O2,\,in} - W_{O2,\,out} - W_{O2,\,rct} \tag{A.2}$$

$$\frac{dm_{N2}}{dt} = W_{N2,\,in} - W_{N2,\,out} \tag{A.3}$$

$$\frac{dm_{w,ca}}{dt} = W_{v,\,ca,\,in} - W_{v,\,ca,\,out} - W_{v,\,ca,\,gen} + W_{v,\,m} \tag{A.4}$$

$$\frac{dm_{H2}}{dt} = W_{H2,\,in} - W_{H2,\,out} - W_{H2,\,rct} \tag{A.5}$$

A. Principal equations in the Fuel Cell System model

$$\frac{dm_{w,an}}{dt} = W_{v,an,in} - W_{v,an,out} - W_{v,m} \tag{A.6}$$

The governing equation for the rotational speed of the compressor is defined by the power conservation principle as:

$$J_{cp}\frac{d\omega_{cp}}{dt} = \tau_{cm} - \tau_{cp} \tag{A.7}$$

The governing equations for the supply manifold pressure and the return manifold pressure are respectively defined using the energy conservation principle and the standard thermodynamics relationships as:

$$\frac{dp_{sm}}{dt} = \frac{\gamma R_a}{V_{sm}}(W_{cp}T_{cp} - W_{sm,out}T_{sm}) \tag{A.8}$$

$$\frac{dp_{rm}}{dt} = \frac{R_a T_{rm}}{V_{rm}}(W_{ca,out} - W_{rm,out}) \tag{A.9}$$

To express the governing equations in terms of the states, the closure relations (A.10) to (A.16) are used . The supply manifold outlet air rate $W_{sm,out}$ is related to p_{sm} and p_{ca} via the linearized nozzle equation:

$$W_{sm,out} = k_{sm,out}(p_{sm} - p_{ca}) \tag{A.10}$$

The inlet oxygen, nitrogen, and cathode vapour mass flow rates, $W_{O2,in}$, $W_{N2,in}$, and $W_{v,ca,in}$ are related to the cathode inlet air mass flowrate, the inlet air humidity and the mass fraction of oxygen and nitrogen in dry air using the ideal gas relations. The outlet oxygen, nitrogen and cathode vapor mass flow rates, $W_{O2,out}$, $W_{N2,out}$, and $W_{v,ca,out}$, are likewise related to the outlet air mass flowrate, the outlet air humidity and the mass fraction of the oxygen and nitrogen in dry air at the cathode outlet using the ideal gas relations. The reacted oxygen and hydrogen and generated water vapor (in the cathode) mass flow rates, $W_{O2,rct}$, $W_{H2,rct}$, and $W_{v,ca,gen}$, are related to the fuel cell current:

$$W_{O2,rct} = M_{O2}\frac{n\,I_{fc}}{4\,F} \tag{A.11}$$

$$W_{H2,rct} = M_{H2}\frac{n\,I_{fc}}{2\,F} \tag{A.12}$$

$$W_{v,ca,gen} = M_v \frac{n\,I_{fc}}{2\,F} \tag{A.13}$$

where the constants 4 and 2 in the denominators denote the of electrons involved in the oxidation and the reduction half-reactions respectively.

The water mass flowrate through the membrane, $W_{v,m}$, is defined using the hydration model. The outlet hydrogen and water masses are assumed to be zero, that is, hydrogen is assumed to react completely in the anode, while water generated by the oxidation half-reaction is assumed to be transported via electro-osmosis through the membrane towards the cathode.

The compressor motor torque τ_{cm} is related to the compressor motor voltage V_{cm} and the compressor motor rotational speed ω_{cp} by the static motor equation:

$$\tau_{cm} = \eta_{cm} \frac{k_t}{R_{cm}} \left(V_{cm} - k_v\,\omega_{cp} \right) \tag{A.14}$$

where k_t, R_{cm}, and k_v are motor constants and η_{cm} is the motor mechanical efficiency. The steady state compressor torque τ_{cp} is related to the supply manifold pressure, the compressor motor rotational speed and the compressor air flowrate via the thermodynamic relations

$$\tau_{cp} = \frac{C_P}{\omega_{cp}} \frac{T_{atm}}{\eta_{cp}} \left[\left(\frac{p_{cm}}{p_{atm}} \right)^{(\gamma-1)/\gamma} - 1 \right] W_{cp} \tag{A.15}$$

The air temperature in the compressor, T_{cp}, is defined using basic thermodynamic relations

$$T_{cp} = T_{atm} + \frac{T_{atm}}{\eta_{cp}} \left[\left(\frac{p_{sm}}{p_{atm}} \right)^{(\gamma-1)/\gamma} - 1 \right] \tag{A.16}$$

The air temperature in the supply manifold, T_{sm}, is obtained from m_{sm}, p_{sm} and V_{sm} using the ideal gas law. The cathode outlet air flowrate $W_{ca,out}$ is related to the cathode pressure and return manifold pressure via a linearized nozzle equation analogous to that in (A.10). The return manifold outlet air flowrate $W_{rm,out}$ is defined using a non-linearized nozzle relation as discussed in Section 4.2.2, while the return manifold air temperature T_{rm} is considered to be constant and equal to the temperature of the fuel cell stack.

A. Principal equations in the Fuel Cell System model

Appendix B

Technical data of Maxwell supercapacitors

Table B.1: Technical specifications of BOOSTCAP BPAK0350-15E supercapacitors from Maxwell Technologies [96].

Specification	Value	Observations
Capacitance, C_R [F]	58	
Voltage, U_R [V]	15	
Maximum energy, $[Wh/kg]$	3.63	Full discharge from nominal voltage $(U_R = 15V)$
Specific power, $[W/kg]$	2850	Idem
Internal resistance, DC $[ohm]$	0.019	Discharging at constant current
Operating temperature, $[C]$	-40 to 65	
Life time[a], $\Delta C/C_R$ [%]	≤ 20	From initial value after 10 years @25°C
Cycle life[b], $\Delta C/C_R$ [%]	≤ 20	From initial value after 500 Kcycles @ 25°C $(I = 5A)$

[a]Life time considers the aging degradation.
[b]Cycle life considers the degradation due to the amount of charge/discharge cycles.

B. Technical data of Maxwell supercapacitors

Bibliography

[1] P. Zegers. Fuel cell commercialization: The key to a hydrogen economy. *J. of Power Sources*, 154(2):497–502, 2006.

[2] International Energy Agency. *Key World Energy Statics*, 2007.

[3] J.M. Ogden, M.M. Steinbugler, and T.G. Kreutz. Comparison of hydrogen, methanol and gasoline as fuels for fuel cell vehicles: implications for vehicle design and infrastructure development. *J. of Power Sources*, 79(2):143–168, 1999.

[4] J.T.S. Irvine. The Bourner lecture: Power sources and the new energy economy. *J. of Power Sources*, 136(2):203–207, 2004.

[5] J. Larminie and A. Dicks. *Fuel Cell Systems Explained*. Wiley and Sons, second edition, 2003.

[6] T. Bose and P. Bénard. Hydrogen as an energy vector. In *Proceedings of the Power Engineering, 2003 Large Engineering Systems Conference on*, pages 196–199, May 2003.

[7] MA Laughton. Fuel cells. *Power Engineering Journal*, 16:37–47, 2002.

[8] R. Helmolt and U. Eberle. Fuel cell vehicles: Status 2007. *J. of Power Sources*, 165:833–843, 2007.

[9] K. Rajashekara. Propulsion system strategies for fuel cell vehicles. *Fuel Cell Technology for Vehicles*, pages 179–187, 2000.

[10] C. Chan. The state of the art of electric and hybrid vehicle. *Proceedings of the IEEE*, 90(2):247–275, 2002.

BIBLIOGRAPHY

[11] H. Tang, S. Peikang, S.P. Jiang, F. Wang, and M. Pan. A degradation study of Nafion proton exchange membrane of PEM fuel cells. *J. of Power Sources*, 170(1):85–92, 2007.

[12] K. Yao, K. Karan, K. McAuley, P. Oosthuizen, B. Peppley, and T. Xie. A review of mathematical models for hydrogen and direct methanol polymer electrolyte membrane fuel cells. *Fuel Cells*, 4(1-2):3–29, 2004.

[13] JT Pukrushpan and A.G.H. Peng. Modeling and control for PEM fuel cell stack system. *American Control Conference. Proceedings of the 2002*, 4.

[14] S. D'Arco, D. Ianuzzi, M. Pagano, and P. Tricoli. Design criteria optimizing the use of fuel cell source in electric power system. In *Proceedings of the 16th IFAC World Congress*, Prague, 2005.

[15] U.S. Department of Energy, Office of Fossil energy and National Energy Technology Laboratory. *Fuel Cell Handbook*, 6th edition, 2002.

[16] W. Yang, B. Bates, N. Fletcher, and R. Pow. Control challenges and methodologies in fuel cell vehicles development. *Fuel Cell Technology for Vehicles*, pages 249–256, 1998.

[17] L. Carrette, K. Friedrich, and U. Stimming. Fuel cells - fundamentals and applications. *Fuel Cells*, 1(1):5–39, 2001.

[18] K. Jeong and B. Oh. Fuel economic and life-cycle cost analysis of a fuel cell hybrid vehicle. *J. of Power Sources*, 105:58–65, 2002.

[19] D. Friedman and R. Moore. PEM fuel cell system optimization. In *Proceedings Electrochemical Society*, volume 27, pages 407–423, 1998.

[20] S. Flipsen. Power sources compared: The ultimate truth? *J. of Power Sources*, 162:927–934, 2006.

[21] J. Amphlett, R. Mann, B. Peppley, P. Roberge, and A. Rodrigues. A model predicting transient responses of proton exchange membrane fuel cells. *J. of Power Sources*, 61:183–188, 1996.

[22] J. Correa, F. Farret, L. Canha, and M. Simoes. An electrochemical-based fuel-cell model suitable for electrical engineering automation approach. *Industrial Electronics, IEEE Transactions on*, 51(5):1103–1112, 2004.

[23] F. Barbir. *PEM Fuel Cells: Theory and Practice*. Elsevier, 2005.

[24] U. Bossel. Well-to-Wheel Studies, Heating Values, and the Energy Conservation Principle. In *European Fuel Cell Forum, 29th October*, 2003.

[25] J. Pukrushpan. *Modelling and Control of Fuel Cell Systems and Fuel Processors*. PhD thesis, University of Michigan, 2003.

[26] K. Wipke, M. Cuddy, and S. Burch. Advisor 2.1: A user-friendly advanced powertrain simulation using a combined backward/forward approach. *IEEE Transactions on Vehicular Technology*, 48:1751–1761, 1999.

[27] T. Markel, A. Brooker, T. Hendricks, V. Johnson, K. Kelly, B. Kramer, M. O'Keefe, S. Sprik, and K. Wipke. Advisor: a system analysis tool for advanced vehicle modeling. *J. of Power Sources*, 110:255–266, 2002.

[28] P. Rodatz, G. Paganelli, A. Sciarretta, and L. Guzzella. Optimal power management of an experimental fuel cell/supercapacitors-powered hybrid vehicle. *Control Engineering Practice*, 13:41–53, 2004.

[29] T. Markel, M. Zolot, K. Wipke, and A. Pesaran. Energy storage system requirements for hybrid fuel cell vehicles. In *Proceedings of the 3rd International Advanced Automotive Battery Conference*, Nice, France, June 2003.

[30] G. Gigliucci, L. Petruzzi, E. Cerelli, A. Garzisi, and A. La Mendola. Demonstration of a residential CHP system based on PEM fuel cells. *J. of Power Sources*, 131(1-2):62–68, 2004.

[31] M. Uzunoglu, O. Onar, and M. Alam. Dynamic behavior of PEM FCPPs under various load conditions and voltage stability analysis for stand-alone residential applications. *J. Power Sources*, 168(1):240–250, 2007.

[32] M. El-Sharkh, A. Rahman, M. Alam, P. Byrne, A. Sakla, and T. Thomas. A dynamic model for a stand-alone PEM fuel cell power plant for residential applications. *J. Power Sources*, 138:199–204, 2004.

[33] M. Uzunoglu and MS Alam. Dynamic modeling, design, and simulation of a combined PEM fuel cell and ultracapacitor system for stand-alone residential applications. *Energy Conversion, IEEE Transaction on*, 21(3):767–775, 2006.

[34] R. Ahluwalia, X. Wang, A. Rousseau, and R. Kumar. Fuel economy of hydrogen fuel cell vehicles. *J. of Power Sources*, 130:192–201, 2003.

[35] J. Pukrushpan, A. Stefanopoulou, and H. Peng. Control of fuel cell breathing: Initial results on the oxygen starvation problem. *IEEE Control Systems Magazine*, 24:30–46, 2004.

[36] J. Golbert and D. Lewin. Fuel efficient model predictive control of pem fuel cells. In *Proceedings of 16th World Congress*, Prague, 2005.

[37] J. Golbert and D. Lewin. Model-based control of fuel cells: (1) regulatory control. *J. of Power Sources*, 135:135–151, 2004.

[38] M. Grujicic, K.M. Chittajallu, E.H. Law, and J.T. Pukrushpan. Model-based control strategies in the dynamic interaction of air supply and fuel cell. *Proceedings of the Institution of Mechanical Engineers, Part A: J. of Power and Energy*, 218(7):487–499, 2004.

[39] M. Grujicic, K.M. Chittajallu, and J.T. Pukrushpan. Control of the transient behaviour of polymer electrolyte membrane fuel cell systems. *Proceedings of the Institution of Mechanical Engineers, Part D: J. of Automobile Engineering*, 218(11):1239–1250, 2004.

[40] A. Vahidi and A. Peng. Model predictive control for starvation prevention in a hybrid fuel cell system. *American Control Conference. Proceedings of the 2004*, 1:834–839.

[41] Z. Liu, L. Yang, Z. Mao, W. Zhuge, Y. Zhang, and L. Wang. Behavior of PEMFC in starvation. *J. of Power Sources*, 157(1):166–176, 2006.

[42] J. Pukrushpan, H. Peng, and A. Stefanopoulou. Control-oriented modelling and analysis for automotive fuel cell systems. *J. of Dynamic Systems*, 126:14–25, 2004.

[43] S. Varigonda, J.T. Pukrushpan, A.G. Stefanopoulou, and American Institute of Chemical Engineers. *Challenges in Fuel Cell Power Plant Control: The Role of System Level Dynamic Models*. American Institute of Chemical Engineers, 2003.

[44] M. Serra, A. Husar, D. Feroldi, and J. Riera. Performance of diagonal control structures at different operating conditions for polymer electrolyte membrane fuel cells. *J. of Power Sources*, 158(2):1317–1323, 2006.

[45] K. Rajashekara. Power conversion and control strategies for fuel cell vehicles. *Industrial Electronics Society*, 3:2865–2870, 2003.

[46] E. Santi, D. Franzoni, A. Monti, D. Patterson, and N. Barry. A fuel cell based domestic uninterruptible power supply. *Applied Power Electronic Conference and Exposition*, pages 605–613, 2002.

[47] D.K. Choi, B.K. Lee, S.W. Choi, C.Y. Won, and D.W. Yoo. A novel power conversion circuit for cost-effective battery-fuel cell hybrid systems. *J. of Power Sources*, 152(1):245–255, 2005.

[48] A. Drolia, P. Jose, and N. Mohan. An approach to connect ultracapacitor to fuel cell powered electric vehicle and emulating fuel cell electrical characteristics using switched mode converter. *Industrial Electronics Society*, 1:897–901, 2003.

[49] P. Atwood, S. Gurski, D.J. Nelson, and K.B. Wipke. Degree of Hybridization Modeling of a Fuel Cell Hybrid Electric Sport Utility Vehicle. *Fuel Cell Power for Transportation*, 2000.

[50] D. Friedman. Maximizing Direct-Hydrogen PEM Fuel Cell Vehicle Efficiency-Is Hybridization Necessary? *SAE International*, pages 265–272, 1999.

[51] S. Akella, N. Sivashankar, S. Gopalswamy, E. Inc, and M. Plymouth. Model-based systems analysis of a hybrid fuel cell vehicle configuration. *American Control Conference, 2001. Proceedings of the 2001*, 3, 2001.

[52] R. Moore, K. Hauer, S. Ramaswamy, and J. Cunningham. Energy utilization an efficiency analysis for hydrogen fuel cell vehicles. *J. of Power Sources*, 159:1214–1230, 2006.

BIBLIOGRAPHY

[53] P. Thounthong, S. Raël, and B. Davat. Control strategy of fuel cell/supercapacitors hybrid power sources for electric vehicle. *J. of Power Sources*, 158(1):806–814, 2006.

[54] G. Paganelli, Y. Guezennec, and G. Rizzoni. Optimizing Control Strategy for Hybrid Fuel Cell Vehicle. pages 71–79, 2002.

[55] P. Rodatz, O. Garcia, L. Guzzella, F. Büchi, M. Bärschi, T. Tsukada, P. Dietrich, R. Kötz, G. Schreder, and A. Woukan. Performance and operational characteristics of hybrid vehicle powered by fuel cell and supercapacitors. *Fuel Cell Power for Transportation*, pages 77–84, 2003.

[56] R. Kötz, S. Müller, M. Bärtschi, B. Schnyder, P. Dietrich, FN Büchi, A. Tsukada, GG Scherer, P. Rodatz, O. Garcia, et al. Supercapacitors for peak-power demand in fuel-cell-driven cars. *ECS Electro-Chemical Society, 52nd Meeting,, San Francisco, Sept*, pages 2–7, 2001.

[57] S. Caux, J. Lachaize, M. Fadel, P. Shott, and L. Nicod. Modelling and control of a fuel cell system and storage elements in transport applications. *J. of Process Control*, 15:481–491, 2005.

[58] S. Caux, J. Lachaize, M. Fadel, P. Shott, and L. Nicod. Energy management of fuel cell system and supercaps elements. In *Proceedings of the 16th IFAC World Congress*, Prague, 2005.

[59] J. Jung, Y. Lee, J. Loo, and H. Kim. Power control strategy for fuel cell hybrid electric vehicles. *Fuel Cell for Transportation*, pages 201–205, 2003.

[60] M. Kim and H. Peng. Power management and design optimization of fuel cell/battery hybrid vehicles. *J. of Power Sources*, 165:819–832, 2007.

[61] J. Schiffer, O. Bohlen, RW de Doncker, and DU Sauer. Optimized Energy Management for FuelCell-SuperCap Hybrid Electric Vehicles VPP Track 4: Energy Storage Components/Systems. *Vehicle Power and Propulsion, 2005 IEEE Conference*, pages 716–723.

[62] JC Amphlett, RF Mann, BA Peppley, PR Roberge, and A. Rodrigues. A practical PEM fuel cell model for simulating vehicle power sources. *Battery Conference on Applications and Advances, Proceedings of the Tenth Annual*, pages 221–226, 1995.

[63] TE Springer, TA Zawodzinski, and S. Gottesfeld. Polymer Electrolyte Fuel Cell Model. *J. of The Electrochemical Society*, 138:2334, 1991.

[64] P.T. Nguyen, T. Berning, and N. Djilali. Computational model of a PEM fuel cell with serpentine gas flow channels. *J. of Power Sources*, 130(1-2):149–157, 2004.

[65] F. Zenith and S. Skogestad. Control of fuel cell power output. *J. of Process Control*, 17(4):333–347, 2007.

[66] M. Ceraolo, C. Miulli, and A. Pozio. Modelling static and dynamic behaviour of proton exchange membrane fuel cells on the basis of electro-chemical description. *J. of Power Sources*, 113(1):131–144, 2003.

[67] PR Pathapati, X. Xue, and J. Tang. A new dynamic model for predicting transient phenomena in a PEM fuel cell system. *Renewable Energy*, 30(1):1–22, 2005.

[68] E. Camacho and C. Bordons. *Model Predictive Control*. Springer-Verlag, 1999.

[69] M. Blanke, M. Kinnaert, J. Lunze, and M. Staroswiecki. *Diagnosis and Fault-Tolerant Control*. Springer, second edition, 2006.

[70] V. Puig, J. Quevedo, T. Escobet, B. Morcego, and C. Ocampo. Control Tolerante a Fallos (Parte II): Mecanismos de Tolerancia y Sistema Supervisor. *Revista Iberoamericana de Automatica e Informatica Industrial*, 1(2):5–21, 2004.

[71] V. Puig, D. Feroldi, M. Serra, J. Quevedo, and J. Riera. Fault-tolerant mpc control of pem fuel cells. In *17th World Congress IFAC*, pages 11112–11117, Seoul, Korea, 2008.

[72] T. Escobet, D. Feroldi, S. de Lira, V. Puig, J. Quevedo, J. Riera, and M. Serra. Model based Fault Diagnosis in PEM Fuel Cell systems. *J. of Power Sources, In press, Corrected proof*.

[73] JJ Gertler and N.L. Inc. *Fault detection and diagnosis in engineering systems*. Marcel Dekker, New York, 1998.

[74] V. Puig, J. Quevedo, T. Escobet, B. Morcego, and C. Ocampo. Control Tolerante a Fallos (Parte I): Fundamentos y Diagnostico de Fallos. *Revista Iberoamericana de Automatica e Informatica Industrial*, 1(1):15–31, 2004.

[75] M. Staroswiecki and G. Comtet-Varga. Analytical redundancy relations for fault detection and isolation in algebraic dynamic systems. *Automatica*, 37:687–699, 2001.

[76] R. Isermann. Model-based fault-detection and diagnosis - status and applications. *Annual Reviews in Control*, 29(1):71–85, 2005.

[77] J. Chen and R.J. Patton. *Robust model-based fault diagnosis for dynamic systems*. 1999.

[78] V. Puig, J. Quevedo, T. Escobet, F. Nejjari, and S. de las Heras. Passive Robust Fault Detection of Dynamic Processes Using Interval Models. *Control Systems Technology, IEEE Transactions on*, 16(5):1083–1089, 2008.

[79] V. Puig, J. Quevedo, T. Escobet, and J. Meseguer. Toward a better integration of passive robust interval-based fdi algorithms. In *In IFAC Safeprocess06*, China, 2006.

[80] N. Fouquet, C. Doulet, C. Nouillant, G. Dauphin-Tanguy, and B. Ould-Bouamama. Model based PEM fuel cell state-of-health monitoring via ac impedance measurements. *J. of Power Sources*, 159(2):905–913, 2006.

[81] J.M. Maciejowski. *Predictive Control: With Constraints*. Prentice Hall, 2002.

[82] J.T. Pukrushpan, A.G. Stefanopoulou, and H. Peng. *Control of Fuel Cell Power Systems: Principles, Modeling, Analysis and Feedback Design*. Springer, 2004.

[83] K. Williams, W. Keith, M. Marcel, T. Haskew, Shepard, and B. Todd. Experimental investigation of fuel cell dynamic response and control. *J. of Power Sources*, 163(2):971–985, 2007.

[84] W. Henson. Optimal battery/ultracapacitor storage combination. *Journal of Power Sources*, 2008.

[85] A. Burke. Ultracapacitors: Why, how and where is the technology. *J. of Power Sources*, 91(1):37–50, 2000.

[86] G. Pede, A. Iacobazzi, S. Passerini, A. Bobbio, and G. Botto. FC vehicle hybridisation: an affordable solution for an energy-efficient FC powered drive train. *J. of Power Sources*, 125(2):280–291, 2004.

[87] Maxwell Technologies. *BC Energy Series: Boostcap Ultracapacitors.*

[88] C. Arbizzani, M. Biso, D. Cericola, M. Lazzari, F. Soavi, and M. Mastragostino. Safe, high-energy supercapacitors based on solvent-free ionic liquid electrolytes. *J. of Power Sources*, 2008.

[89] M. Mastragostino and F. Soavi. Strategies for high-performance supercapacitors for HEV. *J. Power Sources*, 174(1):89–93, 2007.

[90] W. Gao. Performance comparison of a fuel cell-battery hybrid powertrain and a fuel cell-ultracapacitor hybrid powertrain. *IEEE Transactions on Vehicular Technology*, 54(3):846–855, May 2005.

[91] M. Kellaway. Hybrid buses–what their batteries really need to do. *J. of Power Sources*, 168:95–98, 2007.

[92] P. Moseley, B. Bonnet, A. Cooper, and M. Kellaway. Lead-acid battery chemistry adapted for hybrid electric vehicle duty. *J. of Power Sources*, 174(1):49–53, 2007.

[93] L. Lam, R. Louey, N. Haigh, O. Lim, D. Vella, C. Phyland, L. Vu, J. Furukawa, T. Takada, and D. Monma T. Kano. VRLA Ultrabattery for high-rate partial-state-of-charge operation. *J. of Power Sources*, 174(1):16–29, 2007.

[94] R. Ahluwalia and X. Wang. Direct hydrogen fuel cell systems for hybrid vehicles. *J. of Power Sources*, 139:152–164, 2005.

[95] W.G. Pell, B.E. Conway, W.A. Adams, and J. de Oliveira. Electrochemical efficiency in multiple discharge/recharge cycling of supercapacitors in hybrid EV applications. *J. Power Sources*, 80(1-2):134–141, 1999.

BIBLIOGRAPHY

[96] Maxwell Technologies. *Electrical Double Layer Capacitor: Boostcap ultracapacitor Series: BPAK.*

[97] DieselNet. Emission test cycles. Online, 2005. http:// www.dieselnet.com / standards / cycles/.

[98] R. Ahluwalia, X. Wang, and A. Rousseau. Fuel economy of hybrid fuel-cell vehicles. *J. of Power Sources*, 152:233–244, 2005.

[99] J. Kessels. *Energy Management for Automotive Power Nets.* PhD thesis, Technische Universiteit Eindhoven, 2007.

[100] M. Koot, A. Kessels, B. de Jager, W. Heemels, P. van den Bosch, and M. Steinbuch. Energy management strategies for vehicular electric power systems. *IEEE Transaction on Vehicular Technology*, 54(3):771–782, May 2005.

[101] T. Hofman, M. Steinbuch, R.M. van Druten, and A.F.A. Serrarens. Rule-based equivalent fuel consumption minimization strategies for hybrid vehicles. In *Proceedings of the 17th IFAC World Congress*, pages 5652–5657, Seoul, 2008.

[102] F. Philipps, G. Simons, and K. Schiefer. Dynamic investigation of PEFC stacks in interaction with the air supply system. *J. of Power Sources*, 154(2):412–419, 2006.

[103] Gill P., Murray W., and Wright M. *Practical optimization.* London Academic Press, 1981.

[104] National Instrument. Introducing LabVIEW 8.6. Online, 2008. http:// www.ni.com / labview/.